Abstract

WANG, YUN YENG. Constitutive Modeling of the Unloading Behavior of Paper Material Using the Asymptotic Fiber and Bond Model. (Under the direction of Dr. M. K. Ramasubramanian)

Current constitutive models for paper and paperboard material are focused on the prediction of the sheet stress-strain behavior during loading. The unloading process has not been widely addressed. This work will focus on modeling the unloading behavior of paper material in one- and two-dimensional problems.

For the one-dimensional problem, i.e. uniaxial tensile test, the asymptotic fiber and bond model by Sinha (1994) is extended to determine the plastic (permanent strain) of a sample upon unloading. In Sinha's micromechanics model, a representative load bearing, i.e. fiber at a fiber-to-fiber bond site, was used to derive the fiber stress and subsequently the sheet stress. In the asymptotic fiber and bond model, the fiber and bond condition (of elasticity or plasticity) was assumed to be the same throughout the fiber. In this work, the fiber and bond begins in elastic state. As the applied load or strains increase, the bond yields, while fiber remains elastic throughout the loading process. When unloading, both fiber and bond behave elastically.

The model parameters for the asymptotic fiber and bond are obtained by fitting the model to experimental data from uniaxial stress-strain curves. The unloading model is then used to predict the plastic strain after unloading of uniaxially strained samples. The model prediction corresponds well with the experimental data.

For a two-dimensional problem, a sample was deformed in a Mullen burst tester and then unloaded. A Mullen tester is used to conduct burst test by applying a uniform pressure to one surface of the sample that is clamped down on the pressure chamber. In a burst test, the sample deforms into hemispherical shape and eventually fails with a 'H' pattern in the center. For testing the unloading model, the sample is deformed to a given pressure and unloaded. The central displacement of the sample throughout the loading and unloading process is recorded together with the applied pressure, for comparison with model predictions.

Since the asymptotic fiber and bond model has limited application in one-dimensional problems, a combination of continuum and micromechanics methods was

used by Sinha and Perkins (1995) to reap the benefits the two types of approach have to offer. The hybrid model was applied in finite element analysis using the finite element analysis code ABAQUS and its user subroutine UMAT. A similar approach was utilized in this work to model the unloading process in two-dimensional problems.

CONSTITUTIVE MODELING OF THE UNLOADING BEHAVIOR OF PAPER MATERIAL USING THE ASYMPTOTIC FIBER AND BOND MODEL

By

YUN YENG WANG

A dissertation submitted to the Graduate Faculty of
North Carolina State University
in partial fulfillment of the requirements for the Degree of
Doctor of Philosophy

MECHANICAL ENGINEERING

Raleigh

2000

APPROVED BY:

Chair of Advisory Committee

To My Family

Biography

Born Wang Yun Yeng to the late Mr. Wang Seng Wee and Madam Chan Swee Yen. Yun is the third generation of Chinese immigrants in Malaysia. Yun completed her Bachelor's of Science in Mechanical Engineering at the University of Arkansas, Fayetteville followed by a Master's of Science in Nuclear Engineering at North Carolina State University.

Acknowledgement

I would like to extend my sincere thanks to Dr. Ramasubramanian for giving me the opportunity to do this work. The completion of my studies would not be possible without his help, his encouragement, and his compassion. My gratitude also goes to Dr. Richard Perkins of Syracuse University, for his ideas, guidance, and help throughout this work. I would also like to thank my committee members for their feedback and contribution.

The opportunity to pursue what life has to offer is often made available by the hard work and sacrifice of the many generations before me in my family, although fate has a hand in deciding the final outcome. The fruition of this work reflects more on their virtues and labor, rather than my own effort.

A special thanks to my parents, who taught me the value of education and the joy of knowledge. I am also indebted to my siblings, Jo and Yun Hui. Their support, encouragement, and sense of humor have sustained me through many tough times in my life. My special appreciation also goes to Kok Seng, for his support, understanding, and companionship; and to Yueh Wei for the joy she brings and the love she has showered me with.

Finally, I would like to thank all my friends, especially Gary Sweezy and Dinesh Hemnani, for their friendship and their ever willingness to help when I am in need. My thanks also go to Mrs. Joyce Pollard, Mr. Victor Perez, Mr. Rufus ‘Skip’ Richardson, and Mr. Mike Breedlove for their help over the years.

TABLE OF CONTENTS

		Page
LIST OF TABLES		vii
LIST OF FIGURES		viii
LIST OF SYMBOLS		xi
CONSTITUTIVE MODELING OF THE UNLOADING BEHAVIOR OF PAPER MATERIAL USING THE ASYMPTOTIC FIBER AND BOND MODEL		
1	Constitutive Modeling of Paper and Paperboard Material	1
1.1	Introduction	1
1.2	Fiber and Bond Properties	2
1.3	Papermaking Process	6
1.4	Sheet Structure	9
2	Constitutive Models of Paper Material	21
2.1	Continuum Models	21
2.1.1	Hyperelastic Plate Model	22
2.1.2	Composite Laminate Plate Model	23
2.1.3	Mosaic Model	26
2.2	Micromechanics Model	28
2.2.1	Full Plasticity Model	28
2.2.2	Asymptotic Fiber and Bond Model	28
2.2.2.1	Constitutive Behavior of Fiber, Bond, and Sheet	29
2.2.2.2	Critical Yield Strains In Asymptotic Fiber and Bond Model	30
2.2.2.3	Average Fiber Stress in Asymptotic Fiber and Bond Model	36
2.3	Continuum Model based on Incremental Asymptotic Fiber and Bond Model	39
2.3.1	General Finite Element Model for Stress Analysis	39
2.3.2	Continuum Model for Finite Element Analysis	41
2.4	Objective	44
3	Unloading Paper and Paperboard Material	51
3.1	Unloading in One-dimensional Problem	51
3.2	Unloading in Two-dimensional Problem	53
3.3	Cyclic Loading	53
4	Experimental Work	66
4.1	Uniaxial Tensile Test	66
4.1.1	Sample Conditioning	66

4.1.2 Uniaxial Tensile Test 68
4.2 Curve-fitting the Model Parameters 69
4.2.1 Fiber Orientation Concentration Parameter κ 69
4.2.2 Fiber Elastic Modulus and Bond Shear Elastic Modulus 71
4.2.3 Bond Yield Stress, Bond Second Slope, and Hardening Parameters 72

5 Results 84
5.1 Uniaxial Tensile Test 84
5.2 Burst Test 87

6 Conclusion and Future Work 109

References 112

Appendix I 115

List of Tables

		Page
Table 1.1	Comparison of mechanical and chemical pulp obtained from softwood.	6
Table 2.1	Average fiber stress expressions for $\varepsilon_{cb} < \varepsilon_{cf}$	37
Table 2.2	Average fiber stress expressions for $\varepsilon_{cf} < \varepsilon_{cb}$	37
Table 2.3	Average incremental fiber stress expressions for $\varepsilon_{cb} < \varepsilon_{cf}$	38
Table 2.4	Average incremental fiber stress expressions for $\varepsilon_{cf} < \varepsilon_{cb}$	38
Table 2.5	F functions for $\varepsilon_{cb} < \varepsilon_{cf}$	43
Table 2.6	F functions for $\varepsilon_{cf} < \varepsilon_{cb}$	43
Table 4.1	Model parameters for modeling the deformation process where the bond yields first.	66
Table 4.2	Effects of model parameters on the sheet stress-strain curve where bond yields first.	68
Table 4.3	Structural properties of fiber and bond.	69
Table 4.4	Asymptotic fiber and bond model parameters used in modeling.	73
Table 5.1	Final displacements before and after unloading in the uniaxial tensile tests.	86
Table 5.2	Final strains before and after unloading in the uniaxial tensile tests.	86
Table 5.3	Pressure at burst of paper cup stock.	89

List of Figures

Page

Figure 1.1 The configuration of a typical wood fiber 12

Figure 1.2 Load-elongation curves for black spruce fibers (45% yield kraft) for various fibril angles. 13

Figure 1.3 Fiber elastic modulus decreases as the mean fibril angle of S2 layer increases. 14

Figure 1.4 Fiber-to-fiber bond. 15

Figure 1.5 Micro-compression at a fiber-to-fiber bond site. 16

Figure 1.6 Micro-compressions form when the swollen fiber contract in the lateral direction. 17

Figure 1.7 Relative bonded area where $l/l_b = 1$ in the top diagram and $l/l_b = ½$ in the bottom diagram. 18

Figure 1.8 Summerwood fibers of long leaf pine holocelloluse experienced increased fiber strength when subjected to axial restraint during drying. 19

Figure 1.9 Jentzen effect dur to the application of drying restraints. 20

Figure 2.1 Elastic and plastic zones of fiber and bond along the fiber length. 46

Figure 2.2 Free body diagram of a mesoelement. 47

Figure 2.3 Chart of the two possible fiber and bond deformation scenarios. 48

Figure 2.4 Two-slope model approximation of the constitutive behavior of fiber. 49

Figure 2.5 Two-slope model approximation of the constitutive behavior of bond. 50

Figure 3.1 MD and CD stress-strain curve of copy paper subjected to tensile cyclic loading. 56

Figure 3.2 Flowchart for implementing the asymptotic fiber and bond model in UMAT to model the loading and unloading process 57

Figure 3.3 Flowchart of tensile loading process, i.e. $\Delta\varepsilon_s \geq 0$ 60

Figure 3.4 Flowchart of compressive loading process, i.e. $\Delta\varepsilon_s < 0$ 63

Figure 4.1 A schematic of the experimental setup used to measure the pressure-deflection curve of the paper sample 74

Figure 4.2 A schematic of the experimental setup used for tensile test 75

Figure 4.3 The E_{MD}/E_{CD} ratio was experimentally determined to be 2.08. 76

Figure 4.4 κ could range from about 0.5 to 0.7 for E_{MD}/E_{CD} to be 2.08. 77

Figure 4.5 The linear elastic region of the MD curves were fitted using 10 GPa $\leq E_{f0} \leq$ 20 GPa and 0.1 MPa $\leq G_{b0} \leq$ 100 MPa. 78

Figure 4.6 The decrease in S is less significant after G_{b0} = 10 MPa. 79

Figure 4.7 Model generated MD and CD stress-strain curves where ρ_s = 630 kg/m^3, κ = 0.60, E_{f0} = 17 GPa, and G_{b0} = 15 MPa. Assuming no drying restraint effects. 80

Figure 4.8 The MD curves were fitted using 6 MPa $\leq \tau_{p0} \leq$ 10 GPa and 10 kPa $\leq G_2 \leq$ 40 kPa. E_{f0} and G_{b0} were set at 17 GPa and 15 MPa respectively. 81

Figure 4.9 Model generated MD and CD stress-strain curves where ρ_s = 630 kg/m^3, κ = 0.60, E_{f0} = 17 GPa, and G_{b0} = 15 MPa. Assuming no drying restraint effects. 82

Figure 4.10 Model generated MD and CD stress-strain curves using parameters in Table 4.4. 83

Figure 5.1 Calibration curve for the amplified output signals from the pressure transducer 91

Figure 5.2 Calibration curve of the capacitance sensor used to measure the central displacement of the sample in a burst test. 92

Figure 5.3 MD stress-strain curves from micromechanics model for the 1 inch x 7 inch sample during loading and unloading. 93

Figure 5.4 CD stress-strain curves from micromechanics model for the 1 inch x 7 inch sample during loading and unloading. 94

Figure 5.5 The tensile test sample was modeled with 100 4-node bilinear plane stress elements in ABAQUS. 95

Figure 5.6 σ_{MD} in the 100-element model when loaded. 96

Figure 5.7 σ_{MD} in the 100-element model when loaded. 97

Figure 5.8 MD loading-unloading stress-strain curves for the 1 inch x 7 inch sample. The FEA solution was obtained using the automatic time step increment scheme in ABAQUS 98

Figure 5.9 The FEA* (100-element model) solution was obtained with a constant step size in ABAQUS. 99

Figure 5.10 σ_{MD} of sample in burst test at P = 0.72 MPa. The displacement degrees of freedom were constrained at the boundary. 100

Figure 5.11 σ_{CD} of sample in burst test at P = 0.72 MPa. The displacement degrees of freedom were constrained at the boundary. 101

Figure 5.12 σ_{MD} of sample in burst test at P = 0.72 MPa. The displacement and rotational degrees of freedom were constrained at the boundary 102

Figure 5.13 σ_{CD} of sample in burst test at P = 0.72 MPa. The displacement and rotational degrees of freedom were constrained at the boundary. 103

Figure 5.14 In a burst test, the sample generally failed at the center in the shape of the letter H. 104

Figure 5.15 Central displacement curve for a sample loaded to 0.72 MPa and unloaded in a Mulled tester. 105

Figure 5.16 Central displacement curve for a sample loaded to 0.54 MPa and unloaded in a Mullen tester. 106

Figure 5.17 Central displacement curve for a sample loaded to 0.51 MPa and unloaded in a Mullen tester. 107

Figure 5.18 Central displacement curve for a sample loaded to 0.49 MPa and unloaded in a Mullen tester. 108

List of Symbols

Symbol	Description
$\{\partial\}$	differential operator matrix
(Q'_{ij})	transformed reduced stiffness of layer k
[A]	reduced stiffness matrix
[B]	coupling stiffness matrix
[D]	bending stiffness matrix
[E]	material property matrix
[k]	mid-plane curvature
$[k]_n$	element stiffness matrix
[M]	moment applied on plate
[N]	force applied on plate (cf. 2.1.2)
[N]	shape functions (cf. 2.3)
$[\varepsilon]$	mid-plane strains
{d}	nodal displacements
{D}	nodal degree of freedom
{F}	body forces
{P}	external loads applied
$\{r_e\}_n$	element load vector
{u}	displacement field within the element
$\{\Phi\}$	surface tractions
$\{\varepsilon\}$	strain field
$\{\varepsilon_o\}$	initial strains
$\{\sigma_o\}$	Initial stresses
a_1,a_2, a_3	coefficients from linear regression
A_f	fiber cross sectional area
D_f	diameter of a fiber that has not collapsed or the z-directional thickness of a collapsed fiber
E_{2c}	tangent modulus of fiber in compression

Symbol	Description
E_{2c}	fiber tangent modulus (second slope) in compression
E_{2c0}	tangent modulus of unrestrained fiber in compression
E_{2t}	tangent modulus of fiber in tension
E_{2t}	fiber tangent modulus (second slope) in tension
E_{2t0}	tangent modulus of unrestrained fiber in tension
E_f	fiber elastic modulus
E_m,	the elastic modulus of the hemicellulose matrix
$E_{x,f}$	the axial modulus of the microfibrils
$E_{y,f}$	the transverse modulus of microfibrils
$f(\theta)$	probability density function of fiber orientation
G_2	bond tangent modulus (second slope)
G_{20}	bond tangent modulus of unrestrained fiber
G_b	bond shear elastic modulus
G_{b0}	bond elastic shear modulus of unrestrained fiber
G_m	the shear modulus of the hemicellulose matrix
$G_{xy,f}$	the shear modulus of the microfibrils
h	lamina thickness
HE_{2c0}	dimensionless drying restraint parameter for tangent modulus of fiber in compression
HE_{2t0}	dimensionless drying restraint parameter for tangent modulus of fiber in tension
HG_{20}	dimensionless drying restraint parameter for bond tangent modulus
HG_{b0}	dimensionless drying restraint parameter for bond elastic shear modulus
$I_0(\kappa)$	zeroth order modified Bessel function
L	fiber length,
l	distance between the bond centroids
l_b	bond length
m	moisture content
N	number of fibers of length L in a volume V (cf. 1.2)
N	number of laminas (cf. 2.1.2)

Symbol	Description
S, V	surface and volume of the structure
t_b	bond thickness
u_f	fiber displacement along the mesoelement direction
u_s	macroscopic sheet displacement along the mesoelement axial direction
V_f	volume fraction of the microfibrils
V_m	volume fraction of the hemicellulose
w_e	effective width of the fiber
x	volume fraction of voids
y	$E_x/E_{x,\text{ no voids}}$, $E_y/E_{y,\text{ no voids}}$, or $G_{xy}/G_{xy,\text{ no voids}}$
z_k	distance of layer k from the mid-plane
ΔM	moisture content
$H\sigma_{pc0}$	dimensionless drying restraint parameter for fiber yield stress in compression
$H\sigma_{pt0}$	dimensionless drying restraint parameter for fiber yield stress in tension
$H\tau_{p0}$	dimensionless drying restraint parameter for bond yield stress
α_f	coefficient of swelling and shrinkage of fiber material
β'	transformed coefficient of moisture expansion
ε_{bf}	critical strain for fiber yielding after bond has yielded
ε_{cb}	critical strain for initial bond yielding
ε_{cf}	critical strain for initial fiber yielding
ε_f	fiber strain
ε_{fb}	critical strain for bond yielding after fiber has yielded
ε_{pc}	fiber yield strain in compression
ε_{pt}	fiber yield strain in tension
γ_b	bond shear strain
γ_p	bond yield strain
κ	concentration parameter which define the degree of fiber orientation
μ	angle of orientation with greatest concentration of fibers
$\nu_{xy,f}$	the Poisson's ratios of the microfibrils

Symbol	Description
$\nu_{xy,m}$	the Poisson's ratios of the hemicellulose
θ	angle of fiber orientation
θ_0	orientation with the greatest concentration of fibers
ρ_f	fiber density
ρ_s	sheet density
σ_f	fiber stress
σ_{pc}	fiber yield stress in compression
σ_{pc0}	fiber yield stress in compression for unrestrained fiber
σ_{pt}	fiber yield stress in tension
σ_{pt0}	fiber yield stress in tension for unrestrained fiber
τ_b	bond shear stress
τ_p	bond yield stress
τ_{p0}	bond yield stress for unrestrained fiber

1. Constitutive Modeling of Paper and Paperboard Material

1.1 Introduction

Paper material is a network of self-bonding wood fibers. It is utilized in many applications as load-bearing structure and packaging material. In the paper industry, paper and paperboard material are produced in sheet form. They are then converted to end products through various manufacturing processes such as bending, creasing, and scoring. The ability to model the response of paper and paperboard material subjected to various loading conditions greatly facilitates the product design and manufacturing processes.

In general, the constitutive models for paper and paperboard material could be divided broadly into network models and continuum models. In the network models, paper and paperboard are treated as layers of fiber networks that are bonded at the fiber crossing sites. The constitutive behavior of the sheet is derived from the mechanical properties of the network constituents (fiber and bond) and interaction mechanisms in the network structure. Although three-dimensional network models are available, they are computationally intensive to be of practical use. Therefore, in the past, the network model has only been applied in one-dimensional problems, i.e. uniaxial loading. More recently, a finite element approach by Sinha and Perkins (1995) that utilized a continuum model based upon the incremental micromechanics model allowed the application of micromechanics model in two-dimensional problems. This approach is presented in Chapter 2 and would be extended to incorporate unloading mechanisms. Although this type of model is generally more calculation intensive, it allows additional insights into the deformation mechanisms of paper material. The network models also provide a mean to design fiber and bond properties for specific mechanical property needs of the sheet or vice versa. For example, the fiber-to-fiber bond could be strengthened by the addition of chemical additives and this could be taken into account by adjusting the fiber-to-fiber bond properties accordingly when determining the sheet stress.

The continuum models on the other hand treat paper and paperboard as homogenous plate-like continuum. The macroscopic material properties are experimentally determined. These properties are then used in two- and three-dimensional model for common engineering material to describe the deformation of paper material. The continuum approach provides a less calculation intensive alternative. However, it does not offer much insight to the relationship between the constitutive behavior of paper with the properties of the network constituents, the network structure, the papermaking process parameters, and environmental conditions. Therefore, this approach would not be able to accommodate changes in the stress-strain behavior that are caused by factors such as the application of drying restraints, a change in fiber orientation distribution, change in degree of bonding in the fiber network, and so on.

1.2 Fiber and Bond Properties

Prior to conducting any experimental or analytical work, it is essential to have an understanding of the various factors, which affect the constitutive behavior of paper material. Only then would one be able to appreciate the capabilities of contemporary models and identify the root cause of discrepancies between model predictions and experimental findings.

Paper is an orthotropic material and its constitutive behavior is affected by the manufacturing process. Its behavior is also dependent on the loading rate and sensitive to environmental conditions such as moisture and temperature. The factors, which affect the constitutive behavior of paper and paperboard material, could be broadly grouped into three categories and they are the papermaking process parameters, properties of the raw materials, and characteristics of the paper structure.

(i) Fiber and bond properties

- wood species
- growth site
- fibril angles
- fiber irregularities
- fiber length
- microcompression

(ii) papermaking process

- pulping
- bleaching
- beating
- drying restraints and moisture content

(iii) Network Structure

- fiber flocculation
- fiber orientation
- free fiber segment length/degree of bonding

Fibril Angle

A wood fiber typically has a circular or rectangular cross-section and a configuration shown in Figure 1.1. The middle lamella (ML) and primary wall (P) contain mainly lignin, act as a binding agent that keeps the fibers together in wood. Together, they are also known as the compound middle lamella. The secondary cell wall is made up of the S1, S2, and S3 layers. Each layer is essentially a matrix of amorphous hemicellulose, embedded with spirals of cellulose microfibrils. The microfibrils in the S2 layer have considerably smaller helix angle or fibril angle when compared with their counterparts in the S1 and S3 layer. In addition, the S2 layer is also the thickest layer. Consequently, the S2 layer dominates mechanical properties of the fiber.

The mechanical and structural properties of the fibers vary with the wood species and growth sites. In addition, the mechanical properties are also influenced by the fibril angles. Since the microfibrils are considerably stiffer than the hemicellulose, they provide the fiber with its axial elastic modulus and tensile strength. When a fiber is stretched, the fibril spirals tend to straighten out to provide higher tensile strength. Consequently, the tensile strength increases with decreasing fibril angle because the fibrils with smaller angle requires less straightening and therefore, less strain to support a given load (cf. Figure 1.2). Therefore, the fiber elastic modulus decreases with increasing fibril angles in the S2 layer (cf. Figure 1.3).

Fiber Irregularities and Fiber Length

The stress-strain behavior of fiber is dependent on the rate of loading. When measured over a short period of a few seconds, the fiber stress-strain curve could be linearly elastic up to the point of failure. However, if the period of measurement extends over a longer period of time such as several hours, the linear elastic stress-strain curve eventually becomes nonlinear (Jayne, 1959). In addition, the nonlinearity could also arise from the fiber structural irregularities, such as kinks, crimps, and microcompressions. (Niskanen, 1998).

While the fiber stress-strain behavior is affected by the fibril angle, the rate of loading, and fiber structural irregularities, the tensile properties of the network is affected by the fiber length. When a sheet is subjected to an applied load, the stress is transferred to the fibers via bending and shearing at the fiber-to-fiber bonds. Consequently, the ability of the fiber network in supporting a load depends on how well the fibers are bonded in the network. As more fibers are added to the network, the loosely connected regions of fiber network are bonded more effectively together, resulting in improved tensile properties of the sheet. The effectiveness of each fiber in raising the degree of bonding in the network is a function of its length. As the length increases, so does the area available for forming fiber-to-fiber bonds. However, the fiber length effect is not significant in high grammage paper where there is already a high degree of bonding. For a fiber of orientation θ in a planar fiber network, the average number of fiber crossing it would have is given by Komori and Makashima (1977) as

$$n(\theta) = \frac{2D_f NL^2}{V} J(\theta) \qquad \textbf{(1.1)}$$

where

$$J(\theta) = \int_0^{\pi} f(\theta)\left|\sin(\theta - \alpha)\right| d\alpha \qquad \textbf{(1.2)}$$

and D_f = diameter of a fiber that has not collapsed or the z-directional thickness of a collapsed fiber,

L = fiber length,

N = number of fibers of length L in a volume V,

$f(\theta)$ = fiber orientation probability density function.

In paper and paperboard material, there is a distribution of fiber length. Although the fiber length distribution is a characteristic of the wood species, it could also be affected by the degree of beating imposed during the papermaking process. The Erlang functions is used to describe the distribution and it is given by equation 1.3,

$$g(L) = \frac{(L/b)^{c-1} \exp(-L/b)}{[b(c-1)!]} \qquad \textbf{(1.3)}$$

where b is a scale parameter greater than zero, and c is a shape parameter. Together, the product bc gives the average fiber length.

Fiber-to-fiber Bond and Microcompression

While the fiber properties are attributed to the S2 layer, the bond properties could be attributed to the S1 layer (cf. Figure 1.4). When water is removed, the fibers are drawn together to form hydrogen bonds at the crossing sites. During drying, the fibers experience shrinkage, which takes place primarily in the lateral direction. The magnitude of the shrinkage depends on the degree of fiber swelling, which is affected by the pulping and beating process. The fiber-to-fiber bond is formed prior to shrinkage (Page and Tydeman, 1961). Therefore, the contraction, which competes with the fiber longitudinal stiffness, could result in the creation of shear stresses in the bond area, especially around the periphery (cf. Figure 1.5).

The shear stress translates into compressive stress in the crossing fiber, which could lead to deformation in the bonded fiber segments, i.e. micro-compression (cf. Figure 1.6). The effects of these micro-compressions include the distortion of microfibrils in the cell wall (Page and Seth, 1980b). This may result in a lower elastic modulus and a secondary slope in the stress-strain curve. It was suggested that the micro-compression have to be straightened out before the fibers are ‘activated’ and become load bearing elements (Giertz, 1979). This is because, while the microcompression are being straightened out, so are the distorted microfibrils along the fiber longitudinal axis.

While the fiber and bond properties are intrinsic to the species of the wood, they are affected also by the papermaking process. For example, beaten pulp has fewer fiber irregularities due to greater degree of swelling, which tends to straighten out the fiber. Water has the effect of reducing the stiffness of a fiber, so does the removal of the compound middle lamella. A more flexible fiber is capable of molding itself with others to form denser sheets. During the drying process, microcompressions could be reduced by applying drying restraints which inhibits the fibers from shrinkage, resulting in stiffer fibers. Therefore, the fiber properties and in turn, the sheet properties could be modified through the papermaking process such as pulping, beating, and so on.

1.3 Papermaking Process

Pulping

In the papermaking process, wood is converted to pulp through a chemical or mechanical pulping process. The chemical pulps are obtained by cooking wood chips in chemically treated solution. The pulp is then washed and bleached, during which much of the compound middle lamella is removed. This compound middle lamella contains mainly lignin, which acts as a binder that keeps the fibers together in the wood. Consequently, chemical pulp has lower lignin content compared to mechanical pulp. In bleached kraft pulp, the lignin content is almost zero, whereas the lignin content in mechanical pulp is about 30% (Niskanen, 1998). Mechanical pulps on the other hand are obtained by refining wood chips through mechanical actions such as pressing the logs against revolving grindstone. A comparison of the properties for the two pulps is given in Table 1.1. After pulping, chemical pulp may be bleached to improve its brightness. The decision to bleach depends on the end use of the pulp. In addition to its brightness, bleaching may also enhance the bonding ability of the fibers. However, it may also weaken the fiber tensile strength.

Table 1.1 Comparison of mechanical and chemical pulp obtained from softwood (Niskanen, 1998)

Property	Mechanical Pulps	Chemical Pulps
Yield on wood	High	Low
Amount of lignin	High	Low
Amount of hemicellulose	High	Low
Long fibers per unit mass	Few	Many
Specific surface area	Large	Small
Fines content	High	Low
Fiber structure	Stiff, course, straight	Slender, curly, kinky
Fiber shape	Short and thick	Long and thin

Property	Mechanical Pulps	Chemical Pulps
Bending stiffness	High	Low
Degree of collapse	Less collapsed	More collapsed

Beating

When collapsed, fibers attain a ribbon-like form. In paper, these collapsed fibers form a self-bonding network with no added matrix. These fibers are kept together by the hydrogen bonds formed at fiber crossings. A hydrogen bond is one where the proton of a hydrogen atom is shared by two electronegative oxygen (Baum 1993). Since the hydrogen bonds have a bond length of 2.7 angstrom, the surfaces must be very close to each other to allow bonding to occur. Due to the surface tension force, which becomes very large when water is removed, the fibers are drawn together and bonded during drying. The quality of the bond depends on the amount of contact area available at the bond site, which is also dependent on the flexibility of the fibers. Pulp beating leads to increase swelling and moisture content of the fiber. Since water softens the cellulose, beating the pulp result in greater fiber flexibility. Consequently, the more flexible fiber could bend around the others more easily during consolidation to form denser and better bonded network. As a result, beating improves the strength properties of the paper. In addition, swelling also tends to straighten out fiber irregularities, such as kinks and crimps, which also improve the fiber strength properties.

Drying Restraints and Moisture Content

Machined-made papers are dried under restraints. Due to the hydrodynamics effects, the fibers tend to orient themselves in the machine direction (MD). Resulting in the anisotropic nature of the paper structure. In addition, drying restraints also lead to Jentzen effect. Jentzen (1964) discovered that fibers dried under tension have a higher elastic modulus and tensile strength and shorter breaking strains. If the fibers are dried under compression, the reverse effects would be observed (cf. Figure 1.8 and Figure 1.9). While drying, the fibers are restrained from shrinking. As a result, fiber irregularities are straightened out, giving the fibers greater stiffness. Suppose the drying restrain is imposed in the machine direction only. The fibers with orientation in the vicinity of the machine direction would be straightened out more than the fibers with orientation further away. Therefore, fibers in the machine direction become stiffer, giving a directional quality to the sheet properties.

The added stiffness to the fiber could be accounted for, by making the constitutive properties of the fiber functions of the drying restrain strain ε_{DR}. Suppose ε_{xD} and ε_{yD} are imposed on the sheet during the drying process, the fiber elastic modulus is then given by (Perkins and Mark, 1981),

$$E_f = E_{f0}\left(1 + H_1\varepsilon_{DR} + H_2\varepsilon_{DR}^2 + \ldots\right) \quad \textbf{(1.4)}$$

where

$$\varepsilon_{DR} = \left(\varepsilon_{xD} + \alpha_x M\right)\cos^2\theta + \left(\varepsilon_{yD} + \alpha_y M\right)\sin^2\theta \quad \textbf{(1.5)}$$

In equation 1.5, $\alpha_x M$ and $\alpha_y M$ represents the free shrinkage of the sheet during drying which is a function of the moisture content M. Dropping the higher order terms and equation 1.4 and the effective fiber modulus becomes

$$E_f = E_{f0}\left(1 + H_{E_{f0}}\varepsilon_{DR}\right) \quad \textbf{(1.6)}$$

where $H_{E_{f0}}$ is a hardening parameter. Just like the free shrinkage $\alpha_x M$ and $\alpha_y M$, the hardening parameter has to be determined experimentally. Other than the fiber elastic modulus, other constitutive parameters such as the fiber elastic modulus, the bond shear elastic modulus, the fiber yield stress, and bond yield stress (cf. Figure 2.4 and Figure 2.5), are also affected by the drying restraint. These parameters could also be modified in similar manner to account for the effect of drying restraint has on them.

$$E_{2t} = E_{2t0}\left(1 + H_{E_{2t0}}\varepsilon_{DR}\right) \quad \textbf{(1.7)}$$

$$E_{2c} = E_{2c0}\left(1 + H_{E_{2c0}}\varepsilon_{DR}\right) \quad \textbf{(1.8)}$$

$$G_b = G_{b0}\left(1 + H_{G_{b0}}\varepsilon_{DR}\right) \quad \textbf{(1.9)}$$

$$G_2 = G_{20}\left(1 + H_{G_{20}}\varepsilon_{DR}\right) \tag{1.10}$$

$$\sigma_{pt} = \sigma_{pt0}\left(1 + H_{\sigma_{pt0}}\varepsilon_{DR}\right) \tag{1.11}$$

$$\sigma_{pc} = \sigma_{pc0}\left(1 + H_{\sigma_{pc0}}\varepsilon_{DR}\right) \tag{1.12}$$

$$\tau_p = \tau_{p0}\left(1 + H_{\tau_{p0}}\varepsilon_{DR}\right) \tag{1.13}$$

1.4 Sheet Structure

Fiber Flocculation

While in suspension, fibers tend to flocculate which results in the grammage variation within a sheet of paper. Grammage is the measure of the mass per unit area. Grammage may be an indicator of the load bearing capacity of the local region but it is not the sole determining factor. Nevertheless, most constitutive models do not take into account grammage variation in a sheet. Wong et al. (1995) conducted a study on the strain field of a sheet using finite element analysis, where grammage is the only parameter allowed to vary. The sheet was modeled as a plate with plane-stress plate elements of varying thickness to reflect the grammage variation in an actual sheet. Although the expected inverse relationship between local strain and grammage was observed, the correlation between predicted values and experimental data was weak, suggesting there are other factors, such as fiber orientations, which also affect the strain field.

Fiber Orientation

In addition to drying restraints, fiber orientation also contributes to the anisotropic nature of the mechanical properties of paper. As previously mentioned, fibers tend to orient themselves in the machine direction due to the imposed drying restraints. The distribution of the fiber orientation could be described by any convenient mathematical function such as the Fourier series given in equation 1.14

$$f(\theta) = \frac{1}{\pi}[1 + a_1 \cos 2(\theta - \theta_0) + a_2 \cos 4(\theta - \theta_0) + a_3 \cos 6(\theta - \theta_0) + \ldots + a_n \cos 2n(\theta - \theta_0)] \tag{1.14}$$

where θ = angle of fiber orientation

θ_0 = orientation with the greatest concentration of fibers

For a distribution function of fewer parameters, the von Mises function in equation 1.15 could also be used, where μ is usually the machine direction at 0°.

$$f(\theta) = \frac{1}{\pi I_0(\kappa)} \exp[\kappa \cos 2(\theta - \mu)] \tag{1.15}$$

where $I_0(\kappa)$ = zeroth order modified Bessel function

κ = concentration parameter which define the degree of fiber orientation. For a random isotropic material, κ is equal to 0

θ = angle of fiber orientation measured from μ

μ = angle of orientation with greatest concentration of fibers

Free Fiber Segment Length/Degree of Bonding

As suggested by Perkins (1990), the average distance between the centroids of adjacent bonds is the reciprocal of the average number of fiber crossings per unit fiber length. It was also suggested that the fraction of the fiber surface that is bonded could be estimated from, the ratio l/l_b given by (1.16),

$$\frac{l}{l_b} = \frac{\rho_f}{2\rho_s} \tag{1.16}$$

where l = distance between the bond centroids

l_b = bond length.

ρ_s = sheet density

ρ_f = fiber density

When l/l_b is 1, the fiber is essentially bonded to other fibers on one side of its surface (cf. Figure 1.7). When l/l_b is ½, i.e. $\rho_s = \rho_f$, the fiber then is essentially bonded on both the top and bottom surface. When there is a high degree of bonding, the free fiber segment length would be shorter making the stress transfer process more efficient. Consequently the tensile properties improve with the degree of bonding.

From the preceding discussion, one can see that paper is a complex material whose behavior is affected by many parameters in the papermaking process, its environment conditions, and the properties of its network constituents. Therefore, in formulating a model, which could predict the paper behavior or its variation in response to the changes in the parameters discussed above, presents a challenging task.

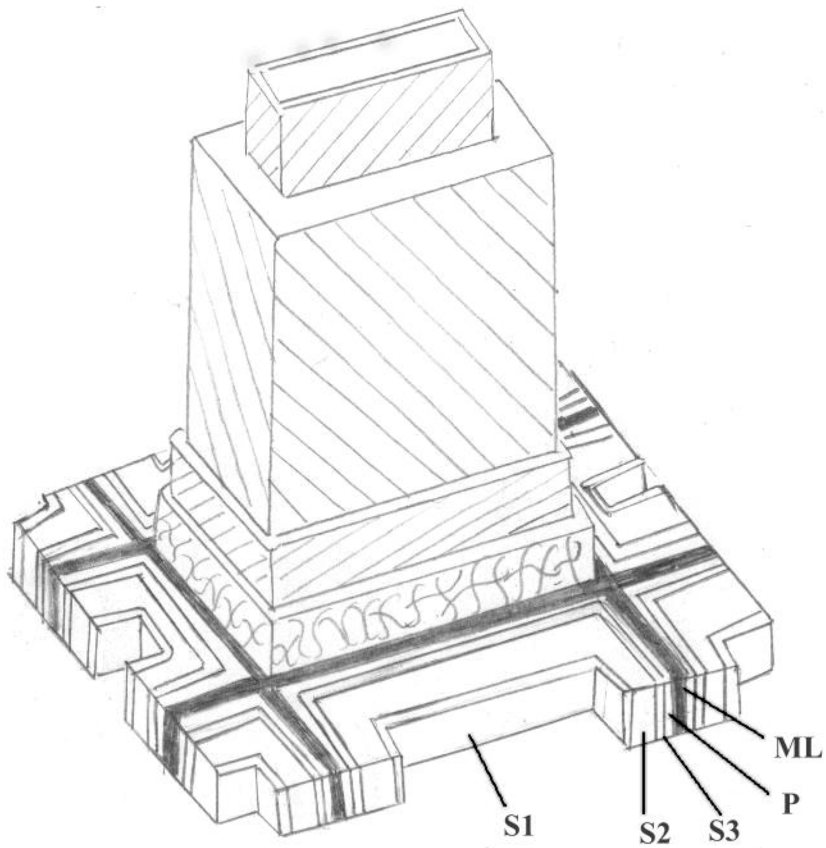

Figure 1.1 Configuration of a typical wood fiber (conifer tracheid) where ML = middle lamella, P = primary wall, and S1, S2, S3 = secondary walls (Niskanen, 1998).

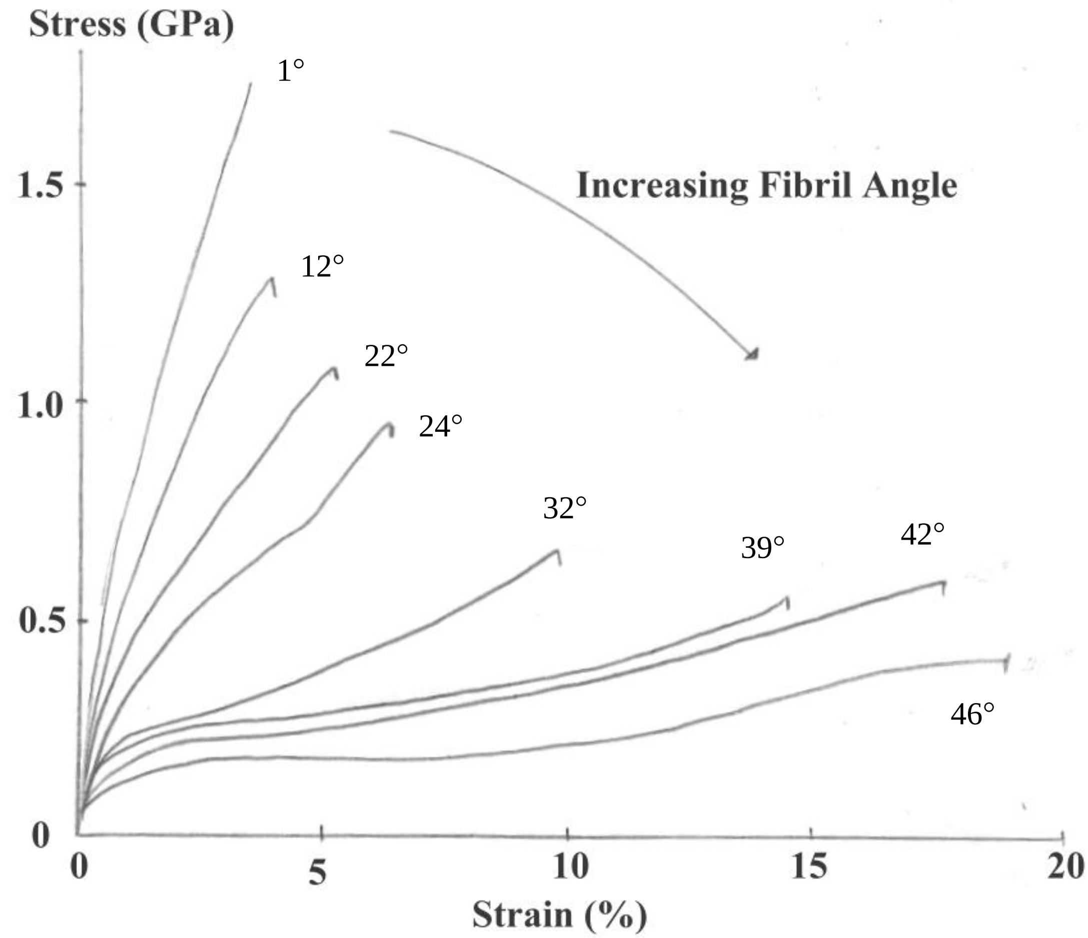

Figure 1.2 Load-elongation curves for black spruce fibers (45% yield kraft) for various fibril angles (Page and El-Hosseiny, 1983).

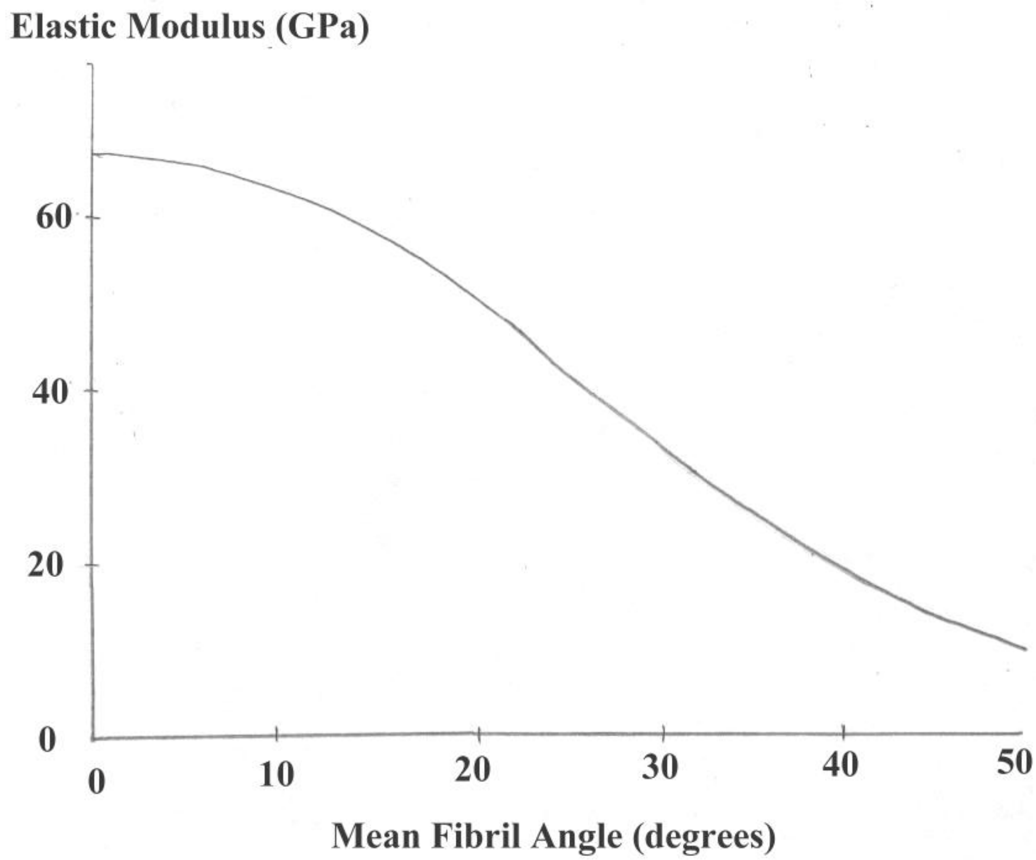

Figure 1.3 Fiber elastic modulus decreases as the mean fibril angle of S2 layer increases. The data which form the curve were collected from sample of holocellulose and 45% yield kraft (Page and El-Hosseiny, 1977).

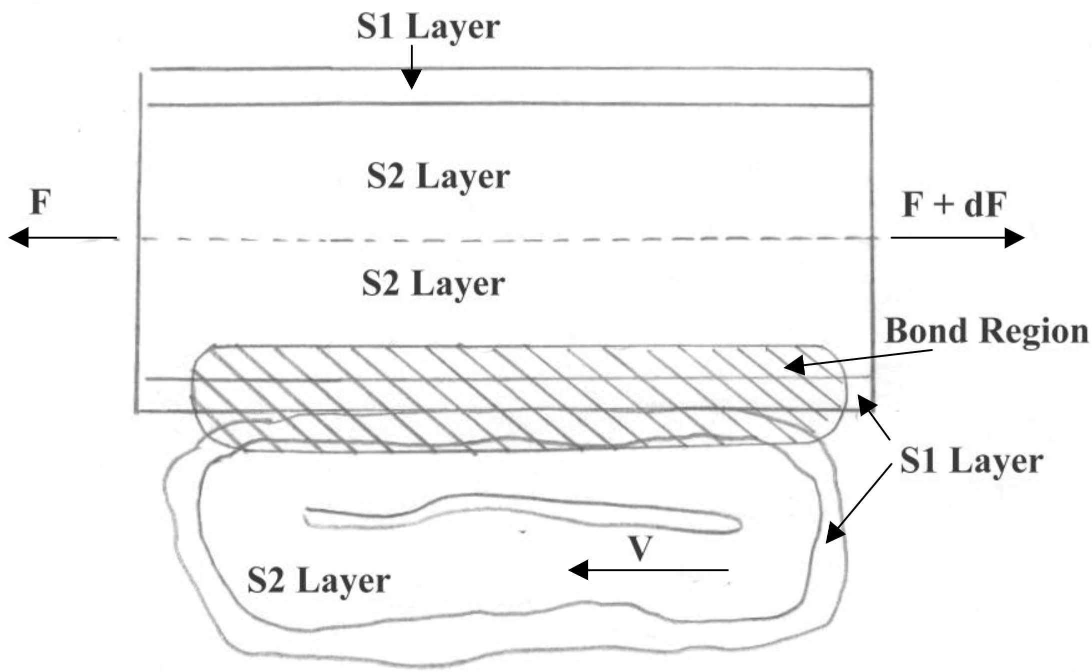

Figure 1.4 Fiber-to-fiber bond. Although the bond could be formed between S1-S1 layer, S1-S2 layer, and S2-S2 layer, it was assumed in this work that the bonds are mainly S1-S1 layer bonds (Ramasubramanian and Perkins, 1988).

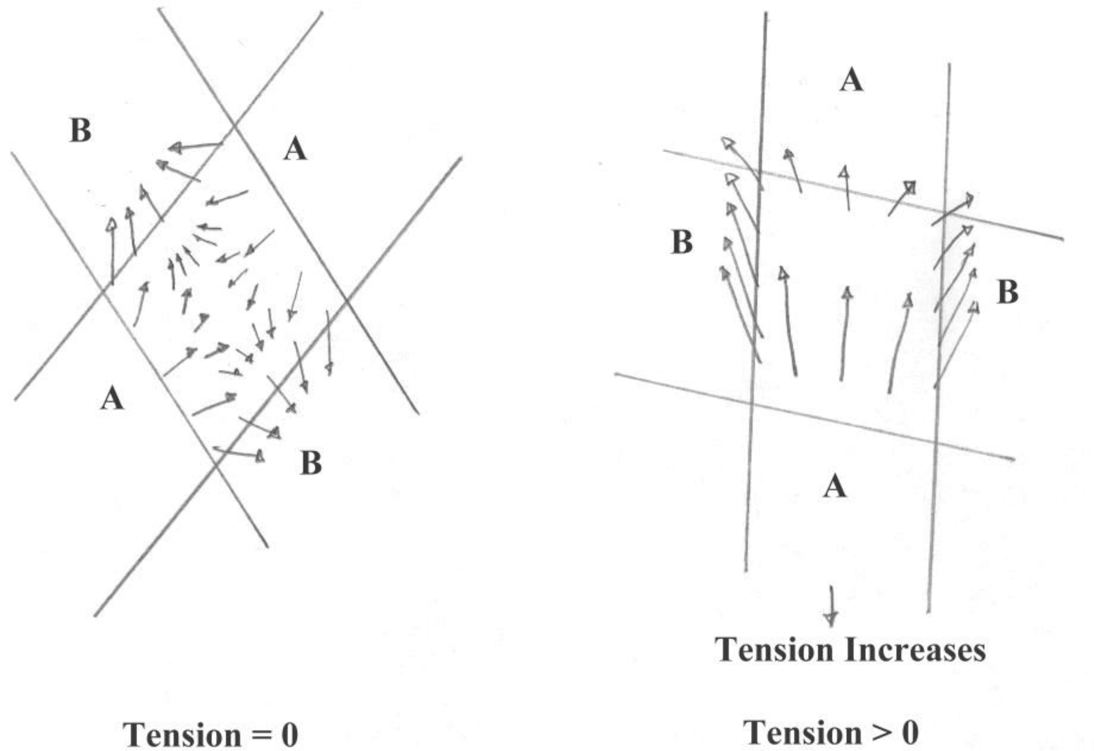

Figure 1.5 The state of stress at a fiber-to-fiber bond site (Van Den Akker, 1962).

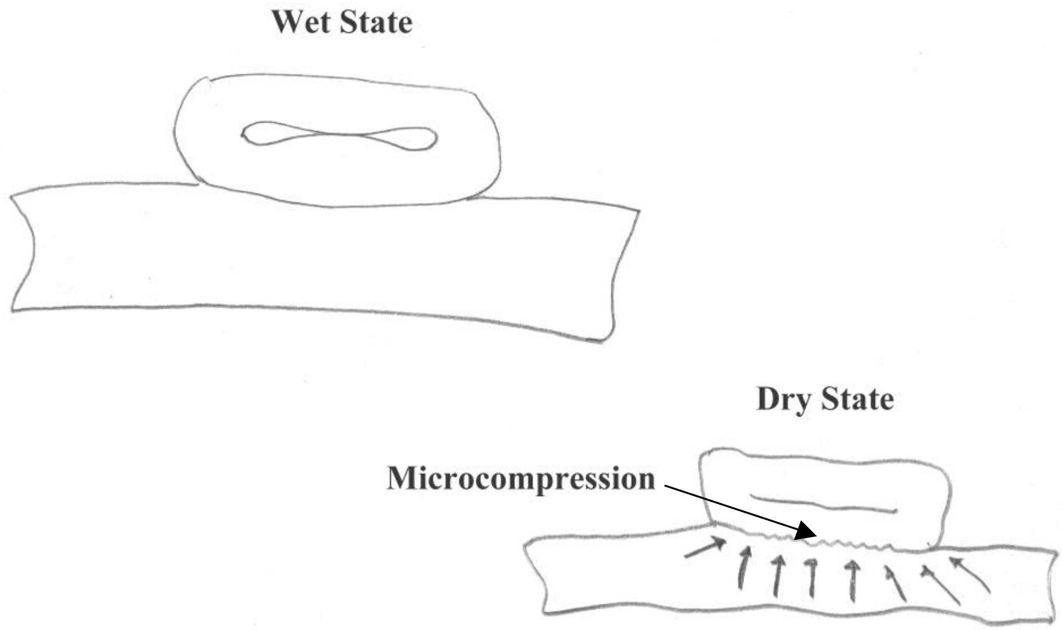

Figure 1.6 Microcompressions form when the swollen fiber contracts in the lateral direction (Giertz, 1979).

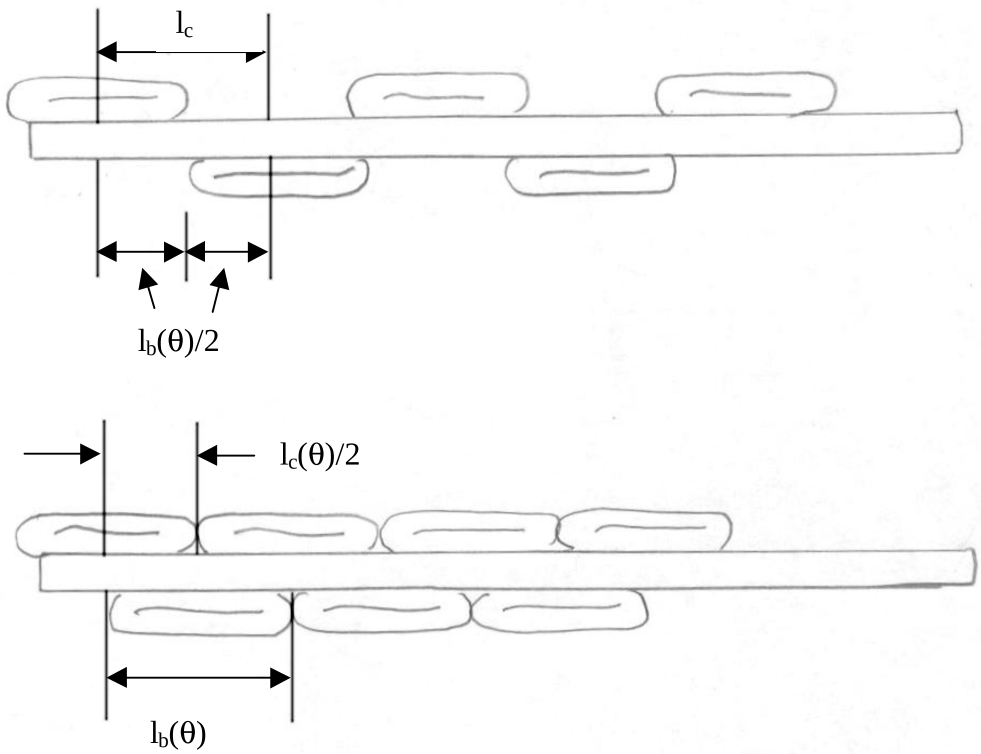

Figure 1.7 Relative bonded area where l/l_b = 1 in the top diagram and l/l_b = ½ in the bottom diagram (Perkins, 1990).

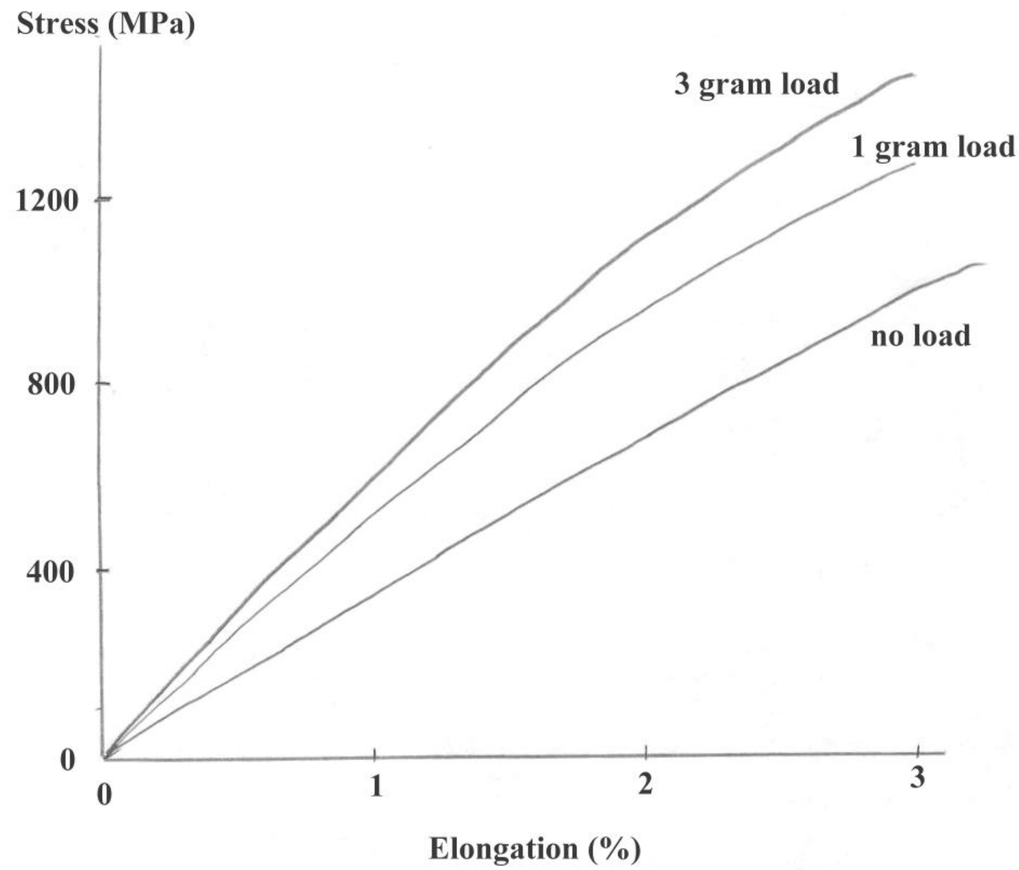

Figure 1.8 Summerwood fibers of long leaf pine holocellulose experienced increased fiber strength when subjected to axial restraint during drying (Jentzen, 1964).

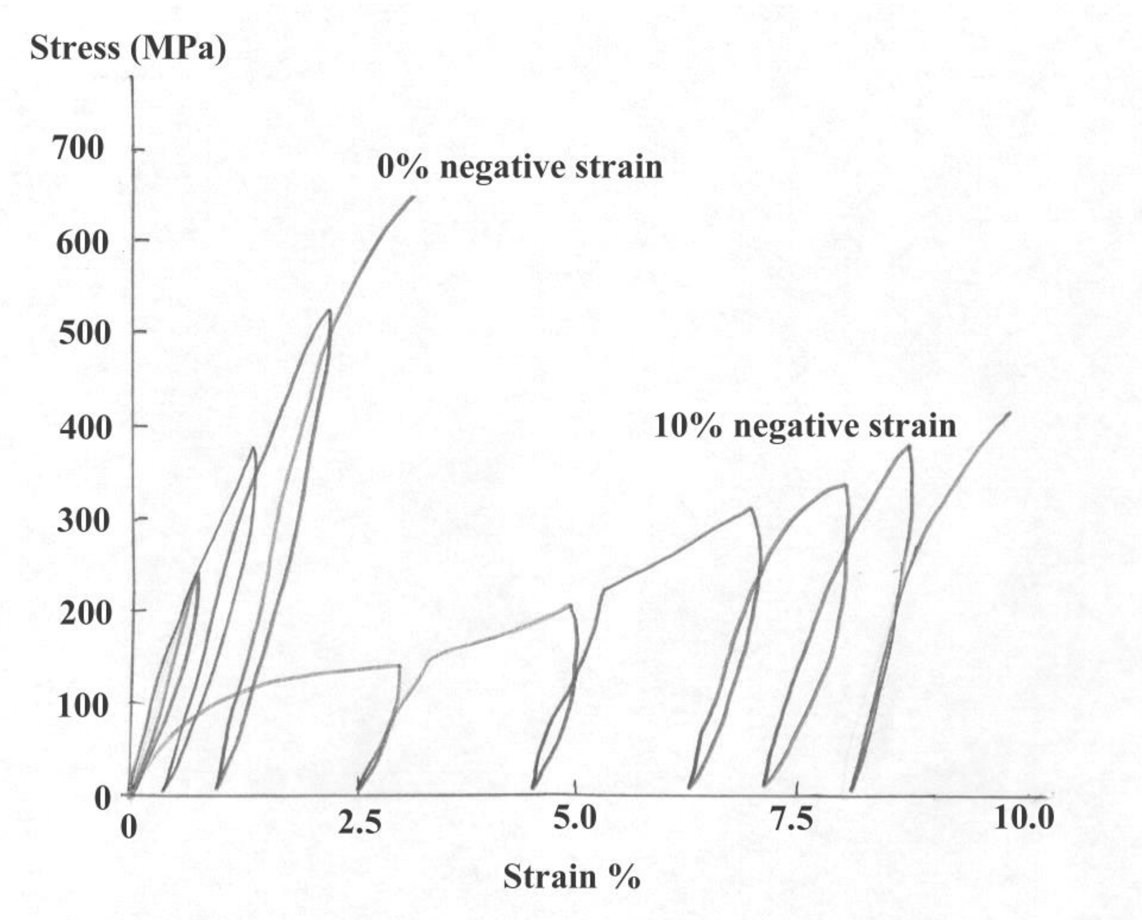

Figure 1.9 The fiber strength decreased while the breaking strain increased when long-leaf pine fibers are dried under compression (Dumbleton, 1972).

2. Constitutive Models of Paper Material

In addition to the understanding of the many factors, which affect the constitutive behavior of paper material, a study of the current models for paper material is also essential. This is so that one could appreciate the merits and beware of the deficiencies of contemporary models in comparison with one another. In the continuum models, the general approach is to treat paper or paperboard as a continuum of cell wall materials. The experimentally determined properties of the sheet are applied in finite element analysis or other general two- or three-dimensional constitutive models, such as the hyperelastic plate model, composite laminate plate model, and mosaic model, to predict the constitutive behavior of paper subjected to various loading conditions.

Although the continuum approach is relatively easy to apply, it is more suitable for high-density paper material since its structure resembles more of a continuum of cell wall material. At low density, the network structure is more apparent. The difference between high- and low-density sheets lies in their relationship with the sheet grammage. The sheet density, given by the division of grammage by the sheet thickness, varies with grammage at low densities ($\rho_s < 450$ kg/m^3) and is independent of grammage at high densities ($\rho_s > 750$ kg/m^3). Since the continuum models do not explicitly address the factors that affect the constitutive behavior, the models also do not provide any explanation to the orthotropic nature of paper material.

In the network models, the constitutive behavior of paper material is derived from the properties and deformation of an elementary load-bearing unit in the fiber network. Therefore, this requires the knowledge of the mechanical properties of the load-bearing unit and its deformation behaviors when the sheet is subjected to applied loads. For example, in the micromechanics approach, one would determine the average fiber stress for a given fiber orientation. The sheet stress, e.g. σ_x, is then obtained from the integral sum of the appropriate fiber stress components, i.e. the x-component of σ_f, of all fiber orientations in the sheet. In this chapter, two micromechanics models, i.e. the full plasticity model and the asymptotic fiber and bond model, will be discussed.

2.1 Continuum Models

Mann et al. (1980) and Baum et al. (1981) determined the orthotropic elastic properties of several paper materials, such as linerboard and carton stock, using the ultrasonic technique. These experimentally determined sheet properties were subsequently utilized by Carlsson et al. (1982) in their finite element analysis of the three-dimensional stress field of a paperboard subjected to bending. Similar approach, i.e. the application of experimentally determined macroscopic properties in finite element analysis, was also used by Muthuraman (1998) to examine the papercup brim forming process. In these works, only the elastic behavior of the sheet was examined. For modeling the nonlinear behavior of paper material beyond its linear elastic regime, a hyperelastic plate model of Suhling et al. (1989) can be used.

2.1.1 Hyperelastic Plate Model

Suhling et al(1989) modeled paper as a hyperelastic material. For small displacement gradient and plane stress condition, the sheet stress σ_{ij} was reduced to the derivative of the strain energy density function W, with respect to the sheet strains ε_{ij} (cf. equation 2.1), where i,j = x,y.

$$\sigma_{ij} = \frac{\partial W}{\partial \varepsilon_{ij}} \qquad \textbf{(2.1)}$$

Following Johnson and Urbanik (1984), the strain energy function of the sheet has to be determined empirically for a given paper material. A hyperbolic tangent function (cf. equation 2.2) was used to describe the stress-strain behavior of a sheet subjected to uniaxial loading. The function was fitted to experimental data of sample subjected to uniaxial load in the machine and cross-machine direction, resulting in two stress-strain functions. These two functions were then integrated to obtain two strain energy density functions, W_{MD} and W_{CD}.

$$\sigma(\varepsilon) = c_1 \tanh(c_2 \varepsilon) + c_3 \varepsilon \qquad \textbf{(2.2)}$$

A single strain energy density function that could be used with equation 2.1 to obtain the stress function $\sigma(\varepsilon)$ (cf. equation 2.2) for samples subjected to uniaxial loading in any directions was desired. Therefore, a general function W was generated from the W_{MD} and

W_{CD} using the cubic spline interpolation such that the errors in the model prediction for the MD and CD stress-strain curve were balanced when compared to experimental data. The resulting W function is then used with equation 2.1 to predict the stress-strain behavior of sampled loaded in different directions. The loading direction was increased in 10° increments from the machine to the cross-machine direction. The model prediction showed relatively good agreement with the experimental data. The orthotropic behavior of paper material is affected primarily by the application of drying restraints and fiber orientation distribution (cf. 1.3). Since the model is semi-empirical and does not address these two factors, the model could not accommodate changes in the constitutive behavior due to drying restraints and fiber orientation distribution. Therefore, for the same paper material, changes in these two factors due to papermaking process would require another curve-fitting process to determine another strain energy density function for the same paper material. One continuum model, which attempts to address the directional dependence of the constitutive behavior on fiber orientation distribution, is the composite laminate plate model.

2.1.2 Composite Laminate Plate Model

In the composite laminate plate model, Salmén et al. (1984) applied the classical laminate plate theory on paper and treated it as a composite layers of cell wall material. Each layer contains a hemicellulose matrix embedded with unidirectional cellulose microfibrils. The actual microfibrils orientation distribution was matched by appropriately varying the orientation angles of the microfibrils of each lamina in the model. It was assumed that the layers in the laminate are subjected to plane stress and bonded perfectly together. In addition, there is no inter-laminar shear deformation. The strain components are also assumed to be linear functions of the thickness coordinate. The constitutive relation of the laminate is then derived using the Kirchhoff plate theory. The general relations for force and moment of the plate are given by equation 2.3.

$$\left[\frac{N}{M}\right] = \left[\begin{array}{c|c} A & B \\ \hline B & D \end{array}\right]\left[\frac{\varepsilon}{k}\right] \qquad \textbf{(2.3)}$$

where [N] = force applied on plate,

[M] = moment applied on plate,

[ε] = mid-plane strains,

[k] = mid-plane curvature,

[A] = reduced stiffness matrix,

[B] = coupling stiffness matrix,

[D] = bending stiffness matrix.

The components of [A], [B], and [D] are related to the transformed reduced stiffness of the laminas and the distances of the laminas from the mid-plane. The values of the components in each matrix also depend on the number of layers in the laminate, the thickness of the laminate, and the stacking sequence of the laminae. For example, when the laminate is symmetric in geometry and material properties with respect to the mid-plane, B_{ij}, A_{16}, A_{26}, D_{16}, and D_{26} become zero. The constitutive behavior of the laminate could be solved for, if the transformed reduced stiffness of each layer is known. For lamina whose orthotropic axes are not aligned with those of the laminate, the transformed reduced stiffness is obtained using the transformation matrix.

$$A_{ij} = \sum_{k=1}^{n} \left(Q'_{ij}\right)_k \left(z_k - z_{k-1}\right) \tag{2.4}$$

$$B_{ij} = \frac{1}{2} \sum_{k=1}^{n} \left(Q'_{ij}\right)_k \left(z_k^2 - z_{k-1}^2\right) \tag{2.5}$$

$$D_{ij} = \frac{1}{3} \sum_{k=1}^{n} \left(Q'_{ij}\right)_k \left(z_k^3 - z_{k-1}^3\right) \tag{2.6}$$

where N = number of laminas

(Q'_{ij}) = transformed reduced stiffness of layer k and

z_k = distance of layer k from the mid-plane.

The elastic properties used to obtain the reduced stiffness matrix of each layer are derived from the material properties of the cell wall. Salmén et al. (1984) utilized the

Halpin-Tsai equations for material containing transversely isotropic continuous reinforcement to determine the lamina properties from the cell wall properties (cf. equation 2.7 – 2.10).

$$E_x = E_{x,f} V_f + E_m V_m \qquad \textbf{(2.7)}$$

$$E_y = E_m \left(1 + 2\eta_E V_f\right) / \left(1 - \eta_E V_f\right) \qquad \textbf{(2.8)}$$

$$G_{xy} = G_m \left(1 + \eta_G V_f\right) / \left(1 - \eta_G V_f\right) \qquad \textbf{(2.9)}$$

$$\nu_{xy} = \nu_{xy,f} V_f + \nu_m V_m \qquad \textbf{(2.10)}$$

where	η_E	=	$(E_{y,f}/E_m - 1)/ (E_{y,f}/E_m + 2)$
	η_G	=	$(G_{xy,f}/G_m - 1)/ (G_{xy,f}/G_m + 1)$
	$E_{x,f}$	=	the axial modulus of the microfibrils
	$E_{y,f}$	=	the transverse modulus of microfibrils
	$G_{xy,f}$	=	the shear modulus of the microfibrils
	E_m, G_m	=	the elastic and shear modulus of the hemicellulose matrix,
	$\nu_{xy,f}$, $\nu_{xy,m}$	=	the Poisson's ratios of the microfibrils and hemicellulose,
	V_f, V_m	=	volume fraction of the microfibrils and hemicellulose.

These lamina properties are then used to determine the reduced stiffness coefficients and allow the modeling of the laminate behavior using equation 2.1. In addition to the microfibrils orientation, this model also addresses the effects of moisture expansion by adding a hygroscopic force [F] (cf. equation 2.11) to [N] in equation 2.1.

$$F_i = \Delta M \sum_{k=1}^{n} \left(Q'_{ij}\right)_k \left(\beta'_j\right)_k h_k \qquad \textbf{(2.11)}$$

where	β'	=	transformed coefficient of moisture expansion
	h	=	lamina thickness
	ΔM	=	moisture content

Salmén et al.(1984) tested the model using papers made from commercial bleached sulphate pulp. For an isotropic sheet, the elastic modulus agree well with experimental data up until about 80% RH. However, for anisotropic papers, even at low moisture content, the model over-predicted the elastic modulus in the longitudinal direction, i.e. E_x, and under-estimated the elastic modulus in the transverse direction, i.e. E_y. Salmén et al. attributed the discrepancy at high moisture content to the break down of fiber-to-fiber bond and the microfibrils, which were not addressed in the model. Subramanian and Carlsson (1994) attributed the over-estimation of the elastic modulus to the exclusion of voids from the model and this was later taken into account in their modeling work using the mosaic model.

2.1.3 Mosaic Model

In Subramanian and Carlsson (1994), the composite laminate plate model was used in conjunction with finite element analysis, to model paper material as a continuum with inclusion of cylindrical voids. The analysis was conducted for various volume fraction of voids. From the results of their finite element analysis work, Subramanian and Carlsson developed an expression to relate the elastic modulus to the volume fraction of voids (cf. equation 2.12).

$$y = 1 + a_1 x + a_2 x^2 + a_3 x^3 \qquad \textbf{(2.12)}$$

where a_1, a_2, a_3 = coefficients from linear regression

y = $E_x/E_{x,\text{ no voids}}$, $E_y/E_{y,\text{ no voids}}$, or $G_{xy}/G_{xy,\text{ no voids}}$

x = volume fraction of voids

Next, using finite element analysis again, Lu et al. (1995) and Lu and Carlsson (1996) modeled paper as a sheet of continuum containing free fiber segments and fiber-to-fiber bond, with no voids. The volume fraction of fiber-to-fiber bonds and free fiber segments were determined using Monte Carlo simulation. In this simulation, the fiber-to-fiber bonds have the higher volume fraction. Therefore, in the finite element analysis, the continuum was modeled as a matrix of fiber-to-fiber bonds, whereas the free fiber segments were modeled as uniformly distributed cylindrical inclusions embedded in the matrix. This is the mosaic approach. The composite laminate plate theory was used to derive the mechanical properties of the fiber-to-fiber bond. In the composite laminate model, the layers of cell wall material were connected to one another in a parallel arrangement. The free fiber segments on the other hand was treated as pieces of cell wall material arranged in series. The arrangement of the free fiber segments and fiber-to-fiber bonds are analogous to springs in series and parallel arrangements. Therefore, although the fiber-to-fiber bonds and free fiber segments are made of the same cell wall material, their elastic properties would differ due to the different arrangements of their cell wall elements. Consequently, the free fiber segments would experience uniform stress, whereas the fiber-to-fiber bonds would experience uniform strain. The two set of elastic properties, one for the fiber-to-fiber bond and one for the free fiber segment, were then used to model a sheet of 500 kg/m^3. The results obtained for E_x, E_y, G_{xy}, and ν_{xy} are then adjusted for the volume void fraction using the expression developed by Subramanian and Carlsson (1994) (cf. equation 2.12).

The finite element simulation was carried out for several materials over a range of relative humidity (0% to 12% R.H.). One of the materials simulated was paper made with bleached chemical pulp. For low and high-anisotropy papers, although the correct trends were obtained, the elastic modulus predicted was greater than the experimental data. The same problem is observed when the mosaic model is applied on paper made of groundwood pulp. This time, the moisture content was fixed at 50% R.H., whereas the densities were varied from ~350 to ~500 kg/m^3. For linerboard, the model again over-predicted the elastic modulus (E_x and E_y). For the shear modulus, the experimental values are in closer agreement with the upper bound solution at low moisture content. Nevertheless, the predicted value for the shear modulus becomes closer to the model prediction as the moisture content increases.

Lu et al. (1996) pointed out that the mosaic model might not work well for low-density sheet because at low densities, paper resembles less like a continuum and the network structure would be a more appropriate depiction of the paper structure. However, the model results for high-density sheet, i.e. paper made from bleached chemical pulp and linerboard, showed that this continuum approach with adjustment for volume fraction of void still led to over-prediction of the elastic properties of the sheet.

2.2 Micromechanics Models

2.2.1 Full Plasticity Model

In micromechanics models by Perkins et al. (24-29), paper is treated as a fiber network consists of fiber-to-fiber bonds, free fiber segments, and voids. The load applied onto the sheet is distributed through the network at the fiber-to-fiber bond sites. Therefore, in micromechanics model, the fiber at a bond site serves as a representative load-bearing unit and is used to derive the fiber stress. In the full plasticity micromechanics model by Perkins et al. (1991), the end effects of fibers are taken into consideration. The fiber ends have zero axial fiber strain which increases to a maximum value at the center due to shear lag mechanism. Therefore, a gradual transition of fiber or bond from elastic to plastic state could occur along the fiber length as the applied strains increase. L_f and L_b (cf. Figure 2.1) denote the boundaries at which these transitions occur in a fiber of half-length L. When $\xi < L_f$, fiber is visco-plastic, and it is elastic when $\xi > L_f$. When $\xi > L_b$, bond is viscoplastic, and it is elastic when $\xi < L_b$. Therefore, in zone 1, fiber is plastic while bond is elastic. In zone 2, both fiber and bond are elastic. In zone 3, fiber is elastic while bond is plastic. The equations from which the values for L_f and L_b are solved are transcendental and have to be solved numerically. Once the boundaries have been determined, the fiber stress in each zone is then calculated from which the sheet stress could be subsequently found.

2.2.2 Asymptotic Fiber and Bond Model

The approach in the asymptotic fiber and bond model is similar to the approach in the full plasticity model, except that the fiber and bond condition is assumed to be constant throughout the fiber length (Sinha, 1994). When the corresponding critical strain has been reached, the fiber or bond along the entire fiber length is considered to have yielded. Thus, the end effect and shear lag mechanism is not addressed. The simplified model reduced considerably the amount of numerical calculation required without compromising the quality of the results. In the past, the asymptotic fiber and bond model has only been applied on the loading process of sheet in one- and two-dimensional problems (Sinha, 1994). A similar approach will be used in this work as well and further extended to include the unloading process of paper in one- and two-dimensional problem. The asymptotic fiber and bond model by Sinha (1994) is presented in this chapter while the extension to include the unloading process is discussed in Chapter 3.

Since the model parameters in micromechanics involve properties of the microconstituents that are difficult to measured experimentally without sophisticated experimental setup, curve-fitting the model to experimental data of macroscopic stress-strain curves provide an alternative solution. Therefore, many of the factors, which affect the sheet stress-strain behavior (cf. 1.2, 1.3, and 1.4), are not explicitly addressed in this model, other than the fiber orientation distribution, moisture content at time of drying, and drying restraint strains. These three factors all contribute to the directional dependence of the sheet mechanical properties.

2.2.2.1 Constitutive Behavior of Fiber, Bond, and Sheet

Paper material behaves linear elastically at the beginning and becomes nonlinear beyond the yield point. In the asymptotic fiber and bond model, the nonlinear sheet behavior is triggered by the yielding of the fiber or bond in the network. Therefore, a two-slope model is used to model the constitutive behavior of fiber and bond.

The constitutive behavior of cellulosic material is dependent on the rate of loading and environmental conditions such as moisture content. In micromechanics model, the constitutive behavior of fiber and bond subjected to constant loading rate is approximated with a two-slope model (cf. Figure 2.4 and Figure 2.5). In this two-slope model, the elastic modulus of fiber is the same in tension and compression. In order to address localized failure, such as fiber buckling, the compressive strength and tangent modulus (second slope) of the fiber cell wall material would be smaller than their respective tensile counterparts. The constitutive model of fiber in tension would then be given by

$$\sigma_f = E_f \varepsilon_f \qquad \sigma_{\mathrm{f}} < \sigma_{pt} \qquad (2.13)$$

$$\sigma_f = \sigma_{pt} + E_{2t}\left(\varepsilon_f - \varepsilon_{pt}\right) \qquad \sigma_{\mathrm{f}} \geq \sigma_{pt} \qquad (2.14)$$

and fiber in compressive is described by

$$\sigma_f = E_f \varepsilon_f \qquad |\sigma_f| < |\sigma_{pc}| \qquad (2.15)$$

$$\sigma_f = \sigma_{pc} + E_{2c}\left(\varepsilon_f - \varepsilon_{pc}\right) \qquad |\sigma_f| \geq |\sigma_{pt}| \qquad (2.16)$$

where σ_f = fiber stress

ε_f = fiber strain

E_f = fiber elastic modulus

E_{2t} = fiber tangent modulus (second slope) in tension

E_{2c} = fiber tangent modulus (second slope) in compression

σ_{pt} = fiber yield stress in tension

σ_{pc} = fiber yield stress in compression

ε_{pt} = fiber yield strain in tension

ε_{pc} = fiber yield strain in compression

The same two-slope model is also applied on the bond. Therefore,

$$\tau_b = G_b \gamma_b \qquad |\tau_b| < |\tau_p| \qquad (2.17)$$

$$\tau_b = \tau_p + G_2\left(\gamma - \gamma_p\right) \qquad |\tau_b| \geq |\tau_p| \qquad (2.18)$$

where τ_b = bond shear stress

γ_b = bond shear strain

G_b = bond shear elastic modulus

G_2 = bond tangent modulus (second slope)

τ_p = bond yield stress

γ_p = bond yield strain

2.2.2.2 Critical Yield Strains in Asymptotic Fiber and Bond Model

In asymptotic fiber and bond model, as the applied strains increase the deformation of fiber and bond could progress in two possible scenarios (cf. Figure 2.3). In case I, bond would yield first, whereas in case II, fiber would yield first. In subsequent sections, the critical strains associated with the fiber and bond conditions in the two cases would be determined. Suppose ε_{cf} is the critical strain of fiber yielding first, whereas ε_{cb}

is the critical strain for bond to yield first. For case I to happen, ε_{cb} has to be less than ε_{cf}. Vice versa, for fiber to yield first, ε_{cf} has to be less than ε_{cb}.

In case I, when the macroscopic sheet strain along the mesoelement axial direction ε_s (cf. equation 2.19), is less than ε_{cb}, both fiber and bond are elastic. When ε_s exceeded ε_{cb}, bond would yield first while fiber remains elastic. When ε_s exceed ε_{bf}, fiber would yield too. Therefore, fiber and bond are now both plastic. In case II, when the local mesoelement strain ε_s, is less than ε_{cf}, both fiber and bond would remain elastic. When ε_s exceeded ε_{cf}, fiber would yield first while bond remains elastic. When ε_s exceed ε_{fb}, bond would yield too. Again, fiber and bond are now both plastic. The derivation of these critical strain ε_{cb}, ε_{cf}, ε_{bf}, and ε_{fb} are shown in subsequent sections.

$$\varepsilon_s = \varepsilon_x \cos^2\theta + \varepsilon_x \sin^2\theta + 2\varepsilon_{xy}\cos\theta\sin\theta \tag{2.19}$$

Elastic Fiber and Bond

When the mesoelement (cf. Figure 2.2) is in equilibrium, equation 2.20 could be obtained from force balance. While the fiber and bond are elastic, they are governed by equation 2.21 and equation 2.22 respectively. Using these constitutive equations and the strain-displacement relation (cf. equation 2.23) with the equilibrium equation, one could solve for fiber displacement and fiber strain (cf. equation 2.24 and equation 2.25).

$$\frac{d}{d\xi}\left(A_f\sigma_f\right) + \tau_b w_e = 0 \tag{2.20}$$

$$\sigma_f = E_f\left(\varepsilon_f - \alpha_f m\right) \tag{2.21}$$

$$\tau_b = G_b\gamma = G_b\left(\frac{u_s - u_f}{t_b}\right) \tag{2.22}$$

$$\varepsilon_f = \frac{d}{d\xi}u_f \tag{2.23}$$

$$u_f = \varepsilon_s\left(\xi - \frac{\sinh(a\xi)}{a\cosh(aL)}\right) \tag{2.24}$$

$$\varepsilon_f = \varepsilon_s \left(1 - \frac{\cosh(a\xi)}{\cosh(aL)}\right) \qquad \textbf{(2.25)}$$

$$a = \frac{G_b w_e}{E_f A_f t_b} \qquad \textbf{(2.26)}$$

where A_f = fiber cross sectional area

w_e = effective width of the fiber (cf. Sinha (1994))

α_f = coefficient of swelling and shrinkage of fiber material

m = moisture content

t_b = bond thickness

u_s = macroscopic sheet displacement along the mesoelement axial direction

u_f = fiber displacement along the mesoelement direction

After deriving the fiber strain, the bond shear stress is now determined from equation 2.20. The bond shear stress for elastic fiber and bond would be governed by equation 2.27.

$$\tau_b = \frac{A_f E_f \varepsilon_s a}{w_e} \frac{\sinh(a\xi)}{\cosh(aL)} \qquad \textbf{(2.27)}$$

Suppose the bond is going to yield first. When the critical ε_s is reached, τ_b would be equal to τ_p. Therefore, τ_p is substituted into equation 2.27. After some rearrangement and the substitution of ξ=L yield the expression for ε_{cb} in equation 2.28. The value of ξ is chosen such that the lowest critical value would be obtained.

$$\varepsilon_{cb} = \frac{\tau_p w_e}{A_f E_f a} \frac{1}{\tanh(aL)} \qquad \textbf{(2.28)}$$

Consider now the scenario where fiber is the first to yield. When fiber reaches its yield point, the fiber strain ε_f is equal to ε_p. Substitute ε_p and $\xi=0$ into equation 2.25 yields the expression for ε_{cf} below.

$$\varepsilon_{cf} = \frac{\varepsilon_p}{\left(1 - \frac{1}{\cosh(aL)}\right)} \qquad \textbf{(2.29)}$$

Elastic Fiber and Plastic Bond

When ε_{cf} is greater than ε_{cb}, the bond would yield first. While the fiber remains elastic and the bond is plastic, their constitutive equations for fiber and bond would now be given by equation 2.21 and equation 2.30 respectively. As the load continues to increase and ε_s reaches ε_{bf}, fibers would eventually yield.

$$\sigma_f = E_f\left(\varepsilon_f - \alpha_f m\right) \qquad \textbf{(2.21)}$$

$$\tau_b = \tau_p + G_2\left(\gamma - \gamma_p\right) \qquad \textbf{(2.30)}$$

The incremental change in fiber strain beyond bond yielding would now be determined. The equilibrium equation for incremental change in fiber stress and bond shear stress is given by equation 2.31. The incremental change in fiber stress and bond shear stress beyond ε_{cb} would be governed by equation 2.32 and equation 2.33 respectively.

$$\frac{d}{d\xi}\left(A_f \Delta\sigma_f\right) + \Delta\tau_b w_e = 0 \qquad \textbf{(2.31)}$$

$$\Delta\sigma_f = E_f\left(\Delta\varepsilon_f - \alpha_f \Delta M\right) \qquad \textbf{(2.32)}$$

$$\Delta\tau_b = G_2\left(\frac{\Delta u_s - \Delta u_f}{t_b}\right) \qquad \textbf{(2.33)}$$

Solving the incremental equilibrium equation yields the incremental fiber displacement and incremental fiber strain beyond ε_{cb} in equation 2.34 and equation 2.35.

$$\Delta u_f = \Delta\varepsilon_s\left(\xi - \frac{\sinh(a_b\xi)}{a_b\cosh(a_bL)}\right) \tag{2.34}$$

$$\Delta\varepsilon_f = \Delta\varepsilon_s\left(1 - \frac{\cosh(a_b\xi)}{\cosh(a_bL)}\right) \tag{2.35}$$

$$a_b = \frac{G_2 w_e}{E_f A_f t_b} \tag{2.36}$$

$$\Delta\varepsilon_s = \varepsilon_s - \varepsilon_{cb} \tag{2.37}$$

The total fiber strain is then given by equation 2.38 and solving for ε_s gives equation 2.27. The second term on the right-hand side in equation 2.39 is negligible and hence dropped. When fiber reaches its yield point, $\varepsilon_f = \varepsilon_p$ and substituting in $\xi=0$ gives the ε_{bf} in equation 2.40.

$$\varepsilon_f = \varepsilon_{cb}\left(1 - \frac{\cosh(a\xi)}{\cosh(aL)}\right) + (\varepsilon_s - \varepsilon_{cb})\left(1 - \frac{\cosh(a_b\xi)}{\cosh(a_bL)}\right) \tag{2.38}$$

$$\varepsilon_s = \frac{\varepsilon_f}{1 - \frac{\cosh(a_b\xi)}{\cosh(a_bL)}} + \varepsilon_{cb}\left[1 - \frac{1 - \frac{\cosh(a\xi)}{\cosh(aL)}}{1 - \frac{\cosh(a_b\xi)}{\cosh(a_bL)}}\right] \tag{2.39}$$

$$\varepsilon_{bf} = \frac{\varepsilon_f}{1 - \frac{1}{\cosh(a_bL)}} \tag{2.40}$$

Plastic Fiber and Elastic Bond

Consider now the opposite scenario where ε_{cb} is greater than ε_{cf} and fiber has yielded. Fiber and bond stresses are now governed by equation 2.41 and equation 2.22 respectively.

$$\sigma_f = \sigma_p + E_2\left(\Delta\varepsilon_f - \alpha_f \Delta M\right) \quad \textbf{(2.41)}$$

$$\tau_b = G_b \gamma = G_b\left(\frac{u_s - u_f}{t_b}\right) \quad \textbf{(2.22)}$$

Repeating the previous steps yields

$$\Delta\sigma_f = E_f\left(\Delta\varepsilon_f - \alpha_f \Delta M\right) \quad \textbf{(2.42)}$$

$$\Delta\tau_b = G_b \Delta\gamma = G_b\left(\frac{\Delta u_s - \Delta u_f}{t_b}\right) \quad \textbf{(2.43)}$$

$$\Delta u_f = \Delta\varepsilon_s\left(\xi - \frac{\sinh(a_f \xi)}{a_f \cosh(a_f L)}\right) \quad \textbf{(2.44)}$$

$$\Delta\varepsilon_f = \Delta\varepsilon_s\left(1 - \frac{\cosh(a_f \xi)}{\cosh(a_f L)}\right) \quad \textbf{(2.45)}$$

$$a_f = \frac{G_b w_e}{E_2 A_f t_b} \quad \textbf{(2.46)}$$

$$\Delta\varepsilon_s = \varepsilon_s - \varepsilon_{cf} \quad \textbf{(2.47)}$$

The total fiber strain is then given by equation 2.48. The fiber yield strain ε_p from equation 2.29 is substituted into equation 2.48 to get equation 2.49.

$$\varepsilon_f = \varepsilon_p + \left(\varepsilon_p - \varepsilon_{cf}\right)\left(1 - \frac{\cosh(a_f \xi)}{\cosh(a_f L)}\right) \quad \textbf{(2.48)}$$

$$\varepsilon_f = \varepsilon_{cf}\left(1 - \frac{\cosh(a\xi)}{\cosh(aL)}\right) + \left(\varepsilon_s - \varepsilon_{cf}\right)\left(1 - \frac{\cosh(a_f \xi)}{\cosh(a_f L)}\right) \quad \textbf{(2.49)}$$

Then, the fiber strain is used with equation 2.20 to determine the bond shear stress given by equation 2.50. The equation is rearranged to solve for ε_s, which is given in equation 2.51.

$$\tau_b = -\frac{A_f}{w_e}\left[E_f \varepsilon_{cf} \sinh(a\xi)\right]\frac{a}{\cosh(aL)} - (\varepsilon_s - \varepsilon_{cf})\sinh(a_f \xi)\frac{a_f}{\cosh(a_f L)}E_2 \qquad \textbf{(2.50)}$$

$$\varepsilon_s = \varepsilon_{cf} + \frac{w_e \tau_b - E_f A_f a \varepsilon_{cf} \dfrac{\sinh(a\xi)}{\cosh(aL)}}{E_2 A_f a_f \dfrac{\sinh(a_f \xi)}{\cosh(a_f L)}} \qquad \textbf{(2.51)}$$

When the bond reaches its yield point, $\tau_b = \tau_p$ and substitute $\xi = L$ into equation 2.51 gives ε_{fb} in equation 2.52.

$$\varepsilon_{fb} = \varepsilon_{cf} - \frac{\tau_p w_e - E_f A_f a \varepsilon_{cf} \tanh(aL)}{E_2 A_f a_f \tanh(a_f L)} \qquad \textbf{(2.52)}$$

2.2.2.3 Average Fiber Stress in Asymptotic Fiber and Bond Model

The fiber stress expression for each state derived in Section 2.2.2.2 is also used to determine the average fiber stress for each fiber and bond condition (cf. equation 2.53).

$$\overline{\sigma}_f = \frac{1}{L}\int_0^L \sigma_f \, d\xi \qquad \textbf{(2.53)}$$

The average fiber stress expressions for each possible fiber and bond condition are listed in Table 2.1and Table 2.2. The average incremental fiber stress expressions for similar conditions are also listed in Table 2.3 and Table 2.4). Detailed derivation of these expressions would not be repeated here. Instead interested reader should refer to Sinha (1994). The sheet stresses are then given by

$$\sigma_x = \frac{\rho_s}{\rho_f}\int_{-\pi/2}^{\pi/2} \overline{\sigma}(\theta)\cos^2\theta \;\; f(\theta) \;\; d\theta \qquad \textbf{(2.54)}$$

$$\sigma_y = \frac{\rho_s}{\rho_f}\int_{-\pi/2}^{\pi/2} \overline{\sigma}(\theta)\sin^2\theta \;\; f(\theta) \;\; d\theta \qquad \textbf{(2.55)}$$

where $f(\theta)$ = probability density function of fiber orientation

θ = fiber orientation

ρ_s = sheet density

ρ_f = fiber density

When applied on one-dimensional problem such as uniaxial tensile test, ε_s reduced to equation 2.56. For a given ε_x, the lateral contraction ratio ν_{xy}, is solved numerically using the false-position method until the boundary condition of $\sigma_y = 0$ is met. Equation 2.43 is evaluated numerically using the multiple-application Simpson's 1/3 rule. When ν_{xy} has been found, σ_x could then be evaluated.

$$\varepsilon_s = \varepsilon_x \left(\cos^2\theta - \nu_{xy_x} \sin^2\theta \right) \qquad \textbf{(2.56)}$$

For application of the model in more complicated geometric and loading condition, Sinha and Perkins (1995) utilized a combined continuum and micromechanics approach to formulate the elemental equation for finite element analysis application.

Table 2.1 Average fiber stress expressions for $\varepsilon_{cb} < \varepsilon_{cf}$.

Fiber and Bond Condition	Average Fiber Stress Expression
$\varepsilon_s \leq \varepsilon_{cb}$ (fiber and bond are elastic)	$\bar{\sigma} = E_f \varepsilon_s \left(1 - \frac{\tanh aL}{aL}\right)$
$\varepsilon_{cb} < \varepsilon_s \leq \varepsilon_{bf}$ (fiber is elastic and bond is plastic)	$\bar{\sigma} = E_f \varepsilon_{cb} \left(1 - \frac{\tanh aL}{aL}\right) + E_f\left(\varepsilon_s - \varepsilon_{cb}\right)\left(1 - \frac{\tanh a_b L}{a_b L}\right)$
$\varepsilon_{bf} < \varepsilon_s$ (fiber and bond are plastic)	$\bar{\sigma} = E_f \varepsilon_{cb} \left(1 - \frac{\tanh aL}{aL}\right) + E_f\left(\varepsilon_{bf} - \varepsilon_{cb}\right)\left(1 - \frac{\tanh a_b L}{a_b L}\right) + E_2\left(\varepsilon_s - \varepsilon_{bf}\right)\left(1 - \frac{\tanh a_{bf} L}{a_{bf} L}\right)$

Table 2.2 Average fiber stress expressions for $\varepsilon_{cf} < \varepsilon_{cb}$.

Fiber and Bond Condition	Average Fiber Stress Expression

Fiber and Bond Condition	Average Fiber Stress Expression
$\varepsilon_s \leq \varepsilon_{cf}$ (fiber and bond are elastic)	$\bar{\sigma} = E_f \varepsilon_s \left(1 - \frac{\tanh aL}{aL}\right)$
$\varepsilon_{cf} < \varepsilon_s \leq \varepsilon_{fb}$ (fiber is plastic and bond is elastic)	$\bar{\sigma} = E_f \varepsilon_{cf} \left(1 - \frac{\tanh aL}{aL}\right) + E_2 (\varepsilon_s - \varepsilon_{cf}) \left(1 - \frac{\tanh a_f L}{a_f L}\right)$
$\varepsilon_{fb} < \varepsilon_s$ (fiber and bond are plastic)	$\bar{\sigma} = E_f \varepsilon_{cf} \left(1 - \frac{\tanh aL}{aL}\right) + E_2 (\varepsilon_{fb} - \varepsilon_{cf}) \left(1 - \frac{\tanh a_f L}{a_f L}\right) + E_2 (\varepsilon_s - \varepsilon_{fbf}) \left(1 - \frac{\tanh a_{fb} L}{a_{fb} L}\right)$

Table 2.3 Average incremental fiber stress expressions for $\varepsilon_{cb} < \varepsilon_{cf}$.

Fiber and Bond Condition	Average Fiber Stress Expression
$\varepsilon_s \leq \varepsilon_{cb}$ (fiber and bond are elastic)	$\Delta\bar{\sigma} = E_f (\Delta\varepsilon_s - \alpha_f \Delta M)\left(1 - \frac{\tanh aL}{aL}\right)$
$\varepsilon_{cb} < \varepsilon_s \leq \varepsilon_{bf}$ (fiber is elastic and bond is plastic)	$\Delta\bar{\sigma} = E_f (\Delta\varepsilon_s - \alpha_f \Delta M)\left(1 - \frac{\tanh a_b L}{a_b L}\right)$
$\varepsilon_{bf} < \varepsilon_s$ (fiber and bond are plastic)	$\Delta\bar{\sigma} = E_2 (\Delta\varepsilon_s - \alpha_f \Delta M)\left(1 - \frac{\tanh a_{bf} L}{a_{bf} L}\right)$

Table 2.4 Average incremental fiber stress expressions for $\varepsilon_{cf} < \varepsilon_{cb}$.

Fiber and Bond Condition	Average Fiber Stress Expression
$\varepsilon_s \leq \varepsilon_{cf}$ (fiber and bond are elastic)	$\Delta\bar{\sigma} = E_f (\Delta\varepsilon_s - \alpha_f \Delta M)\left(1 - \frac{\tanh aL}{aL}\right)$
$\varepsilon_{cf} < \varepsilon_s \leq \varepsilon_{fb}$ (fiber is plastic and bond is elastic)	$\Delta\bar{\sigma} = E_2 (\Delta\varepsilon_s - \alpha_f \Delta M)\left(1 - \frac{\tanh a_f L}{a_f L}\right)$

Fiber and Bond Condition	Average Fiber Stress Expression
$\varepsilon_{fb} < \varepsilon_s$ (fiber and bond are plastic)	$\Delta\overline{\sigma} = E_2\left(\Delta\varepsilon_s - \alpha_f \Delta M\right)\left(1 - \frac{\tanh a_{fb} L}{a_{fb} L}\right)$

2.3 Continuum Model based on Incremental Asymptotic Fiber and Bond Model

2.3.1 General Finite Element Model for Stress Analysis

For solving two- and three-dimensional problems with complicated geometry and arbitrary loading conditions, finite element analysis is a common approach and sometimes the only mean of solution. In general, the actual structure is approximated with an assemblage of small elements with simpler geometry, which are easier to analyze. An admissible displacement field is selected and the displacements within an element are interpolated from the nodal degree of freedom of the element. Following the Rayleigh-Ritz method, the total potential energy of the structure is determined. Applying the principle of minimum potential energy would result in a set of algebraic equations from which the nodal displacements could be solved.

Equation 2.57 shows the displacement field for an element in matrix notation. The formulation of the shape functions in [N] depends on the type of element and desired accuracy in the solution. The strains of the element are given by the derivatives of {u}.

$$\{u\} = [N]\{d\} \qquad \textbf{(2.57)}$$

$$\{\varepsilon\} = [\partial]\{u\} = [\partial][N]\{d\} = [B]\{d\} \qquad \textbf{(2.58)}$$

where {u} = Displacement field within the element
[N] = Shape functions
{d} = Nodal displacements
$\{\partial\}$ = Differential operator matrix

The potential energy of a single body is given by the sum of its strain energy and its work potential. Π = strain energy + work potential. Equation 2.59 gives the potential energy of a linear elastic material, where the first integral gives the strain energy and the rest combined gives the work potential.

$$\Pi_P = \int_V \left(\frac{1}{2}\{\varepsilon\}^T [E]\{\varepsilon\} - \{\varepsilon\}^T [E]\{\varepsilon_o\} + \{\varepsilon\}^T \{\sigma_o\} \right) dV - \int_V \{u\}^T \{F\} dV - \int_S \{u\}^T \{\Phi\} dS - \{D\}^T \{P\} \tag{2.59}$$

where	{u}	=	displacement field
	{ε}	=	strain field
	[E]	=	material property matrix
	$\{\varepsilon_o\}$, $\{\sigma_o\}$	=	initial strains and initial stresses
	{F}	=	body forces
	{Φ}	=	surface traction
	{P}	=	external loads applied
	{D}	=	nodal degree of freedom
	S, V	=	surface and volume of the structure

For a discretized body that does not have any initial strains and stresses, its potential energy is the given by the sum of potential energies of all its elements (cf. equation 2.60).

$$\Pi_P = \frac{1}{2} \sum_{n=1}^{numel} \{d\}_n^T [k]_n \{d\}_n - \sum_{n=1}^{numel} \{d\}_n^T \{r_e\}_n - \{D\}^T \{P\} \tag{2.60}$$

$$[k] = \int_{Ve} [B]^T [E][B] dV \tag{2.61}$$

$$\{r_e\} = \int_{Ve} [B]^T [E]\{\varepsilon_o\} dV - \int_{Ve} [B]^T \{\sigma_o\} dV + \int_{Ve} [N]^T \{F\} dV - \int_{Se} [N]^T \{\Phi\} dS \tag{2.62}$$

where	$[k]_n$	=	element stiffness matrix
	$\{r_e\}_n$	=	element load vector
	numel	=	number of elements

The potential energy in equation 2.60 could also be rewritten in terms of global stiffness matrix and global load vector.

$$\Pi_P = \frac{1}{2}\{D\}^T[K]\{D\} - \{D\}^T[R] \qquad \textbf{(2.63)}$$

where

$$[K] = \sum_{n=1}^{numel}[k]_n \qquad \textbf{(2.64)}$$

$$\{R\} = \{P\} + \sum_{n=1}^{numel}\{r_e\}_n \qquad \textbf{(2.65)}$$

Applying equation 2.66 yields equation 2.67, which is a set of algebraic equations from which the nodal displacements could be solved.

$$\left\{\frac{\partial\ \Pi}{\partial\ \mathrm{D}}\right\} = \{0\} \qquad \textbf{(2.66)}$$

$$[K]\{D\} = \{R\} \qquad \textbf{(2.67)}$$

2.3.2 Continuum Model for Finite Element Analysis

The finite element model presented to this point is just a general model for stress analysis involving common engineering material such as metal with linear elastic behavior. Applications with paper material often involve nonlinear behavior. However, if the load is applied in increments and the increments are small enough, the response could be approximated as linear response.

Therefore, an incremental finite element approach is needed. The elemental $\Delta\sigma_{ij}$ is assumed to be sufficiently small such that it is still linearly related to $\Delta\varepsilon_{ij}$ by the instantaneous slope of the incremental stress-strain curve. In addition, for paper materials, the moisture and temperature effects also provide additional work potential to the element. The elemental stiffness matrix is now given by equation 2.68, while the elemental load vector has two addition terms to account for the moisture and temperature effect (cf. equation 2.69).

$$[k] = \int_{Ve} [B]^T \left[\frac{\partial \ \Delta\sigma_{ij}}{\partial \ \Delta\varepsilon_{ij}} \right] [B] dV \qquad \textbf{(2.68)}$$

$$\begin{aligned} \{\Delta r_e\} = &-\int_{Ve} [B]^T \left[\frac{\partial \ \Delta\sigma_{ij}}{\partial \ \Delta\varepsilon_{ij}} \right] \{\Delta\varepsilon_M\} dV - \int_{Ve} [B]^T \left[\frac{\partial \ \Delta\sigma_{ij}}{\partial \ \Delta\varepsilon_{ij}} \right] \{\Delta\varepsilon_T\} dV \\ &+ \int_{Ve} [N]^T \{\Delta F\} dV - \int_{Se} [N]^T \{\Delta\Phi\} dS \end{aligned} \qquad \textbf{(2.69)}$$

When the incremental potential energy is minimized (cf. equation 2.70) a matrix equation from which the incremental nodal displacement could be solved for is obtained (cf. equation 2.71) is obtained.

$$\left\{ \frac{\partial \ \Delta\Pi}{\partial \ \Delta \mathrm{D}} \right\} = \{0\} \qquad \textbf{(2.70)}$$

$$[K]\{\Delta D\} = \{\Delta R\} \qquad \textbf{(2.71)}$$

The Jacobian matrix [$\partial \Delta\sigma_{ij} / \partial \Delta\varepsilon_{ij}$] in equation 2.68 for an element is determined by applying the incremental micromechanics model a planar element, whose stress and strain fields are assumed to be uniform (cf. equation 2.72). Again, the results of the derivation would be presented here but not the detailed derivation, which could be found in Sinha (1994). The incremental finite element model based on the asymptotic fiber and bond model is implemented in the commercial finite element code ABAQUS via its UMAT user subroutine.

$$\begin{Bmatrix} \Delta\sigma_x \\ \Delta\sigma_y \\ \Delta\sigma_{xy} \end{Bmatrix} = \begin{bmatrix} k_{11} & k_{12} & k_{13} \\ k_{21} & k_{22} & k_{23} \\ k_{31} & k_{32} & k_{33} \end{bmatrix} \begin{Bmatrix} \Delta\varepsilon_x \\ \Delta\varepsilon_y \\ \Delta\varepsilon_{xy} \end{Bmatrix} \qquad \textbf{(2.72)}$$

where

$$k_{11} = \frac{\rho_s}{\rho_f} \int_0^{\infty} \int_{-\pi/2}^{\pi/2} F \cos^4\theta \quad f_\theta \, f_\lambda \; d\theta \;\; d\lambda \qquad \textbf{(2.73)}$$

$$k_{12} = \frac{\rho_s}{\rho_f} \int_0^{\infty} \int_{-\pi/2}^{\pi/2} F \sin^2\theta \ \cos^2\theta \quad f_\theta f_\lambda \ d\theta \ d\lambda \tag{2.74}$$

$$k_{13} = \frac{\rho_s}{\rho_f} \int_0^{\infty} \int_{-\pi/2}^{\pi/2} F \sin\theta \ \cos^3\theta \quad f_\theta f_\lambda \ d\theta \ d\lambda \tag{2.75}$$

$$k_{22} = \frac{\rho_s}{\rho_f} \int_0^{\infty} \int_{-\pi/2}^{\pi/2} F \sin^4\theta \quad f_\theta f_\lambda \ d\theta \ d\lambda \tag{2.76}$$

$$k_{23} = \frac{\rho_s}{\rho_f} \int_0^{\infty} \int_{-\pi/2}^{\pi/2} F \sin^3\theta \ \cos\theta \quad f_\theta f_\lambda \ d\theta \ d\lambda \tag{2.77}$$

$$k_{33} = k_{12} \tag{2.78}$$

The F functions are listed in Table 2.5 and Table 2.6.

Table 2.5 F functions for $\varepsilon_{cb} < \varepsilon_{cf}$

Fiber and Bond Condition	F Functions
$\varepsilon_s \le \varepsilon_{cb}$ (fiber and bond are elastic)	$E_f\left(1-\frac{\tanh aL}{aL}\right)$
$\varepsilon_{cb} < \varepsilon_s \le \varepsilon_{bf}$ (fiber is elastic and bond is plastic)	$E_f\left(1-\frac{\tanh a_b L}{a_b L}\right)$
$\varepsilon_{bf} < \varepsilon_s$ (fiber and bond are plastic)	$E_2\left(1-\frac{\tanh a_{bf} L}{a_{bf} L}\right)$

Table 2.6 F functions for $\varepsilon_{cf} < \varepsilon_{cb}$

Fiber and Bond Condition	F Functions
$\varepsilon_s \le \varepsilon_{cf}$ (fiber and bond are elastic)	$E_f\left(1-\frac{\tanh aL}{aL}\right)$

Fiber and Bond Condition	F Functions
$\varepsilon_{cf} < \varepsilon_s \leq \varepsilon_{fb}$ (fiber is elastic and bond is plastic)	$E_2\left(1-\frac{\tanh a_f L}{a_f L}\right)$
$\varepsilon_{fb} < \varepsilon_s$ (fiber and bond are plastic)	$E_2\left(1-\frac{\tanh a_{fb} L}{a_{fb} L}\right)$

2.4 Objective

Regardless of the type of model, after an extensive literature review (Ramasubramanian and Wang, 1999), it was clear that the focus of constitutive modeling of paper material thus far has been mainly on the loading process. The unloading behavior after yielding has not been addressed.

Therefore, the focus of this work would be to model the unloading behavior of a sheet in a one-dimensional and two-dimensional problem using the same approach by Sinha and Perkins (1995) for loading. The micromechanics model in Sinha (1994), i.e. the asymptotic fiber and bond model, would be extended to address the unloading behavior of high-density paperboard (720 kg/m^3) materials.

The asymptotic fiber and bond model derives the sheet stress from the mechanical properties and interaction mechanisms of a representative load-bearing unit in the fiber network. The load-bearing unit in this model is a fiber segment, which is bonded on one side. At a given strain, the average fiber stress is calculated from the equilibrium condition of the load-bearing unit as a function of the fiber orientation angle. The sheet stress is then calculated by an integral sum of the appropriate fiber stress components of fibers in all orientations. In determining the average fiber stress, the knowledge of the micro-constituents and network properties, such as the fiber elastic modulus, fiber-to-fiber bond modulus, fiber orientation distribution, and so on is required. However, the measurements of these model parameters are difficult to accomplish and are not readily available. Therefore, uniaxial tensile test would be conducted on a sample stock so that the model could be fitted to the experimental data to obtain the parameter values. The extended model would then be used to predict the permanent or plastic strains of uniaxially strained samples in the machine and cross machine direction.

Finally, for a two-dimensional problem, the same combined continuum and micromechanics approach by Sinha and Perkins would be used to model the unloading process of samples subjected to uniform pressure on one surface. A Mullen Tester for conducting burst test would be used to deform the sample, but not to failure, and then unloaded. The deformed sample is hemispherical in shape. The model would be used with the commercial finite element software ABAQUS to determine the pressure-displacement curve at the center of the sample.

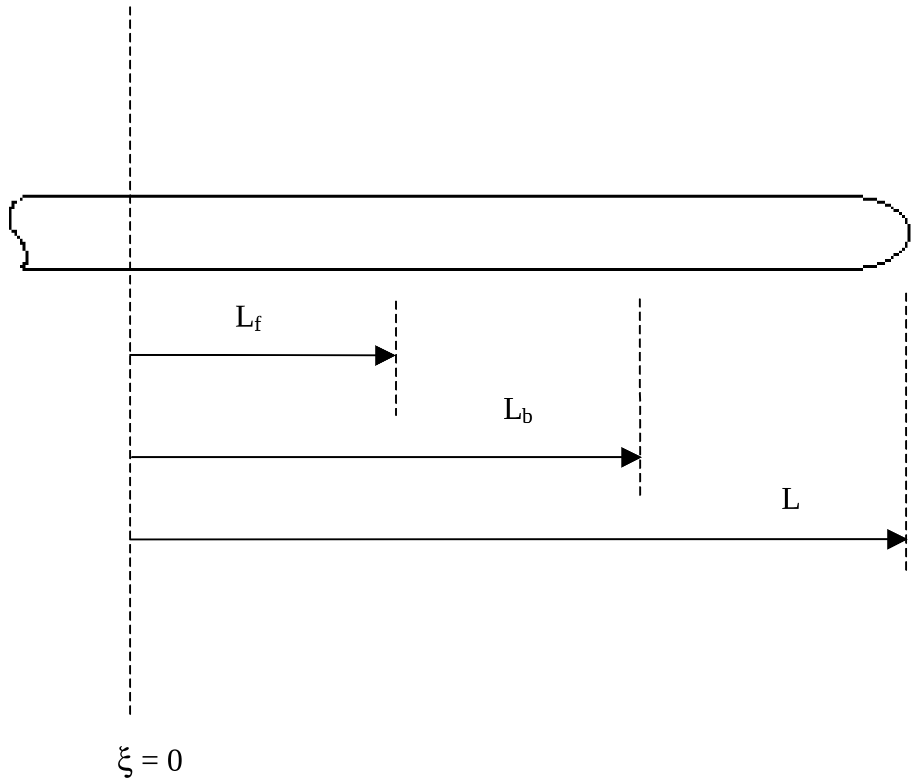

Figure 2.1 Elastic and plastic zones of fiber and bond along the fiber length (Sinha, 1994).

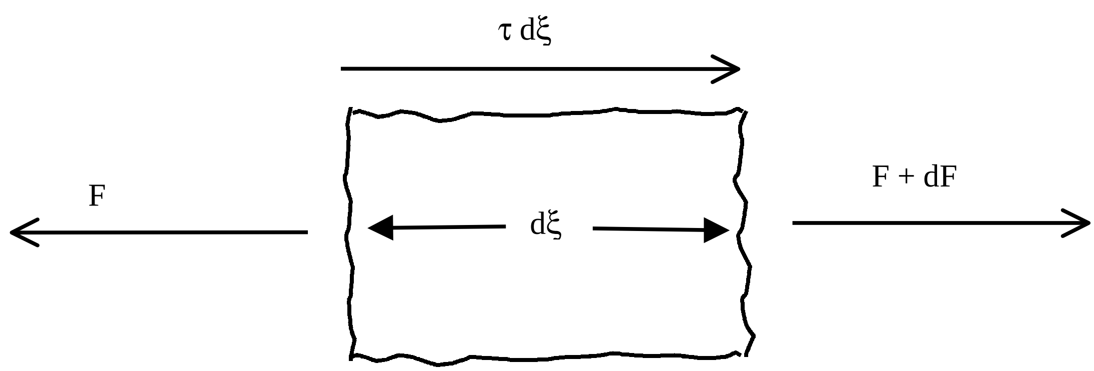

Figure 2.2 Free body diagram of a mesoelement (Sinha, 1994).

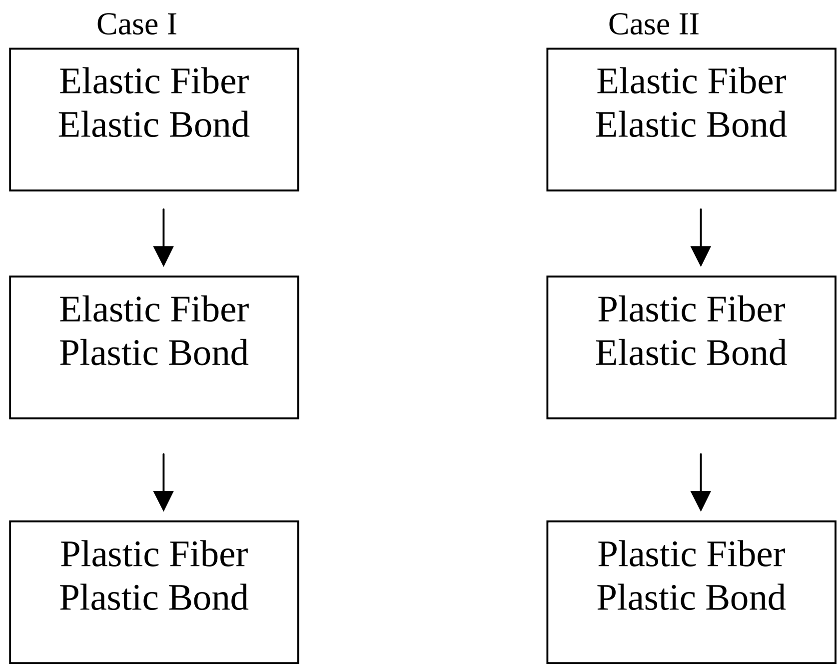

Figure 2.3 Chart of the two possible fiber and bond deformation scenarios

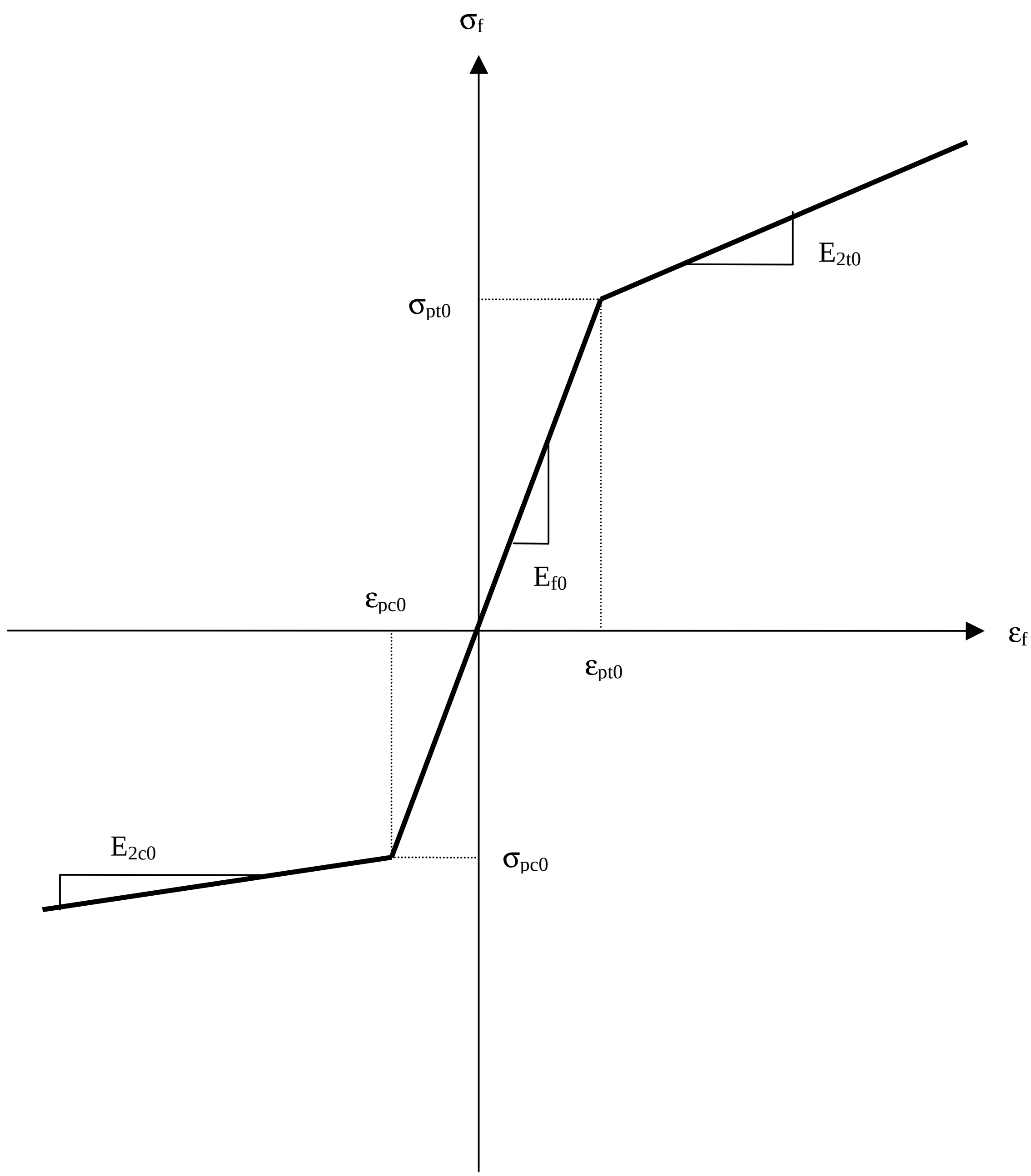

Figure 2.4 Two-slope model approximation of the constitutive behavior of fiber.

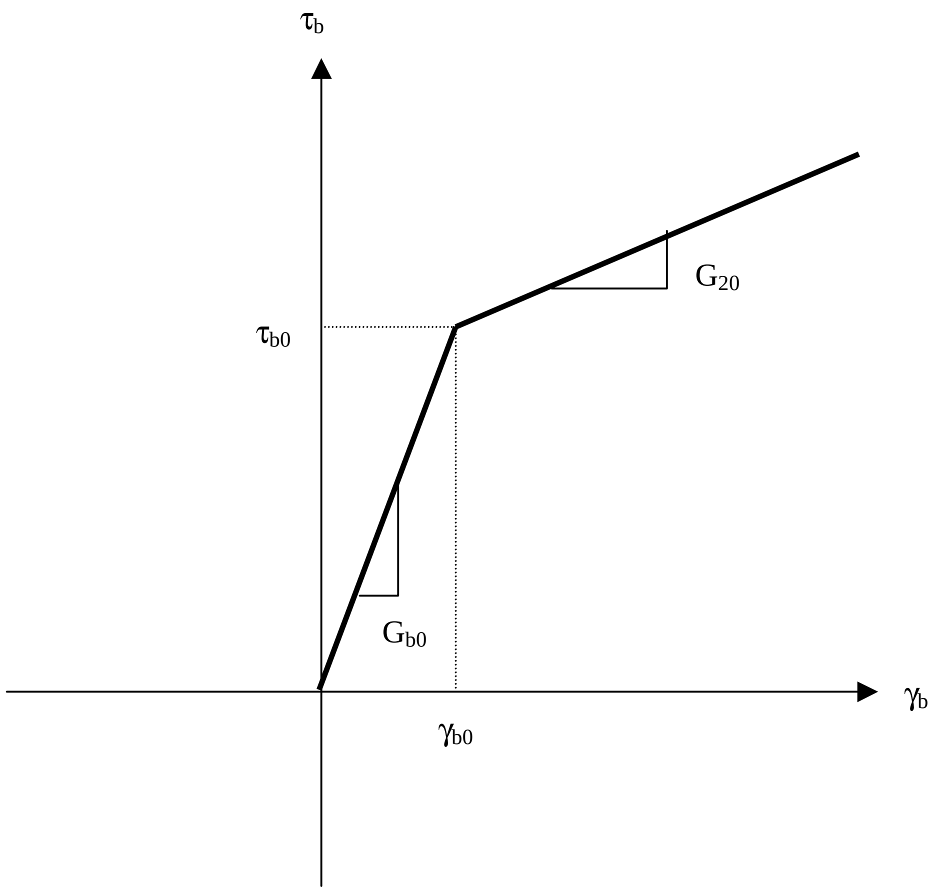

Figure 2.5 Two-slope model approximation of the constitutive behavior of bond (Sinha, 1994).

3. Unloading of Paper and Paperboard Material

3.1 Unloading in One-dimensional Problem

Consider a sheet subjected to a uniaxial tensile load in the x-direction. In this work, the sheet strain is considered to consist of two components (cf. equation 3.1), i.e. an elastic strain component and a plastic strain component. The elastic component represents the strain recovered upon unloading.

$$\varepsilon_x = \varepsilon_{x,el} + \varepsilon_{x,pl} \tag{3.1}$$

While the sheet has not reached its yield point, $\varepsilon_x < \varepsilon_{yield}$, $\varepsilon_{x,pl} = 0$. Therefore, the sheet returns to its undeformed state upon unloading. Although in practice, the total strain should also include a visco-elastic component, it will not be addressed here. If the sheet has exceeded its yield strain, the elastic component is recovered upon unloading and the remaining strain is named the “plastic” component, for ease of reference.

In a typical loading-unloading curve (cf. Figure 3.1), the unloading-reloading path forms a hysteresis loop, which resulted from energy loss. Although, the unloading and reloading path may have different slopes, they could be adequately approximated by the initial elastic modulus of the sheet. Therefore, fiber and bond are assumed to behave elastically when the sheet is being unloaded.

While the fiber and bond are elastic, so is the sheet. The sheet stress σ_x would be given by equation 3.2. Since $\sigma_x = E_x\varepsilon_x$ in linear elasticity, the elastic modulus of the sheet would be equal to the sheet stress divided by the sheet strain (cf. equation 3.3).

$$\sigma_x = \frac{\rho_s}{\rho_f} E_f \varepsilon_x \int_{-\pi/2}^{\pi/2} \left(\cos^2\theta - \nu \sin^2\theta\right)\left(1 - \frac{\tanh(aL)}{aL}\right)\cos^2\theta \; f(\theta) d\theta \tag{3.2}$$

$$E_x = \frac{\rho_s}{\rho_f} E_f \int_{-\pi/2}^{\pi/2} \left(\cos^2\theta - \nu \sin^2\theta\right)\left(1 - \frac{\tanh(aL)}{aL}\right)\cos^2\theta \; f(\theta) d\theta \tag{3.3}$$

When the sheet has yielded, the elastic strain $\varepsilon_{x,el}$ that is recovered upon unloading would then be given by division of the sheet stress by the sheet elastic modulus (cf. equation 3.4).

$$\varepsilon_{x,el} = \frac{\int_{-\pi/2}^{\pi/2} \overline{\sigma}(\theta)\cos^2\theta \ \ f(\theta)d\theta}{E_f \int_{-\pi/2}^{\pi/2} \left(\cos^2\theta - \nu \sin^2\theta\right)\left(1 - \frac{\tanh(aL)}{aL}\right)\cos^2\theta \ \ f(\theta)d\theta} \tag{3.4}$$

When implementing the model, for a given ε_x, the integrals in equation 3.2 – 3.4 are evaluated numerically using the multiple application Simpsons's 1/3 rule given by equation 3.5. Once $\varepsilon_{x,el}$ is determined, the permanent plastic sheet strain could be obtained from equation 3.1.

$$\int_{\theta_1}^{\theta_2} G(\theta)d\theta = \frac{\theta_2 - \theta_1}{3(n-1)}\left(G(\theta_1) + 2\sum_{i=2,4,...}^{n-1} G(\theta_i) + 4\sum_{i=3,5,...}^{n-2} G(\theta_i) + G(\theta_n)\right) \tag{3.5}$$

While E_x and $\varepsilon_{x,el}$ in a one-dimensional problem is relatively easy to determine, the loading-unloading behavior of problems with arbitrary geometry and complex loading conditions could not be solved using the same approach. The solution to such problems requires the application of the continuum model based on incremental asymptotic fiber and bond model in finite element analysis. In fact, the uniaxial loading problem could be solved graphically by drawing a straight path with a slope of the sheet elastic modulus at the unloading point to the point of zero stress to obtain the plastic strain at the end of unloading. Therefore, the application of the model in the uniaxial loading problem only serves as a confirmation of the feasibility and accuracy of predicting the unloading process using the model by assuming elastic fiber and elastic bond behavior during unloading. The uniaxial loading problem serves as a stepping stone from where the model proceed to be applied in a nontrivial problem, i.e. the two dimensional problem of a sample deformed in a burst test.

3.2 Unloading in Two-dimensional Problem

In incremental approach, the macroscopic sheet strain in the mesoelement axial direction is given by the sum of the incremental strain $\Delta\varepsilon_s$ (cf. equation 3.6 and 3.7).

$$\Delta\varepsilon_s = \Delta\varepsilon_x \cos^2\theta + \Delta\varepsilon_y \sin^2\theta + 2\Delta\varepsilon_{xy} \cos\theta \sin\theta \tag{3.6}$$

$$\varepsilon_s = \sum_{i=1}^{n} \left(\varepsilon_s\right)_i \tag{3.7}$$

When fiber is unloading, ε_s would have an opposite sense to that of $\Delta\varepsilon_s$. Both fiber and bond would behave elastically. Therefore, the F function, which corresponds to elastic fiber and bond condition (cf. Table 2.5 and Table 2.6), would be used in the Jacobian matrix (cf. 2.3.2) to calculate the corresponding change in σ_{ij}.

The continuum model based on the modified incremental asymptotic fiber and bond model to include unloading behavior was implemented in ABAQUS via its UMAT subroutine (cf. flowchart in Figure 3.2, Figure 3.3, Figure 3.4, and Appendix A). The subroutine is capable of addressing cyclic loading, which oscillates between tensile and compressive state. During cyclic loading, the critical strains have to be modified accordingly so that the ensuing plastic deformation would occur at the correct stress limit.

3.3 Cyclic Loading

Consider a fiber of orientation θ. The fiber is loaded in tension until bond has yielded. It is then unloaded and the fiber strain would have a nonzero plastic component, $\varepsilon_{f,pl} \neq 0$. This nonzero value of the fiber plastic strain component is then added to the critical strains in compression. If the fiber is subsequently compressed, the updated critical strains allow the load-bearing unit to yield at the correct stress limit (cf. equation 3.8, 3.9, 3.10, 3.11, 3.12 and 3.13).

$$\varepsilon_{s,pl} = \varepsilon_s - \varepsilon_{s,el} \tag{3.8}$$

$$\varepsilon_{s,el} = \frac{\varepsilon_s}{E_f\left(1-\frac{\tanh aL}{aL}\right)} \quad (3.9)$$

$$\varepsilon_{cb} = \varepsilon_{cb,0} + \varepsilon_{s,pl} \quad (3.10)$$

$$\varepsilon_{cf} = \varepsilon_{cf,0} + \varepsilon_{s,pl} \quad (3.11)$$

$$\varepsilon_{bf} = \varepsilon_{bf,0} + \varepsilon_{s,pl} \quad (3.12)$$

$$\varepsilon_{fb} = \varepsilon_{fb,0} + \varepsilon_{s,pl} \quad (3.13)$$

For a fiber subjected to multiple cycle of loading and unloading process, the critical strains are still adjusted in similar manner. In compression, the original critical strains are adjusted by addition of the cumulative absolute value of the plastic strains (cf. equation 3.14). In tension, the offset value in equation 3.14 is subtracted from the original critical strains instead.

$$\varepsilon_{offset} = \sum_{i=1}^{n}\left|\varepsilon_{s,pl}^{i}\right| \quad (3.14)$$

The updated critical strains are then compared with ε_s to determine the state of fiber and bond so that the appropriate F function (cf. Table 2.5 and Table 2.6) could be selected for subsequent calculation of $\Delta\sigma_{ij}$.

The implementation of the asymptotic fiber and bond model is shown in the flowcharts in Figure 3.2 to Figure 3.4. Consider now an undeformed sheet subjected to tensile loading in the machine direction. The values of the model parameters are defined in the subroutine, although they can also be defined in the input file for use in the UMAT subroutine. In this work, ε_{cb} is greater than ε_{cf} in tension and compression. Therefore, bond would yield first when the critical strain ε_{cb} is reached.

The fiber orientation distribution, θ, is discretized into 30 angles varying from -$\pi/2$ to $\pi/2$. For a given loading condition on the sheet, the algorithm begins with $\theta=-\pi/2$

and calculates the corresponding $\varepsilon_s(\theta)$. The critical strains are calculated and so are the model parameters that are affected by the application of drying restraints.

Suppose $\varepsilon_s(\theta)$ is loaded in tension ($\mathrm{sgn}(\varepsilon_s) = \mathrm{sgn}(\Delta\varepsilon_s)$ and $\Delta\varepsilon_s > 0$) beyond the yield point ε_{cb}. Bond would yield and the total strain of ε_s could be broken into two components, i.e. the elastic and plastic strain component (cf. equation 3.8). The $\varepsilon_{s,el}$ is recovered when the sheet is unloaded. Therefore, the F function for elastic fiber and elastic bond would be used to calculate the Jacobian matrix (cf. equation 2.72 – 2.78, Table 2.5). This matrix in turn is used to determine the corresponding change in fiber stress during the unloading process (cf. equation 2.72). The k_{ij}'s in the Jacobian matrix are obtained by evaluating the integral of the F functions in equation 2.73 to 2.78 numerically using the Simpson's 1/3 rule (cf. equation 3.5). The elastic and plastic strain components of ε_s are also stored for decision making in the algorithm and updating the critical strains of subsequent loading cycle (cf. 3.10 – 3.14).

Supposed $\varepsilon_s(\theta)$ is then compressed. The algorithm determines if the elastic strain component of $\varepsilon_s(\theta)$ in tension has exceeded the critical strain. If exceeded, the critical strains in compression are updated (cf. equation 3.10 – 3.13), else the critical strain in compression remain unchanged. When ε_s has increased beyond ε_{cb} in compression, it is then unloaded. While it is being unloaded, again the F function for elastic fiber and elastic bond again is used to calculate the Jacobian matrix.

When the next tensile load is applied, $\varepsilon_s(\theta)$ has yielded both in tension and compression. Therefore, $\varepsilon_{s,el} > \varepsilon_{cb,el}$ in tension and in compression. This serves as checking criteria in the algorithm before the critical strains are updated for subsequent cyclic load (cf. 3.14). From this point forward, the critical strain for subsequent cyclic load would only be updated using equation 3.14.

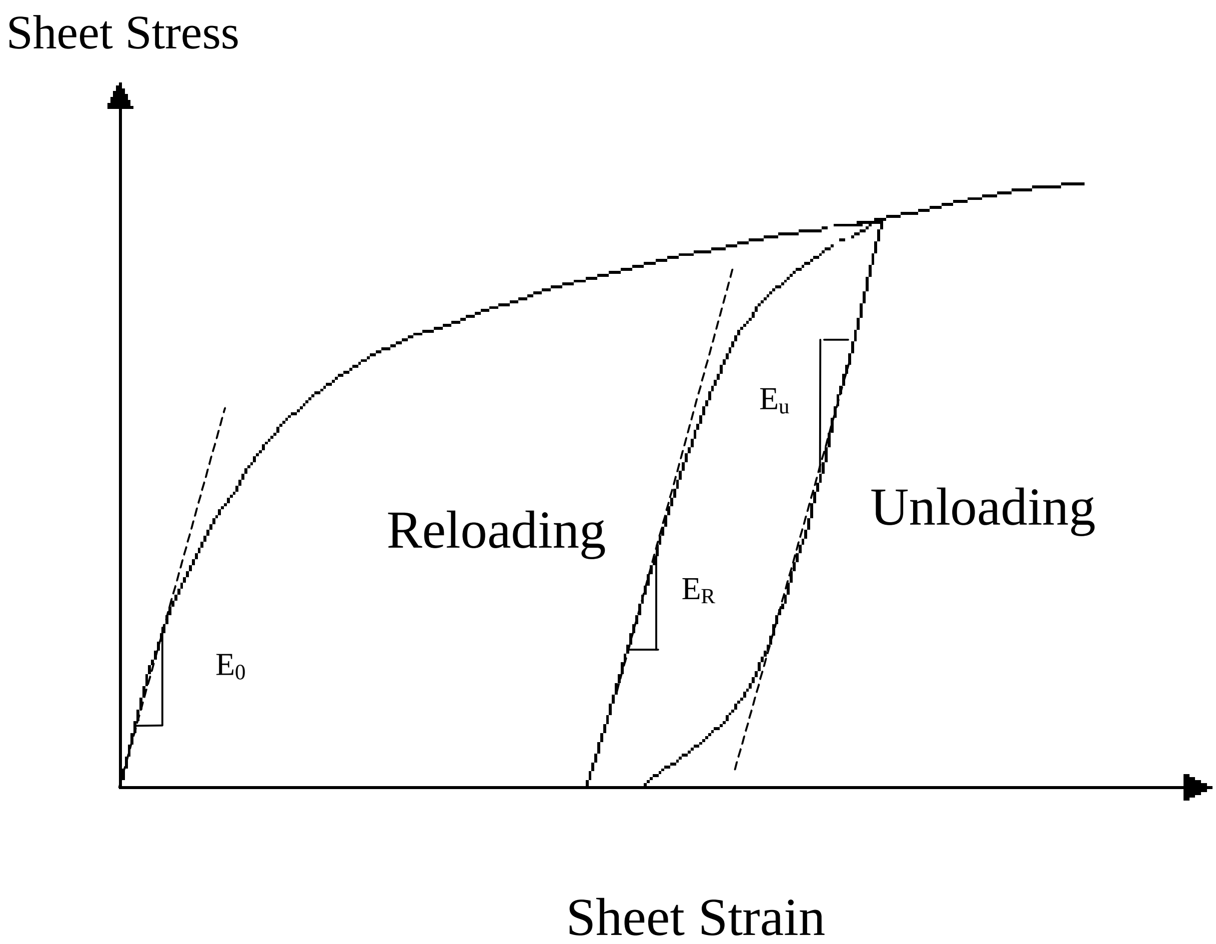

Figure 3.1 Sketch of a representative loading-unloading stress-strain curve for paper material. The unloading and reloading path of the stress-strain curve is approximated with the sheet initial elastic modulus, i.e. $E_0 \approx E_u \approx E_R$.

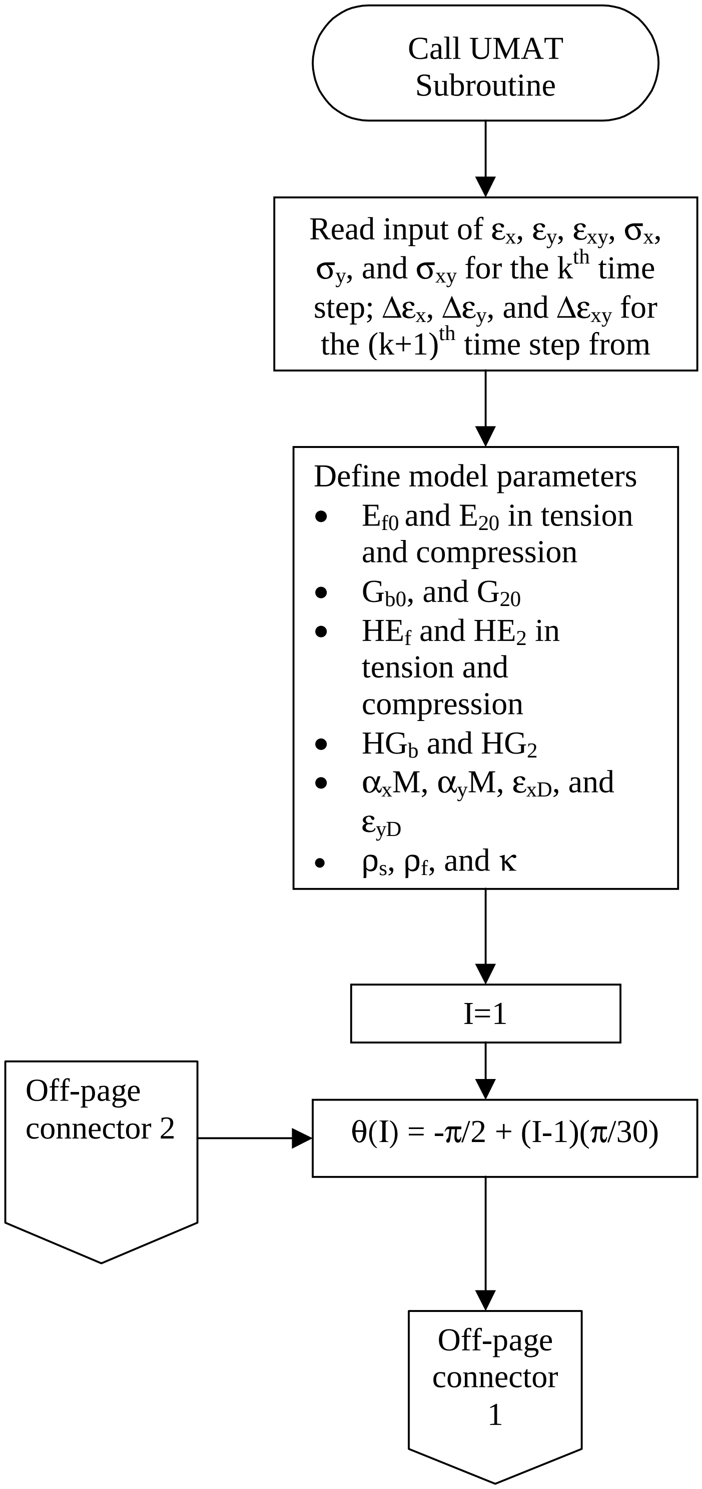

Figure 3.2 Flowchart for implementing the asymptotic fiber and bond model in UMAT to model the loading and unloading process.

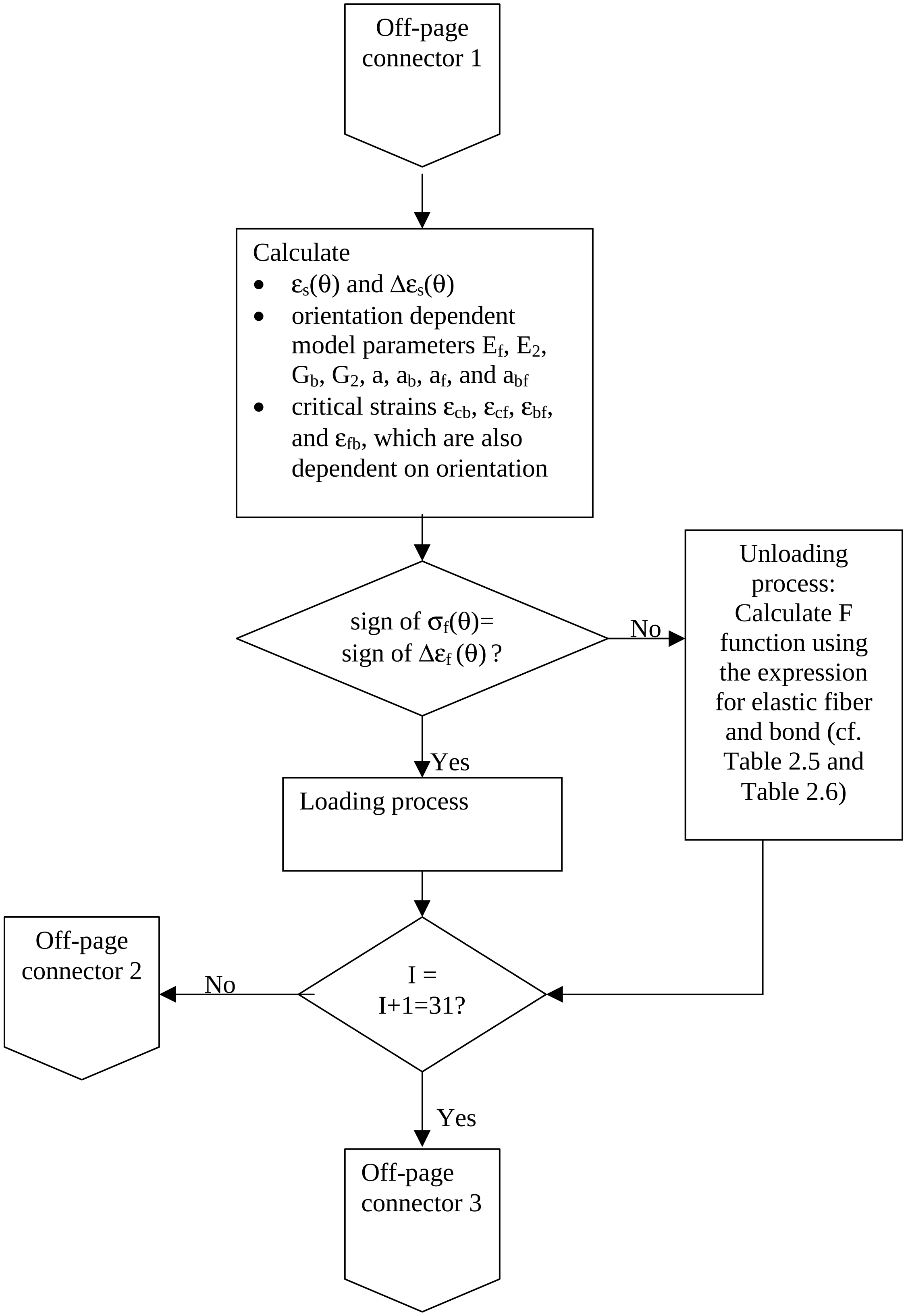

Figure 3.2 Flowchart for implementing the asymptotic fiber and bond model in UMAT to model the loading and unloading process.

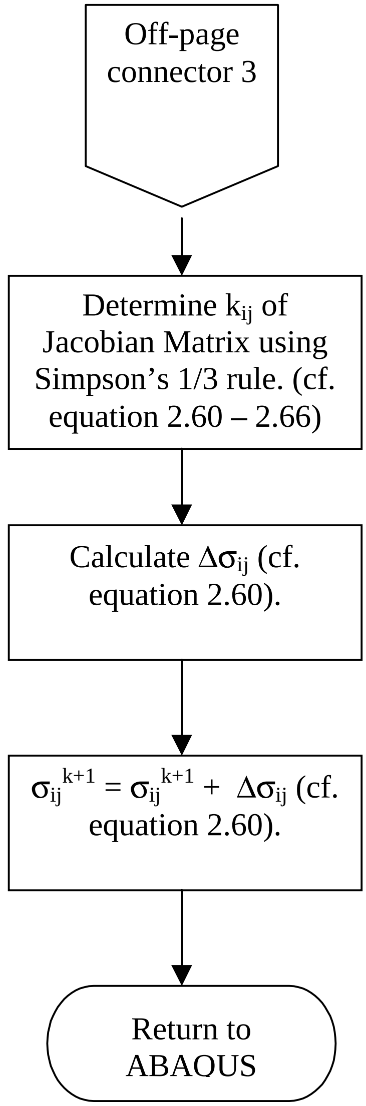

Figure 3.2 Flowchart for implementing the asymptotic fiber and bond model in UMAT to model the loading and unloading process. (Continue)

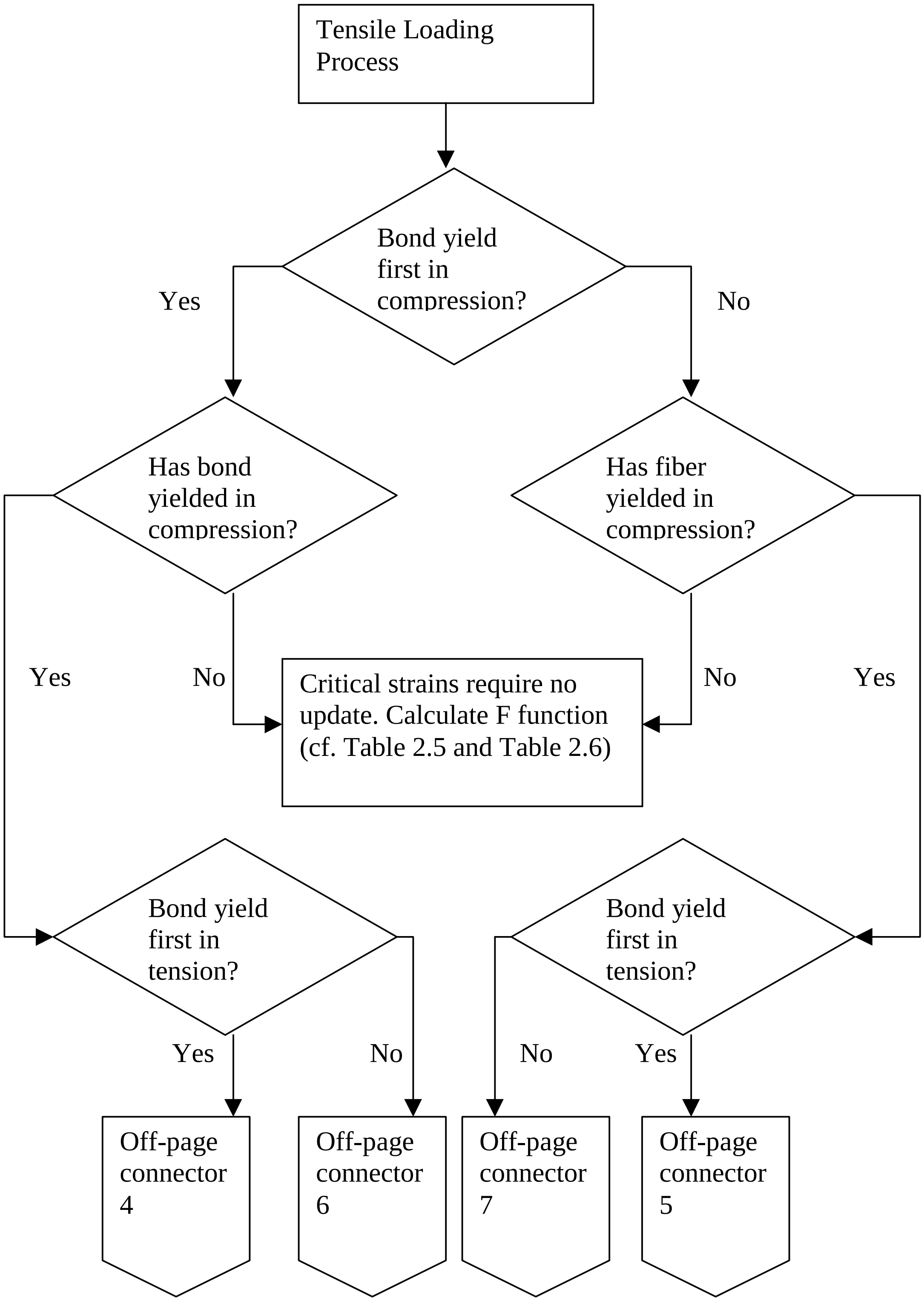

Figure 3.3 Flowchart of tensile loading process, i.e. when $\Delta\varepsilon_s \geq 0$

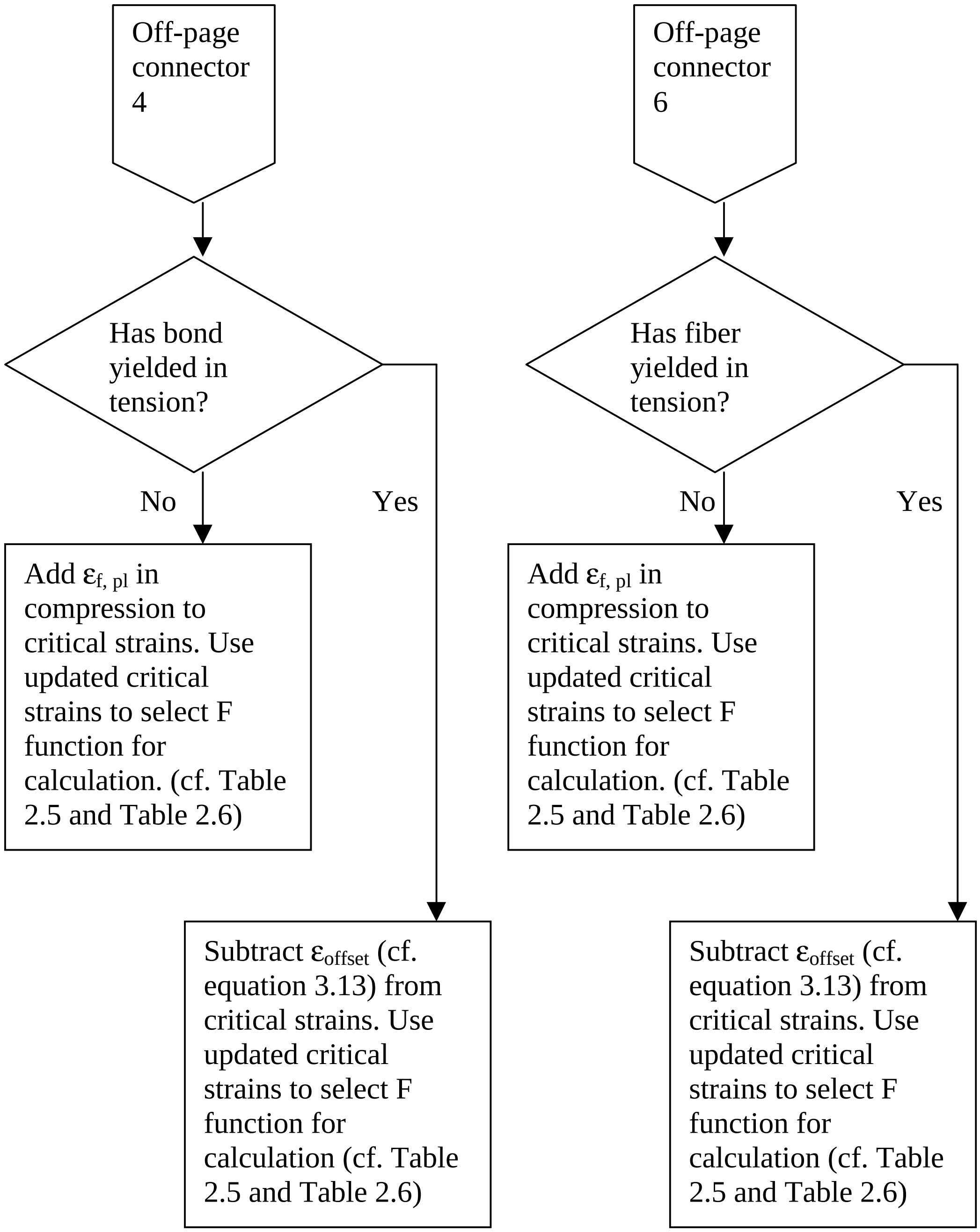

Figure 3.3 Flowchart of tensile loading process, i.e. when $\Delta\varepsilon\sigma \geq 0$. (Continue)

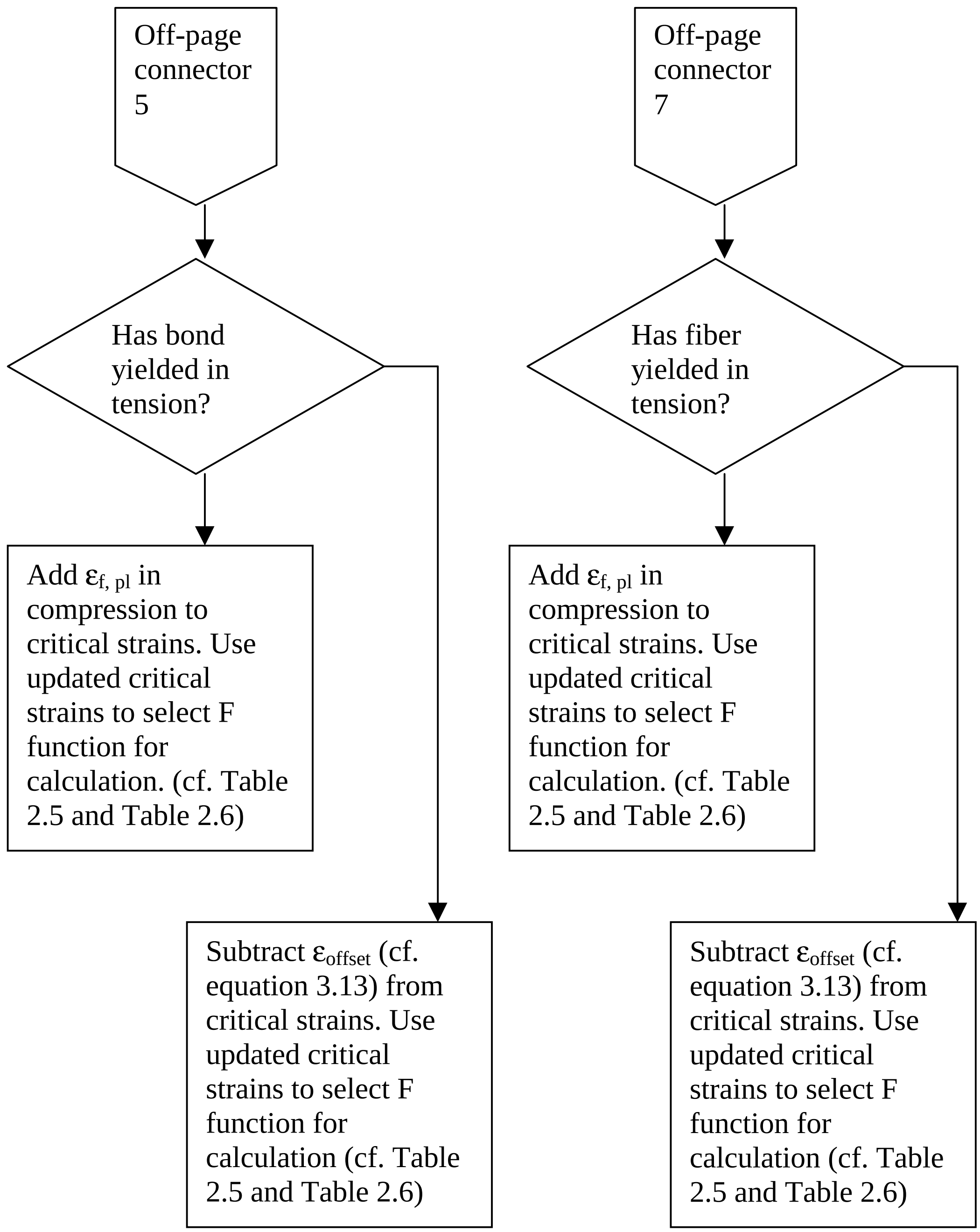

Figure 3.3 Flowchart of tensile loading process, i.e. when $\Delta\varepsilon\sigma \geq 0$. (Continue)

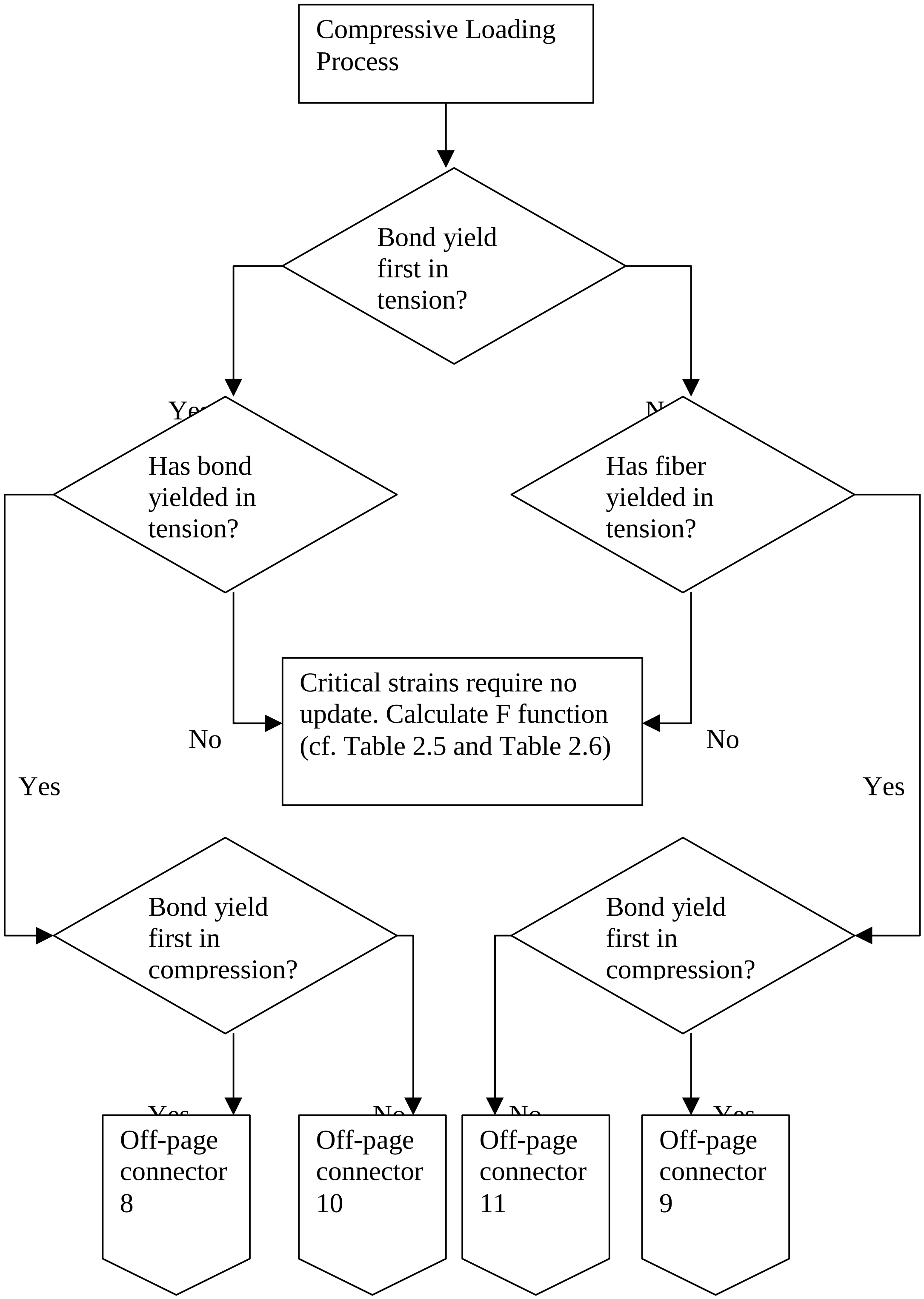

Figure 3.4 Flowchart of compressive loading process, i.e. $\Delta\varepsilon_s$<0

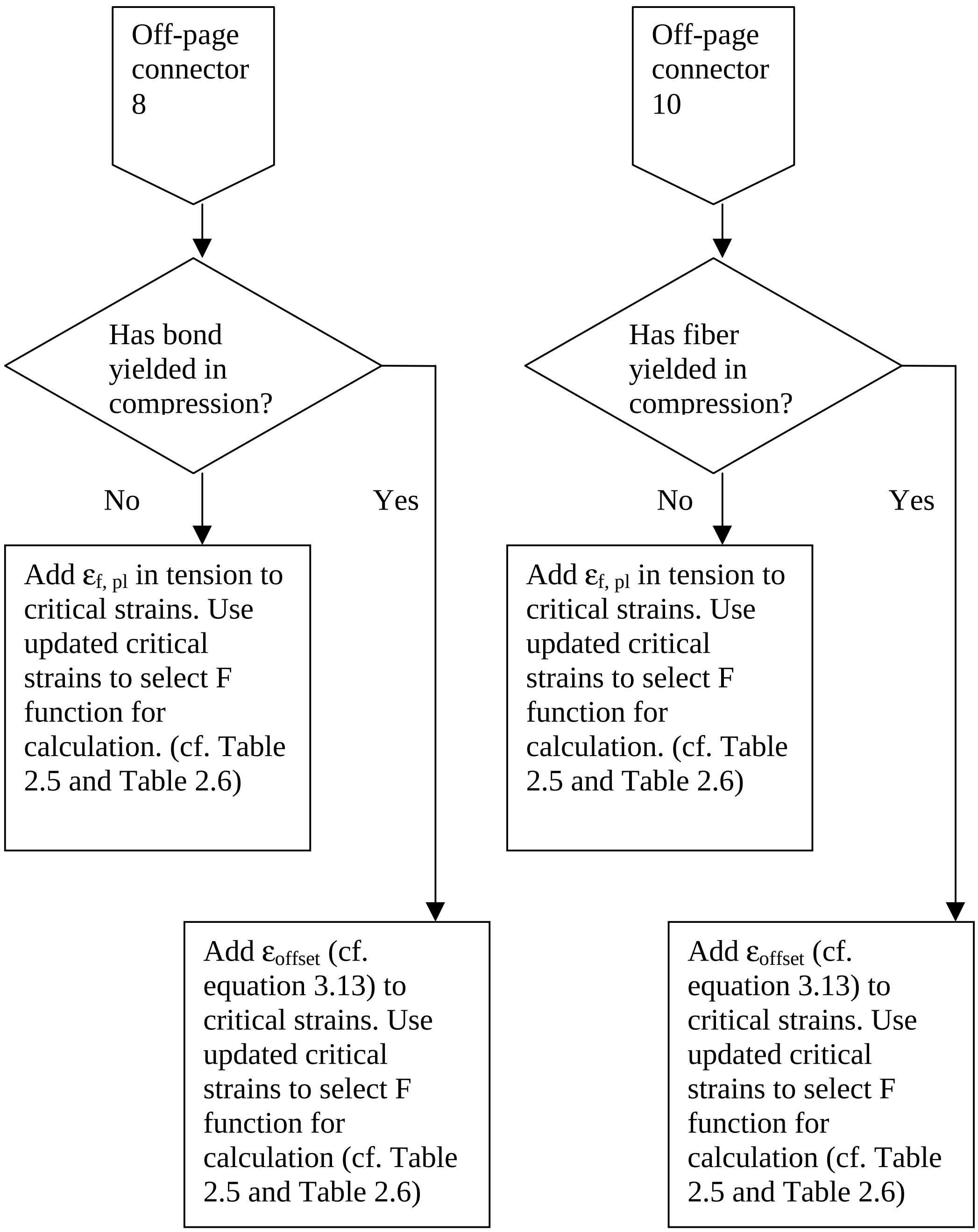

Figure 3.4 Flowchart of compressive loading process, i.e. $\Delta\varepsilon\sigma<0$. (Continue)

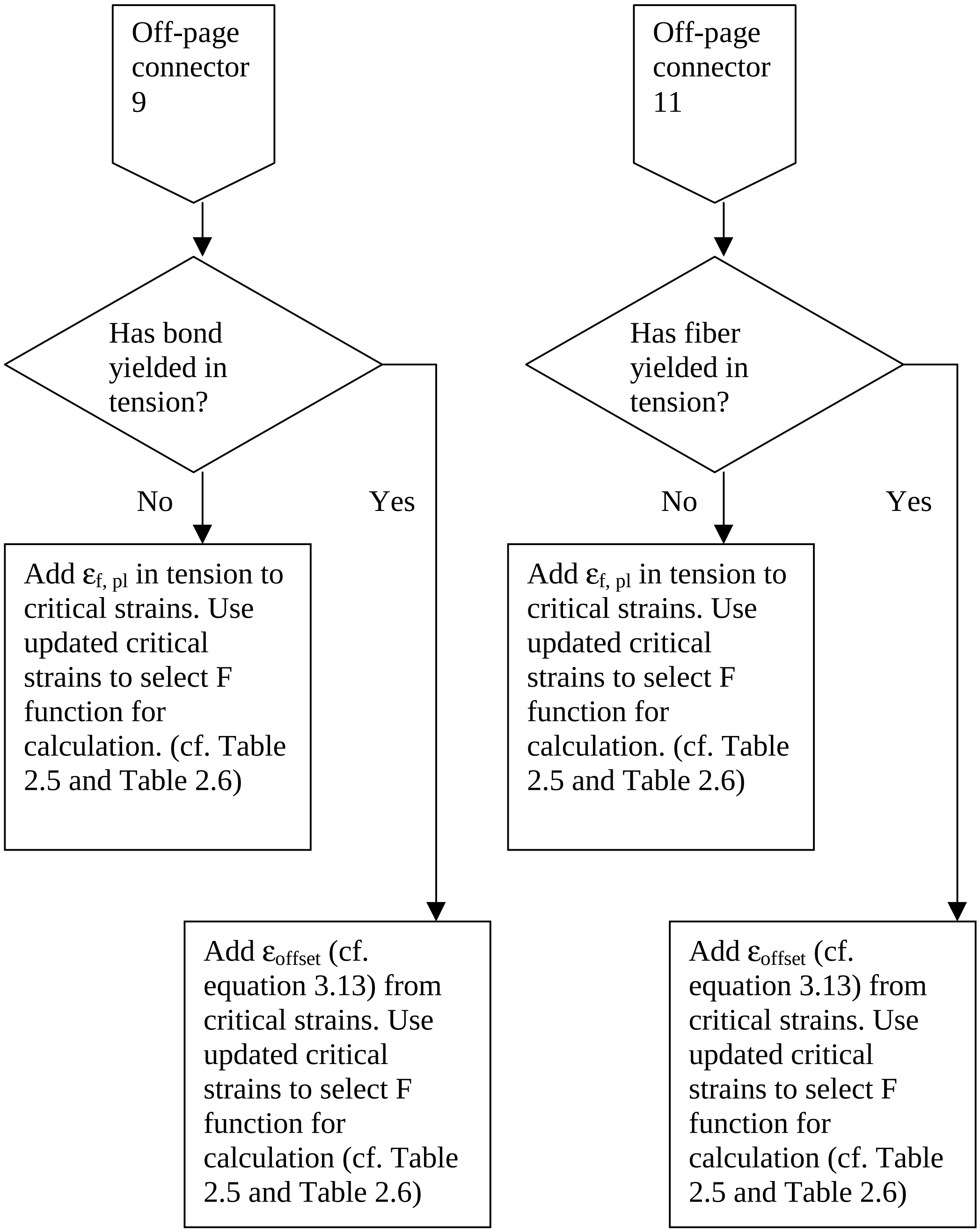

Figure 3.4 Flowchart of compressive loading process, i.e. $\Delta\varepsilon\sigma<0$. (Continue)

4. Experimental Work

4.1 Uniaxial Tensile Test

4.1.1 Sample Conditioning

The unloading model would be tested on a high-density paper cup stock of 720 kg/$m^{3,}$ which was coated on one side. Before applying the asymptotic fiber and bond model, the parameters listed in Table 4.1 needs to be known first. However, these parameters are difficult to measure because of the microscopic size of the constituents that made up the load-bearing unit in the model. Therefore, these parameters were obtained by fitting the asymptotic fiber and bond model to experimental data obtained from uniaxial tensile test of the paper cup stock.

Table 4.1 Model Parameters for modeling deformation process where the bond yields first.

Parameter Type	Description	Parameter
Sheet Properties	Concentration parameter	κ
	Direction of greatest concentration	μ
	Lateral contraction ratio	ν
	Free shrinkage of sheet in the x- and y-direction due to drying	$\alpha_x M$, $\alpha_y M$
	Drying restraint strains	ε_{xD}, ε_{yD}
Fiber Properties	Fiber elastic modulus	E_{f0}
	Drying restraint parameter of fiber elastic modulus	HE_{f0}
Bond Properties	Bond shear elastic modulus	G_{b0}
	Drying restraint parameter of bond shear elastic modulus	HG_{b0}
	Bond yield stress	τ_{p0}
	Drying restraint parameter of bond yield stress	$H\tau_{p0}$
	Bond second slope	G_{b2}
	Drying restraint parameter of bond second slope	HG_{20}

In machine made papers, the fibers tend to align and concentrate more in the machine direction due to hydrodynamics effects. Therefore, μ was assumed to be in the machine direction and serves as the reference from which the angle of fiber orientation θ is measured. If the sheet were left to dry freely, the shrinkage due to M moisture content would lead to shrinkage of $\alpha_x M$ and $\alpha_y M$ amount in the machine and cross-machine direction respectively. During the papermaking process, the sheet is restrained in the machine direction. Due to this drying restraint, the paper is prohibited from undergoing free shrinkage in the machine direction. Therefore, $\varepsilon_{xD} = 0$. The sheet in the cross-machine direction on the other hand is free from any restraint. Therefore, $\varepsilon_{yD} = -\alpha_y M$. Therefore, the expression for the macroscopic drying restraint strain measure ε_{DR} was reduced to $\varepsilon_{DR} = \alpha_x M \cos^2 \theta$. Since the free shrinkage of the paper cup stock was not known, $\alpha_x M$ was given an assumed the value of 4.5%. This value was obtained from the work of Sinha (1994) for paper of similar density. The actual $\alpha_x M$ could provide more insights into the effects of hardening on the various properties of fiber and bond. However, the lack of this knowledge would not hinder the application of the asymptotic fiber and bond model for a sheet, which is restrained only in one direction. This is because ε_{DR} and hence, $\alpha_x M$ is paired with the hardening parameters HE_{f0}, HG_{b0}, $H\tau_{p0}$, and HG_{20} to describe the directional effects due to drying restraints. These hardening parameters are fitted to the various features of the sheet stress-strain curves and could be adjusted accordingly to accommodate the inaccuracies in the assumed value of $\alpha_x M$.

In a sensitivity study by Sinha (1994), a systematic variation of the model parameters was conducted to investigate the effects of the model parameters on sheet stress-strain curve. The conclusion is summarized in Table 4.2. In that study, the onset of the nonlinearity in the sheet stress-strain curve was attributed to the viscoplastic behavior of the fiber-to-fiber bond, in keeping with experimental observation and conventional wisdom. Therefore, the same assumption is made in this unloading analysis as well, i.e. fibers remain elastic throughout the entire deformation process.

Table 4.2 Effects of model parameters on the sheet stress-strain curve where bond yields first

Model Parameter	Effect
Fiber elastic modulus E_{f0}	Elastic modulus of sheet.
Bond shear elastic modulus G_{b0}	No significant effects observed.
Bond yield stress τ_{p0}	Yield point of sheet stress-strain curve.
Bond second slope G_{20}	Nonlinearity (second slope) of sheet stress-strain curve.

The model parameters E_{f0}, G_{b0}, τ_{p0}, and G_{20} are best determined from sheets that were dried freely. In order to reduce the effects of drying restraints on the already made paper cup stock, several samples were conditioned in a humidifying chamber at R.H. 85% and 23.0°C for 24 hours. The samples were then allowed to dry freely in a temperature and humidity controlled room for another 24 hours. The room atmosphere conformed to the TAPPI standard for conditioning and testing, i.e. 50.0% ± 2.0% R.H. and 23.0 ± 1.0°C.

4.1.2 Uniaxial Tensile Test

The uniaxial tensile tests were conducted with conditioned and unconditioned paper cup stock. The samples were cut into 1 inch x 10 inch strips. When mounted on the Instron tensile tester, a grip distance of 7 inches was used and a loading rate of 1 inch/min was applied to the upper grip while the lower grip remained stationary. The uniaxial stress-strain curves were obtained for the machine and cross-machine direction for each type of sample. It was noted that the loading curves of the conditioned sample do not show significant difference from those of the unconditioned samples. Two possible reasons for this observation were drawn. One, the humidifying process could be ineffective in eliminating the drying restraint effects. Or, the time between manufacturing and testing of the stock was long enough that the drying restraint effects could have diminished over time. Later analysis showed that the first explanation was more plausible.

Since the Instron machine was incapable of stopping precisely at a given load, the unloading process was stopped manually. After a sample was stretched to a given strain, the motion of the upper grip was reversed. As the grip returns to the starting position, the applied load on the grip decreases. An approximate value to the plastic strain after unloading was obtained when the applied load was relatively close to zero but not exactly zero. This is because it was difficult to stop the grip at exactly zero value. The strip became unstable when the applied load is close to zero. The load could decrease very rapidly and buckling would occur. Therefore, the approximate strains are higher than the actual plastic strains.

4.2 Curve-fitting the Model Parameters

In addition to the assumed value of μ and $\alpha_x M$, the structural properties of fiber and bond in Table 4.3 also assumed the values obtained from literature. The paper stock density was measured and found to be 720 kg/m^3.

Table 4.3 Structural properties of fiber and bond.

Structural Fiber or Bond Parameter	Value
Average fiber length L_{av}	1 mm
Fiber width w_f	40x10^{-3} mm
Fiber thickness t_f	4x10^{-3} mm
Bond thickness t_b	0.4x10^{-3} mm
Fiber density ρ_f	1500 kg/m^3

4.2.1 Fiber Orientation Concentration Parameter κ

The first parameter to be determined was the fiber orientation concentration parameter κ. The mesoelement strain ε_s expression for the sample subjected to uniaxial load in the machine and cross-machine direction is reduced to equation 4.1 and 4.2 respectively. From continuum mechanics, equation 4.3 would govern the relationship between the two lateral contraction ratios, i.e. ν_{MD} and ν_{CD}, where ν_{MD} is the ratio of CD contraction over the MD stretch and ν_{CD} is the ratio of MD contraction over CD stretch.

In other words, ν is the ratio of lateral strain over the longitudinal strain and the subscript denotes the direction of the longitudinal strain.

$$\varepsilon_s = \varepsilon_{MD}\left(\cos^2\theta - \nu_{MD}\sin^2\theta\right) \qquad \textbf{(4.1)}$$

$$\varepsilon_s = \varepsilon_{CD}\left(\sin^2\theta - \nu_{CD}\cos^2\theta\right) \qquad \textbf{(4.2)}$$

$$\frac{\nu_{MD}}{\nu_{CD}} = \frac{E_{MD}}{E_{CD}} \qquad \textbf{(4.3)}$$

The sheet stress in the machine and cross-machine direction would then be given by equation 4.4 and 4.5 respectively.

$$\sigma_{MD} = \frac{\rho_s}{\rho_f}\int_{-\pi/2}^{\pi/2} E_f\,\varepsilon_{MD}\left(\cos^2\theta - \nu_{MD}\sin^2\theta\right)\left(1-\frac{\tanh aL}{aL}\right)\cos^2\theta\;\; f(\theta)\;\; d\theta \qquad \textbf{(4.4)}$$

$$\sigma_{CD} = \frac{\rho_s}{\rho_f}\int_{-\pi/2}^{\pi/2} E_f\,\varepsilon_{CD}\left(\sin^2\theta - \nu_{CD}\cos^2\theta\right)\left(1-\frac{\tanh aL}{aL}\right)\sin^2\theta\;\; f(\theta)\;\; d\theta \qquad \textbf{(4.5)}$$

The two equations above were divided by the sheet strains ε_{MD} and ε_{CD} respectively, to obtain the expressions for the sheet elastic modulus in equation 4.6 and 4.7.

$$E_{MD} = \frac{\sigma_{MD}}{\varepsilon_{MD}} = \frac{\rho_s}{\rho_f}\int_{-\pi/2}^{\pi/2} E_f\left(\cos^2\theta - \nu_{MD}\sin^2\theta\right)\left(1-\frac{\tanh aL}{aL}\right)\cos^2\theta\;\; f(\theta)\;\; d\theta \qquad \textbf{(4.6)}$$

$$E_{CD} = \frac{\sigma_{CD}}{\varepsilon_{CD}} = \frac{\rho_s}{\rho_f}\int_{-\pi/2}^{\pi/2} E_f\left(\sin^2\theta - \nu_{CD}\cos^2\theta\right)\left(1-\frac{\tanh aL}{aL}\right)\sin^2\theta\;\; f(\theta)\;\; d\theta \qquad \textbf{(4.7)}$$

For a sheet that is not affected by drying restraint effects, the fiber orientation would be the only cause of sheet anisotropy. The ratio of E_{MD}/E_{CD} is then a function of the fiber orientation concentration parameter κ and the lateral contraction ratios only.

$$\frac{E_{MD}}{E_{CD}} = \frac{\int_{-\pi/2}^{\pi/2} \left(\cos^2\theta - \nu_{MD}\sin^2\theta\right)\cos^2\theta \;\; f(\theta) \;\; d\theta}{\int_{-\pi/2}^{\pi/2} \left(\sin^2\theta - \nu_{CD}\cos^2\theta\right)\sin^2\theta \;\; f(\theta) \;\; d\theta} \tag{4.8}$$

The sheet elastic modulus E_{MD} and E_{CD} were then determined from the experimental data. They were found to have the value of 3.385 GPa and 1.622 GPa respectively, resulting in an E_{MD}/E_{CD} ratio of 2.09. The integrals in the ratio were evaluated numerically using the multiple application Simpson's 1/3 rule and equation 4.3 was applied in equation 4.8 to eliminate the need of fitting for ν_{CD}. The E_{MD}/E_{CD} ratios were calculated for different combinations of κ and ν_{MD} values, where $0.0 \leq \kappa \leq 1.0$ and $0.0 \leq \nu \leq 1.0$. The combinations were varied systematically and the resulting ratios from these combinations are shown in Figure 4.3 and Figure 4.4. These figures show that for an E_{MD}/E_{CD} ratio of 2.09, κ could take on any value between 0.50 and 0.70. Therefore, κ assumed the average value of 0.6, which corresponds to a lateral contraction ratio ν_{MD} of about 0.5.

4.2.2 Fiber Elastic Modulus and Bond Shear Elastic Modulus

The elastic region of the stress-strain curves from the conditioned samples was used to determine the fiber elastic modulus E_{f0} and the bond shear elastic modulus G_{b0}. Now that the fiber orientation concentration parameter κ has been determined, the only unknown parameters in the sheet elastic stress-strain curve would be E_{f0} and G_{b0} (cf. equation 4.4 and 4.5). Initially only the MD curves were used for curve-fitting the two parameters. For samples that were loaded in the machine direction, they were subjected to the boundary condition of $\sigma_{CD} = 0$.

For a given ε_{MD}, the lateral contraction ratio ν_{MD} was determined again using the false-position method with equation 4.5 until the boundary condition of $\sigma_{CD} = 0$ was met. Then, the MD elastic stress-strain curve was calculated for different combinations of E_{f0} and G_{b0}. The combinations of E_{f0} and G_{b0} were systematically varied for the range of 10 GPa $\leq E_{f0} \leq$ 20 GPa and 0.1 MPa $\leq G_{b0} \leq$ 100 MPa. The residuals, i.e. the difference between the fitted curve and experimental data, were squared and summed. The sum, denoted by S, decreases as E_{f0} increases and reaches a minimum at E_{f0} = 18 GPa. A contour plot of S as a function of E_{f0} and G_{b0} is shown in Figure 4.5. Although S continues to decrease as G_{b0} increases, the change in S is not significant and S plateaus off after G_{b0} has reached 10 MPa. Figure 4.6 shows a plot of S vs. G_{b0} at E_{f0} = 18 GPa. Therefore, E_{f0} was given the value of 18 GPa and G_{b0} of 15 MPa. The elastic MD curve generated with these elastic parameters corresponds to a ν_{MD} of 0.506. This agrees with the ν_{MD} that was previously determined together with the fiber orientation concentration parameter κ.

The elastic parameters obtained were tested on the CD stress-strain curves. Figure 4.7 shows the MD and CD linear elastic stress-strain curves for the sheets generated with these parameters. The predicted CD curve shows good agreement with the experimental data. The curve-fitting process was continued further with the bond yield stress and the bond second slope.

4.2.3 Bond Yield Stress, Bond Second Slope, and Hardening Parameters

When the nonlinearity of the sheet stress-strain curve was due to bond yielding while fiber remains elastic, the nonlinear sheet stress is dependent of the bond yield stress and the bond second slope only. When curve-fitting for τ_{p0} and G_{20}, the MD curves of the conditioned samples again were used. The experimental data were fitted for combinations of τ_{p0} and G_{20} in the range of 6 MPa $\leq \tau_{p0} \leq$ 10 GPa and 10 kPa $\leq G_{20} \leq$ 40 kPa respectively. The minimum S corresponds to τ_{p0} = 9 MPa and G_{20} = 30 kPa.

Once τ_{p0} and G_{20} were obtained, these parameters were tested and used to generate the CD stress-strain curve. The results shown in Figure 4.9 show that the predicted CD curve deviates significantly from the experimental data. The model under-estimated the CD curves and it is known that drying restraint in the machine direction has a more significant strengthening effect on the tensile properties in the machine direction. Therefore, this led to the conclusion that the humidifying process did not eliminate the drying restraint effects completely. Nevertheless, the values obtained thus far provide good initial estimates for the parameters. The bond plastic parameters were reduced and their corresponding hardening parameters were increased in a trial and error process until the predicted MD and CD curves matched the experimental data (cf. Figure 4.10). The bond plastic parameters now have the values of τ_{p0} = 6.5 MPa and G_{20} = 10 kPa . The corresponding hardening parameters were $H\tau_p$ = 2 and HG_2 = 70. The model parameters obtained and used in subsequent work are summarized in Table 4.4.

Table 4.4 Asymptotic fiber and bond model parameters used in modeling

Parameter	Values
κ	0.6
μ	0° (MD)
$\alpha_x M$, $\alpha_y M$	0.045, 0
ε_{xD}, ε_{yD}	0,0
E_{f0}	18 GPa
HE_{f0}	0
G_{b0}	15 MPa
HG_{b0}	0
τ_{p0}	6.5 MPa
$H\tau_{p0}$	2.0
G_{b2}	10 kPa
HG_{20}	70

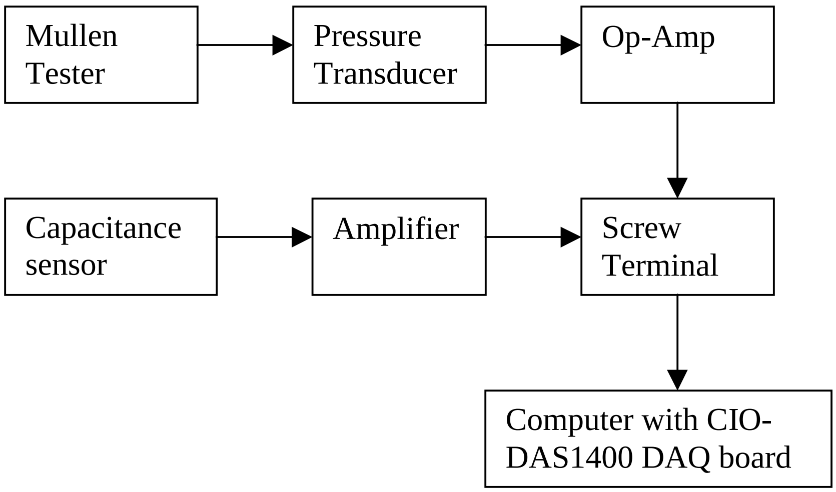

Figure 4.1 A schematic of the experimental setup used to measure the pressure-deflection curve of the paper sample.

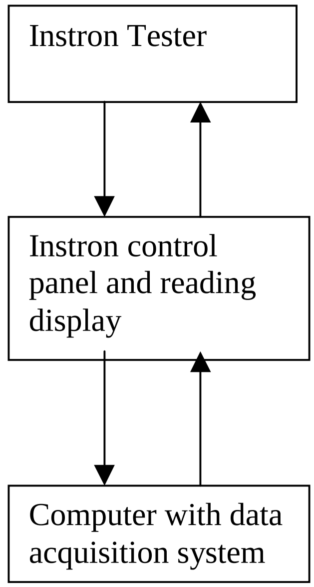

Figure 4.2 A schematic of the experimental setup used for tensile test.

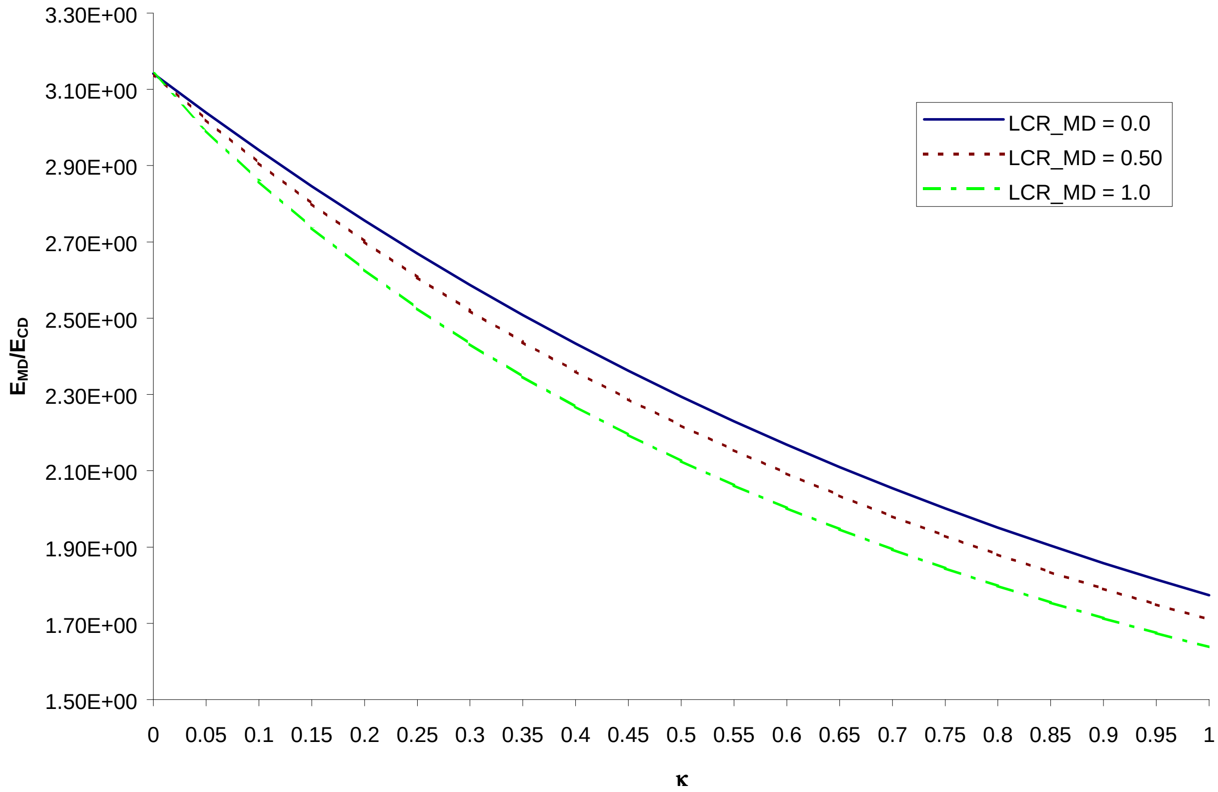

Figure 4.3 The E_{MD}/E_{CD} ratio was experimentally determined to be 2.08. E_{MD}/E_{CD} was calculated for $0.0 \leq \kappa \leq 1.0$ and $0.0 \leq \nu \leq 1.0$ to find the corresponding κ value.

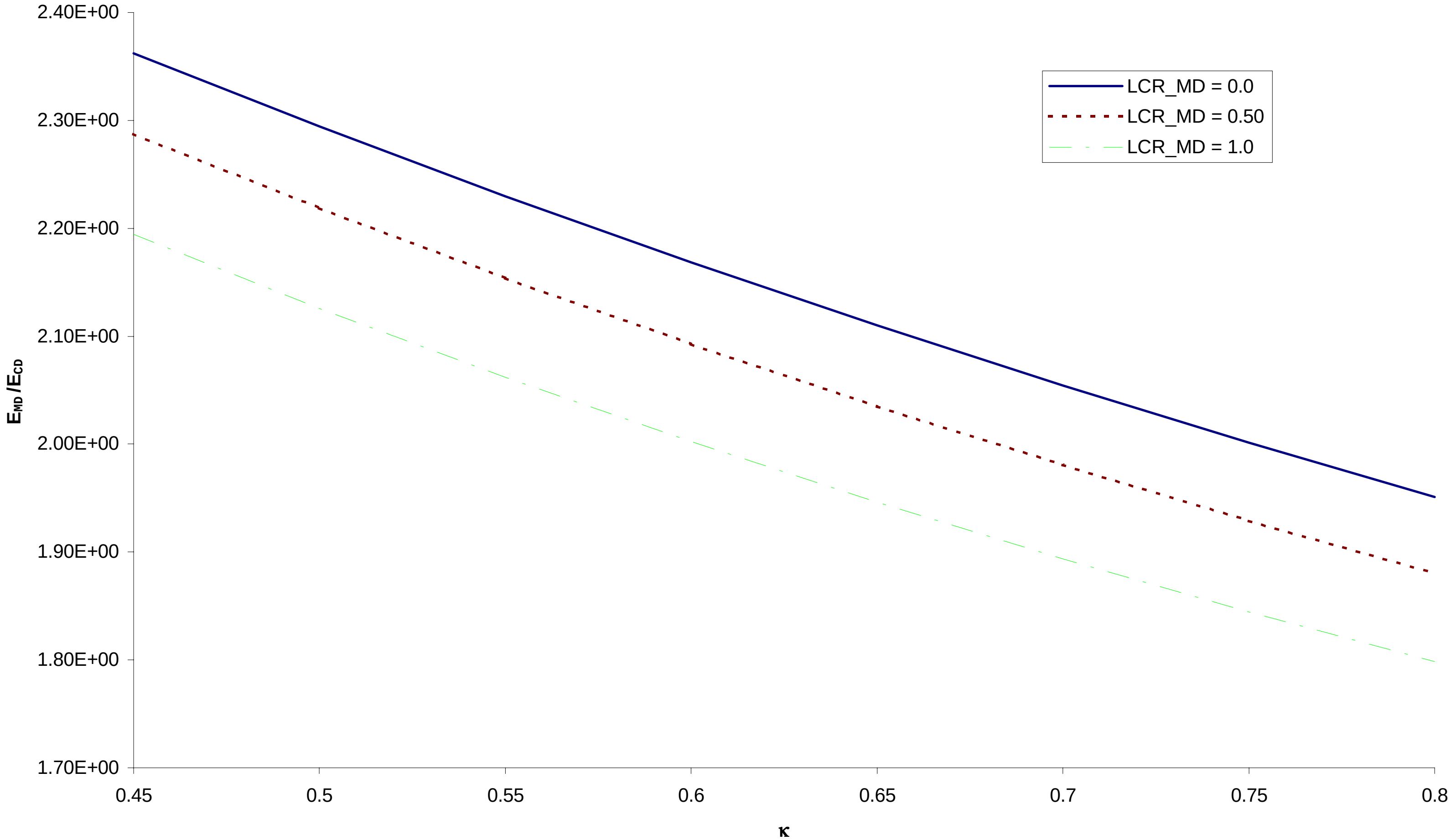

Figure 4.4 κ could range from about 0.5 to 0.7 for E_{MD}/E_{CD} to be 2.08. Therefore, an intermediate value of 0.6 was assumed for κ.

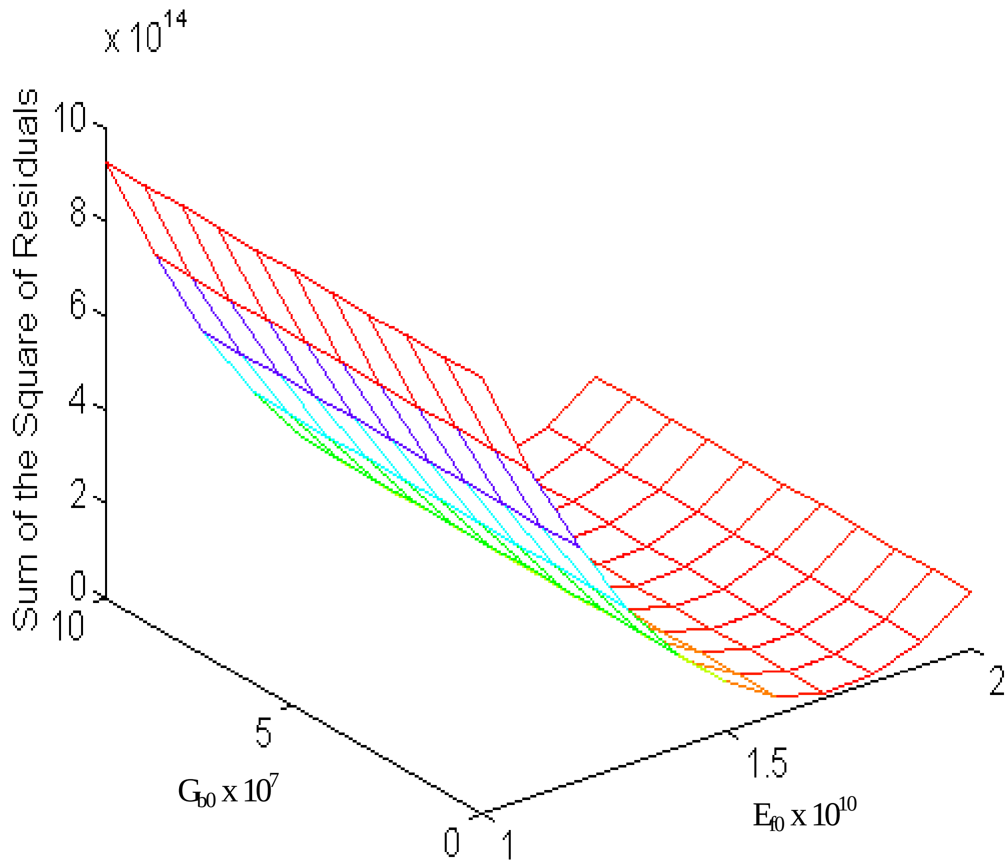

Figure 4.5 The linear elastic region of the MD curves were fitted using 10 GPa ≤ E_{f0} ≤ 20 GPa and 0.1 MPa ≤ G_{b0} ≤ 100 MPa. The sum of the square of residuals is minimum at E_{f0} = 18 GPa.

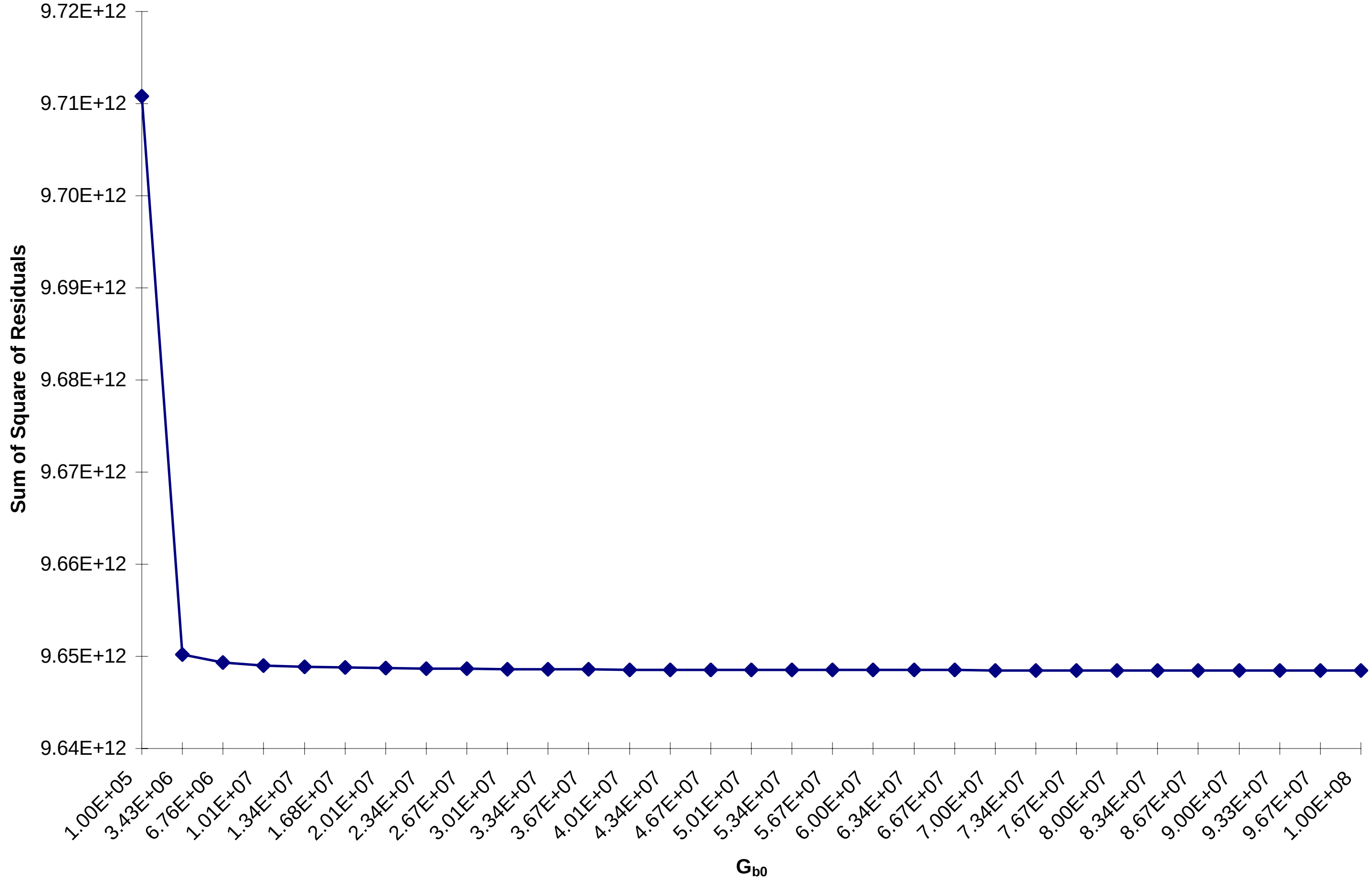

Figure 4.6 The decrease in S is less significant after G_{bo} = 10 MPa.

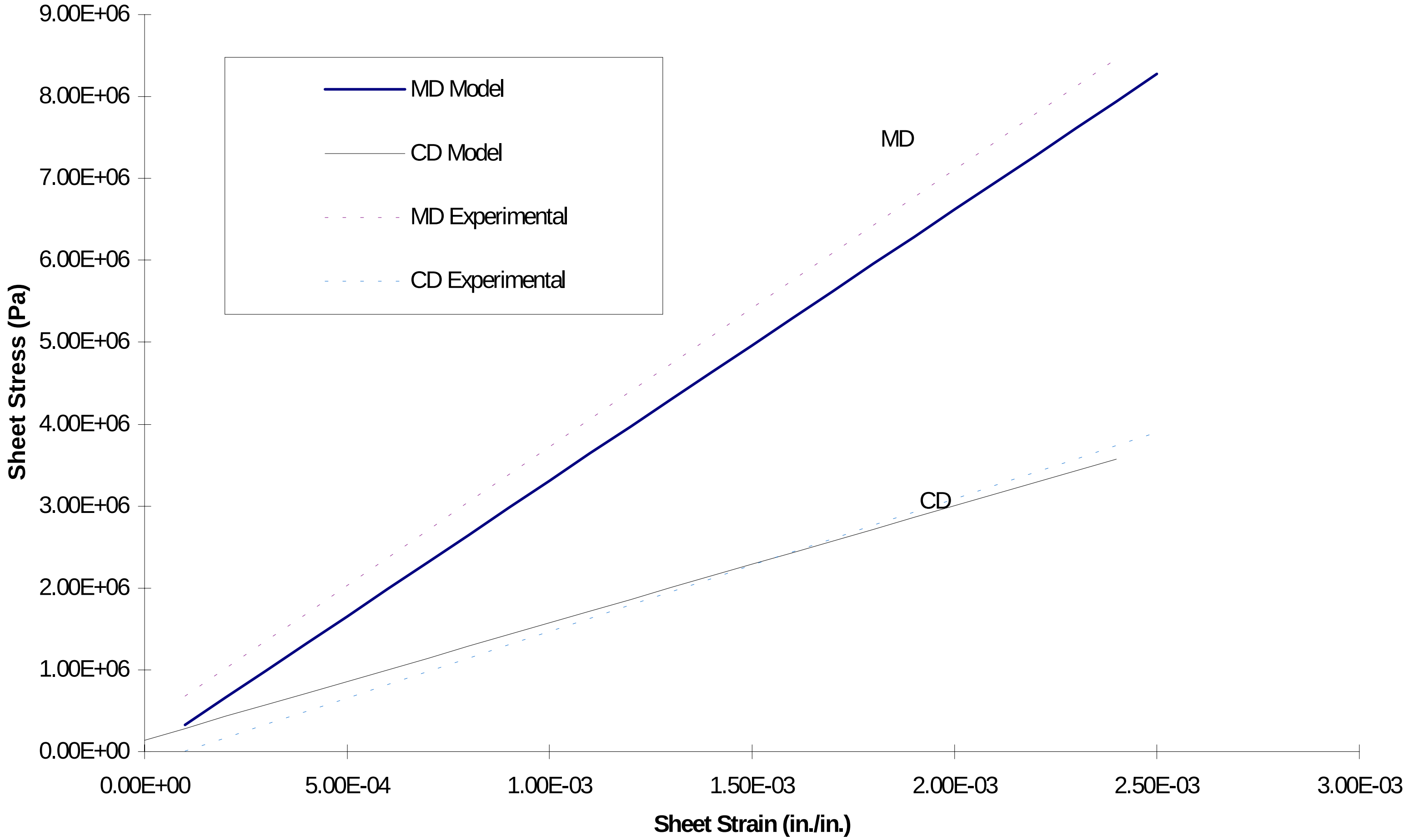

Figure 4.7 Model generated MD and CD stress-strain curves where ρ_s = 630 kg/m3, κ = 0.60, E_{f0} = 17 GPa, and G_{b0} = 15 MPa. Assuming no drying restraint effects.

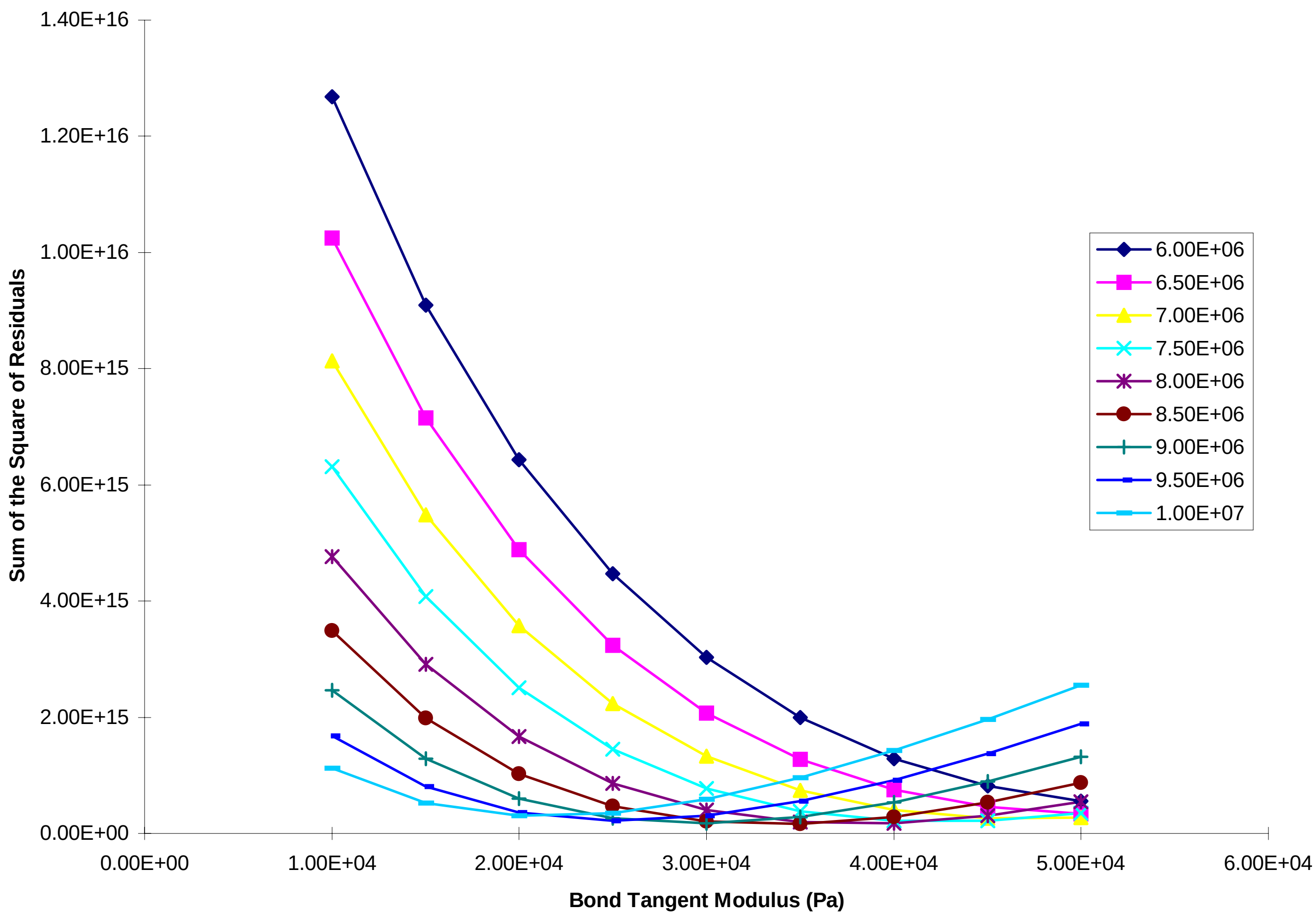

Figure 4.8 The MD curves were fitted using 6 MPa ≤ τ_{p0} ≤ 10 GPa and 10 kPa ≤ G_2 ≤ 40 kPa. E_{f0} and G_{b0} were set at 17 GPa and 15 MPa respectively.

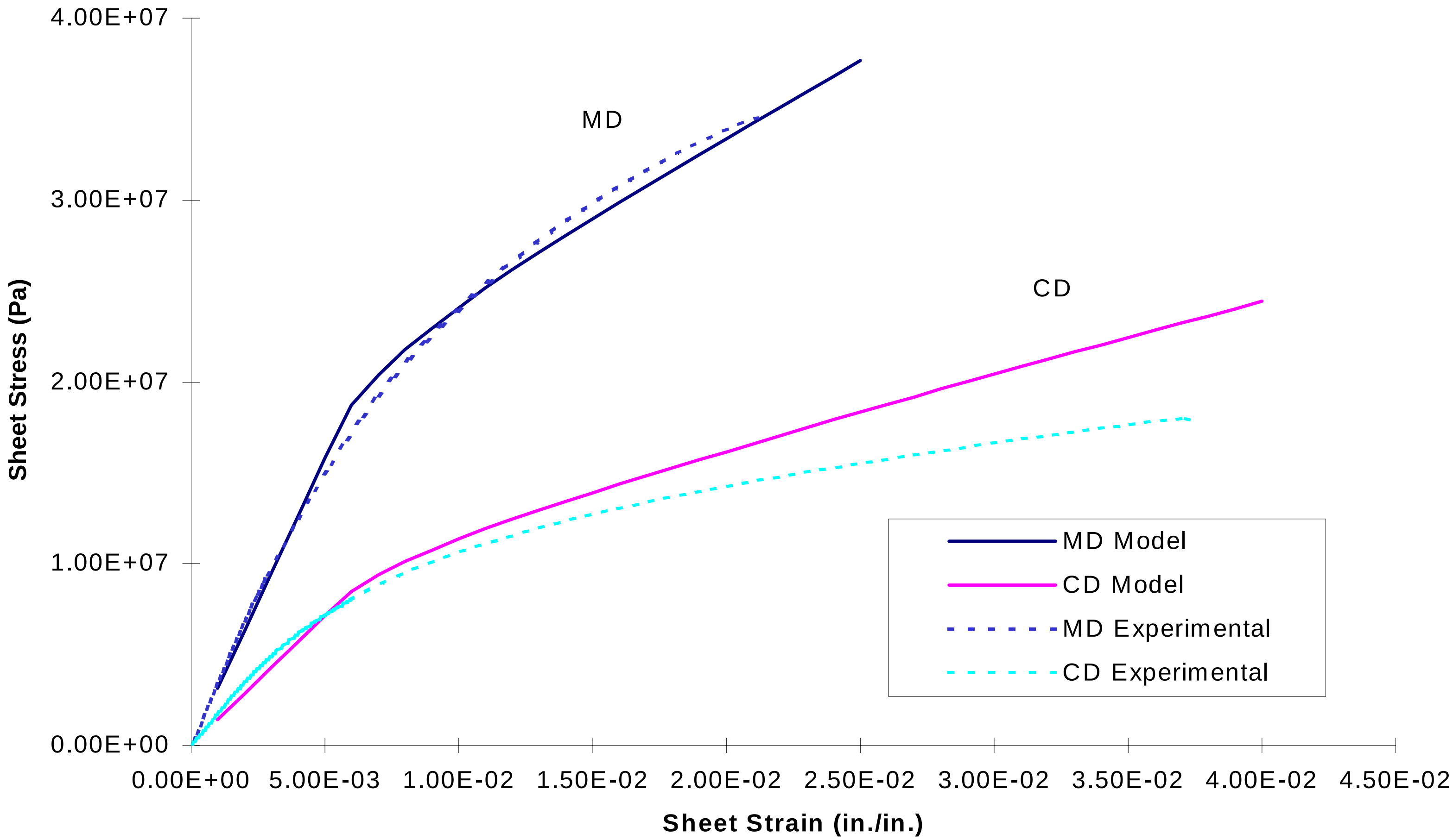

Figure 4.9 Model generated MD and CD stress-strain curves where ρ_s = 630 kg/m3, κ = 0.60, E_{f0} = 17 GPa, G_{b0} = 15 MPa, τ_{p0} = 9 MPa, and G_{20} = 30 kPa. Assuming no drying restraint effects.

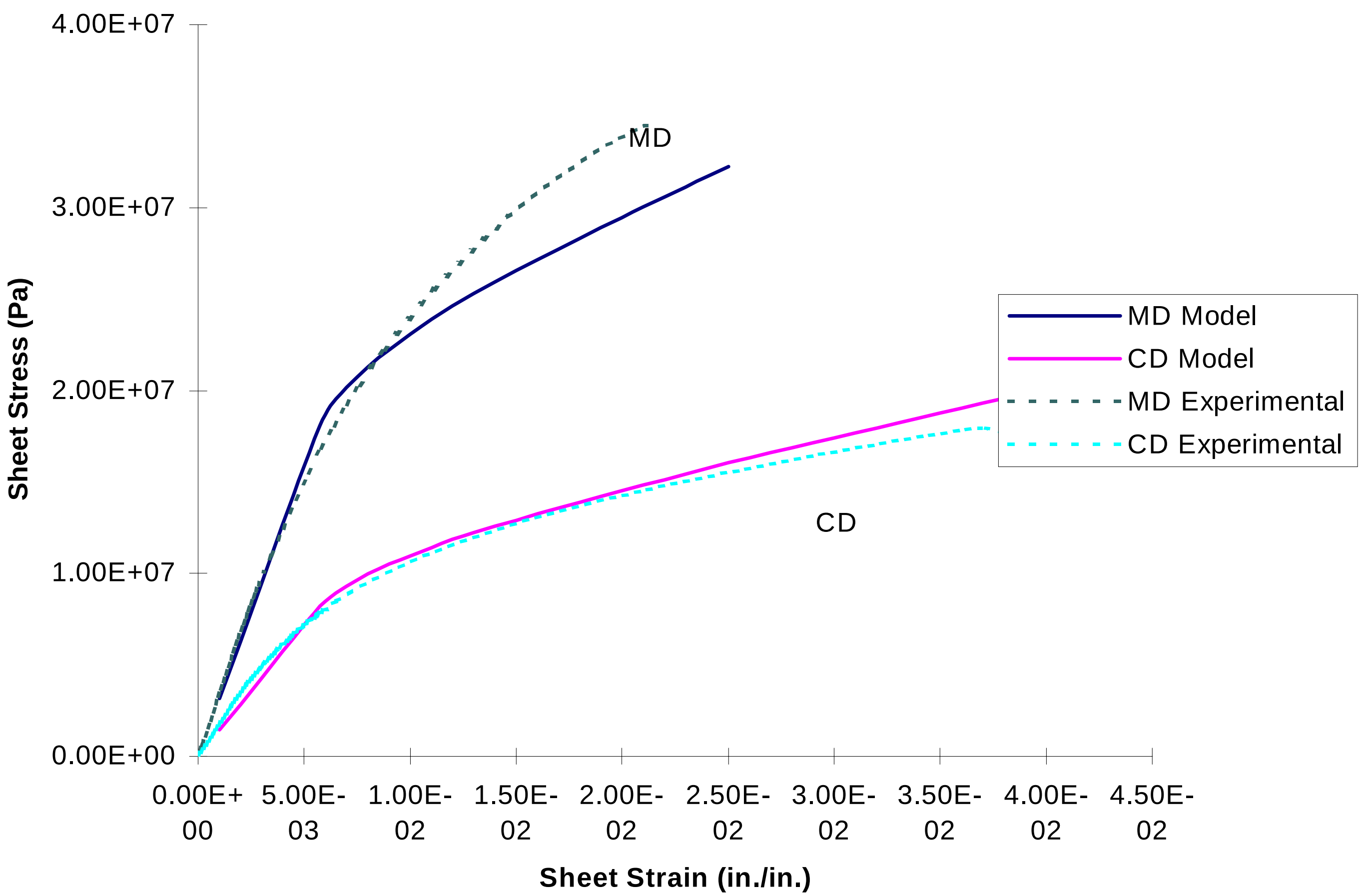

Figure 4.10 Model generated MD and CD stress-strain curves using parameters in Table 4.4.

5. Results

5.1 Uniaxial Tensile Test

In ABAQUS, nonlinear equilibrium problems are solved using the Newton's method. For static stress/displacement analysis using the *STATIC option, an initial time increment and a time period of the analysis are given by the user. After the first time step, an automatic step size increment scheme is used in the analysis to optimize computational efficiency, unless otherwise specified by the user. The solution obtained from finite element analysis using the continuum model based one incremental asymptotic fiber and bond mode over-predicted the nonlinear sheet stress in Sinha (1994). The source of discrepancy was unknown then but it was suspected to be numerical in nature. In this work, the source was found to be inappropriately large time step near the yield point of the sheet.

Figure 5.3 and Figure 5.4 show the stress-strain curves obtained from the extended asymptotic fiber and bond model, for the uniaxial loading and unloading process of the 1 inch x 7 inch sample. The parameter values in Table 4.4 were used. The uniaxial tensile tests were conducted in the machine and cross-machine direction. Five sets of experimental data were collected for each direction. The final displacements before and after unloading obtained in these ten sets of data are shown in Table 5.1. The MD and CD loading curves were generated with the micromechanics model until the two curves reached their respective average strains shown in Table 5.2. Then, the unloading curves were generated until zero applied stress was reached. The model prediction corresponds well with the experimentally obtained data.

For the MD curve, the final/plastic strain after unloading obtained from the model was 8.45×10^{-3} m/m. Compare to the average value obtained from the experimental data, the discrepancy is about 10.77%. For the CD curve, the final/plastic strain obtained from the model was 2.04×10^{-2} m/m. Compare to the average value obtained from the experimental data, the discrepancy is about 0.48%. Since the plastic strain was obtained when the applied load was decreased until close to zero but not completely zero, the higher values in the experimentally obtained plastic strains was expected (cf. 4.1.2). The discrepancy is also compounded by less than perfect choice of parameter values. Despite these, the overall model prediction was still satisfactory.

The continuum model based on incremental asymptotic fiber and bond model was also used to generate the same stress-strain curves in ABAQUS. In order to eliminate convergence as the source of the discrepancy between the micromechanics solution and finite element solution, the MD stress-strain curve was generated using a 1-element, 50-element, and 100-element finite element model. The type of element used was a 4-node bilinear plane stress element (CPS4). Each node of this element has two degrees of freedom, i.e. u_x and u_y. The nodes on the left boundary were constrained in the two degrees of freedom while the right boundary was displaced (cf. Figure 5.5) by the amount of the average MD displacement in Table 5.1, i.e. 3.120 x 10^{-3}m. For unloading, the right boundary was displaced in the opposite direction until the average displacement at unloading was reached, i.e. 1.752 x 10^{-3}m.

The results of the center element on the right boundary (element 48 in the 50-element model and element 98 in the 100-element model) were used to obtain the stress-strain curves. A contour plot of the stress and strain distribution shows higher stress concentration around the restrained left boundary. The stress distribution grew uniform when moved away from the restrained edge (cf. Figure 5.6 and Figure 5.7). The results obtained from the 1-element, 50-element, and 100-element model showed similar over-prediction in the nonlinear region. Therefore, convergence was ruled out as the cause of discrepancy. The automatic time step increment scheme was used in these analyses in ABAQUS. Upon closer inspection, it was observed that the time step increment grew larger as the elastic curve approached the yield point. The large time/strain increment applied to the last point in the elastic region results in the large stress increment into the nonlinear region. Therefore, the predicted yield point greatly exceeded the actual value, thus giving a considerably higher starting point for the nonlinear region. The discrepancy between the finite element solution and micromechanics solution was eliminated when a smaller time step was used (cf. Figure 5.8).

Recall that (cf. 4.1.2) the plastic strains at unloading were approximate value obtained when the applied stress was close to zero but not zero. The finite element solution reflects this approximation. When the right boundary was displaced to the average value of 1.692 x 10^{-3} m, the sheet stress was not zero. The unloading path from the finite element analysis closely approximates the unloading path obtained from the micromechanics model. Therefore, the plastic strain at zero stress that could be obtained from the finite element analysis by further displacing the right boundary to the left, would not differ significantly from the micromechanics solution.

Table 5.1 Final displacements before and after unloading in the uniaxial tensile tests.

Sample	**Final Displacement Prior to Unloading**		**Final Displacement After Unloading**	
	(inch)	(m)	(inch)	(m)
MD 1	0.1219	3.096 x 10^{-3}	0.062	1.575 x 10^{-3}
MD 2	0.1220	3.099 x 10^{-3}	0.068	1.727 x 10^{-3}
MD 3	0.1232	3.129 x 10^{-3}	0.066	1.676 x 10^{-3}
MD 4	0.1233	3.132 x 10^{-3}	0.068	1.727 x 10^{-3}
MD 5	0.1237	3.142 x 10^{-3}	0.069	1.752 x 10^{-3}
Average	0.1228	3.120 x 10^{-3}	0.067	1.692 x 10^{-3}
CD 1	0.2023	5.138 x 10^{-3}	0.147	3.73 x 10^{-3}
CD 2	0.2036	5.171 x 10^{-3}	0.142	3.61 x 10^{-3}
CD 3	0.2040	5.182 x 10^{-3}	0.144	3.66 x 10^{-3}
CD 4	0.2026	5.146 x 10^{-3}	0.146	3.71 x 10^{-3}
CD 5	0.2017	5.123 x 10^{-3}	0.145	3.68 x 10^{-3}
Average	0.2028	5.152 x 10^{-3}	0.145	3.68 x 10^{-3}

Table 5.2 Final strains before and after unloading in the uniaxial tensile tests

Sample	Final Strain Before Unloading (m/m)	Final Strain After Unloading (m/m)
MD 1	0.01726	8.818 x 10^{-3}
MD 2	0.01728	9.667 x 10^{-3}
MD 3	0.01745	9.384 x 10^{-3}
MD 4	0.01746	9.667 x 10^{-3}
MD 5	0.01752	9.809 x 10^{-3}
Average	0.01739	9.469 x 10^{-3}
CD 1	0.02849	2.078 x 10^{-2}
CD 2	0.02867	2.008 x 10^{-2}
CD 3	0.02873	2.036 x 10^{-2}
CD 4	0.02853	2.064 x 10^{-2}
CD 5	0.02841	2.050 x 10^{-2}
Average	0.02857	2.048 x 10^{-2}

5.2 Burst Test

In addition to the one-dimensional problem of uniaxial tensile test, the unloading model would also be tested in a two dimensional problem. The model would be used to predict the central deflection of a sample undergoing a burst test (which is not carried to failure) and then unloaded. The same paper cup stock was used in the experiment carried out on a Mullen tester (cf. Figure 4.1), which was equipped with a pressure transducer.

Eight samples were tested for their burst strength and the value range from 9.4 kg/cm^2 to 13.3 kg/cm^2. The voltage output for this range of pressure was in the hundreds of millivolts. This was too small for the data acquisition system, which measures voltage from 0 to 10 V. Therefore, an op-amp, which provide a gain of 37, was built to amplify the output voltage from the pressure transducer. Other than that, inspection with an oscilloscope also showed that the output signals from the pressure transducer fluctuate significantly. Therefore, an averaging function was added to the data acquisition program written in LabTech. The averaged output voltage from the op-amp gave the same reading as the output voltage measured using a multimeter.

The measurement of the central deflection of the sample presents a difficulty in the experimental process. This is mainly due to the limited space available above the sample and under the three-legged clamp. In the end, a capacitance sensor (HPB-500 Button Probe, Capacitec) measuring 0.5 inch in outer diameter was used in the measurement process. A ½ inch x ½ inch metal target was placed onto each sample using double sided adhesive tape. The output voltage of the capacitance sensor changes with the distance between the sensor and the target.

The amplified output voltage of the pressure transducer and the output voltage from the capacitance sensor are supplied to a CIO-DAS1400 DAQ board (Computer Boards, Inc.) and read using LabTech. The output signal of the pressure transducer varies linearly with the applied pressure (cf. Figure 5.1). The calibration equation for the amplified pressure transducer signals is pressure (kg/cm^2) = 0.036345 + [0.757366 x voltage (V)]. The output signal of the capacitance sensor is linear only with a limited range (cf. Figure 5.2) and the calibration equation in this region is given by distance (inch) = 0.008387 + [0.078428 x voltage (V)].

In the experimental work, the sample was clamped onto the Mullen tester and a sample area of 3.0 cm in diameter was subjected to the applied pressure. The area was modeled with 96 shear deformable shell elements. The innermost ring was made up of 6-node triangular thin shell elements (STRI65), while the rest were 8-node doubly curved thin shell elements (S8R5). The boundary of the model was constrained in the displacement degrees of freedom only, i.e. u_x, u_y, and u_z. Although the sample was clamped down during the test, the rotational degrees of freedom were not restrained in the finite element analysis because the sample is flexible and thin enough to bend at the clamped edge. In addition, finite element analysis performed for sample that was modeled with only the displacement degrees of freedom constrained, showed higher stress concentration in the center of the sample (cf. Figure 5.10 and Figure 5.11). Samples that were modeled with both the displacement and rotational degrees of freedom constrained showed higher stress concentration at the boundary edge (cf. Figure 5.12 and Figure 5.13). Since the sample always burst in the center in the shape of the letter 'H' (cf. Figure 5.14), the results of the later would not be consistent with experimental observation because the samples do not fail at the edge.

For the shell elements used in ABAQUS, i.e. STRI65 and S8R5, the shear elastic modulus are needed to calculate the transverse shear stiffness. Since the asymptotic fiber and bond model does not predict these properties, experimental values obtained using the ultrasonic technique by Baum (1981) were used. The experimental result showed that for the coated paper cup stock used in this work, $G_{CD\text{-}ZD}$ = 0.109 GPa and $G_{MD\text{-}ZD}$ = 0.119 GPa. The corresponding transverse stiffness are given by

$$k_{11}^{ts} = \frac{5}{6}G_{13}t\ ,\ k_{22}^{ts} = \frac{5}{6}G_{23}t\ \text{, and}\ k_{12}^{ts} = 0.0$$

respectively. The average thickness of the sample measured was 0.48 mm. Therefore, k_{11} = 49.5 N/m and k_{12} = 45.3 N/m.

The first analysis was on a sample subjected to a uniformly applied pressure of 0.72 MPa before unloading. The analysis was also repeated for an applied pressure of 0.54 MPa, 0.51 MPa, and 0.49 MPa. The results are shown in Figure 5.15 to Figure 5.18. Despite the over-prediction over the finite element solution, the results were thought to agree well with the experimental data. The over-prediction could be caused by unsuitable model parameters that could be remedied by improving the fit of the experimental data from the uniaxial tests. In addition, the paper cup was coated with polyethlyne, which changes the bending characteristics of the material. Table 5.3 shows the measured burst pressure of the paper cup stock. The burst pressure for sample whose coated surface was subjected to the applied pressure dominated the lower spectrum of the burst pressure. The pressure was applied to the surface that was not coated when the pressure-displacement data used in this work was collected.

Table 5.3 Pressure at burst of paper cup stock.

Surface Subjected to Applied Pressure	Sample	Pressure at Burst (kg/cm^2)
Coated	1	10.3
Coated	2	11.1
Coated	3	13.2
Coated	4	9.4
Not coated	5	12.0
Not coated	6	12.7
Not coated	7	13.3
Not coated	8	11.1

The experimentally obtained pressure-displacement curves show a step increase before 0.1 MPa. The specific cause of this step increase is unclear at this point. Initially, it was speculated that the metal target of the capacitance sensor, which was placed onto the sample surface with a double-sided adhesive tape, may have strengthened the sample surface. As the applied pressure increased, the sample surface began to stretch, eventually to a point where the adhesive tape also started stretching. As a result, additional pressure was needed to stretch the adhesive tape together with the sample. Hence, the sudden increase in the applied pressure.

Therefore, several samples were tested without the metal target. After the pressure has been applied and the sample has deformed, only then the metal target was placed onto the sample to measure the displacement. The displacements obtained do not show significant difference from the displacements collected with the metal target adhered to the sample.

It was observed during the experimental process that the applied pressure increased slowly initially. Once the sample started to bulge, the applied pressure would increase at a faster rate. It was also noticed that the sudden pressure increase occurs at about the same point in very curve. Since displacements of deformed samples measured, using a caliper, show similar results with the values obtained with the capacitance sensor, any error the unexplained pressure increase may have caused would not be significant.

The unloading model has shown promising results in the one-dimensional and two-dimensional application. Although in some cases, the model predictions over-estimated the experimental values, the discrepancy is considered tolerable after taking into consideration of the spread in the mechanical properties/behavior of paper material.

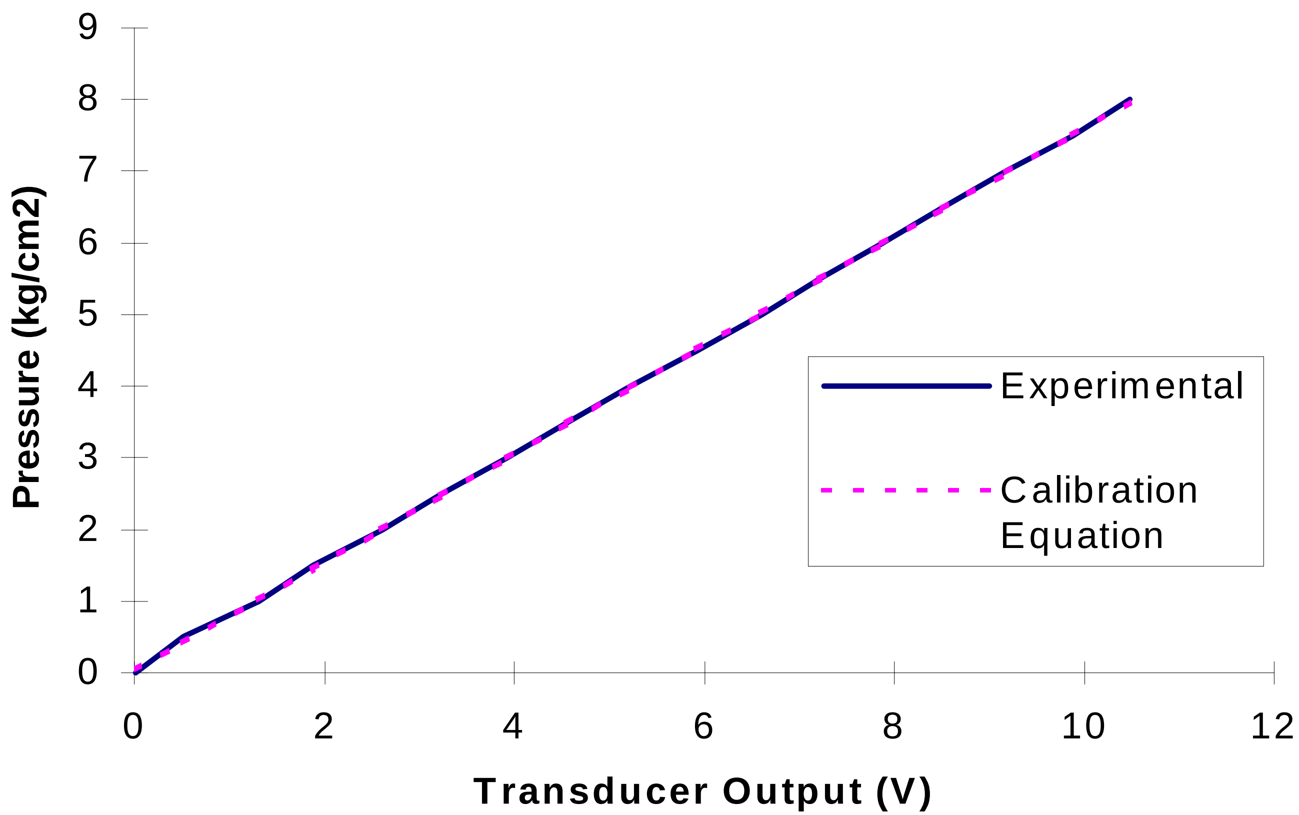

Figure 5.1 Calibration curve for the amplified output signals from the pressure transducer. The original voltage signal was amplified with an op-amp with a gain of about 37.

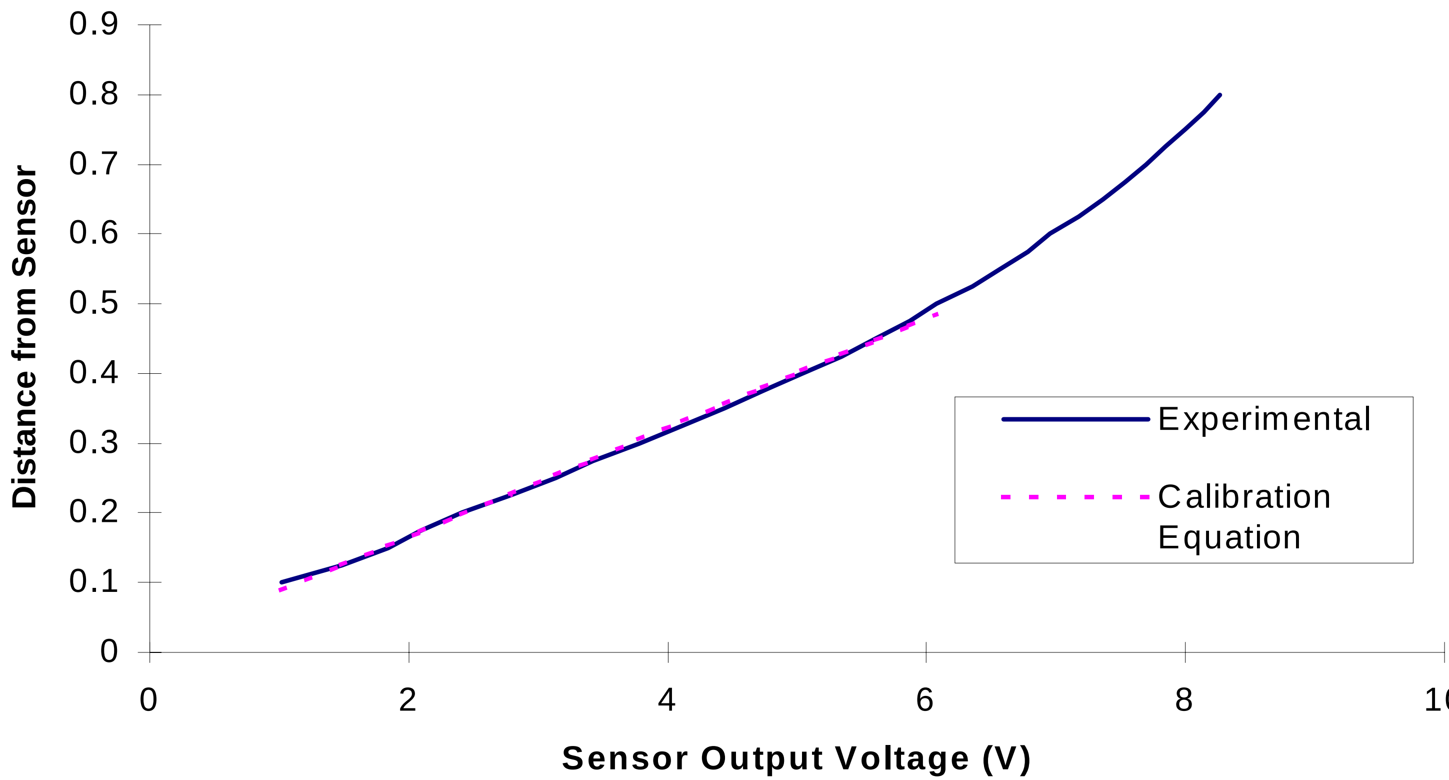

Figure 5.2 Calibration curve of the capacitance sensor used to measure the central displacement of the sample in a burst test.

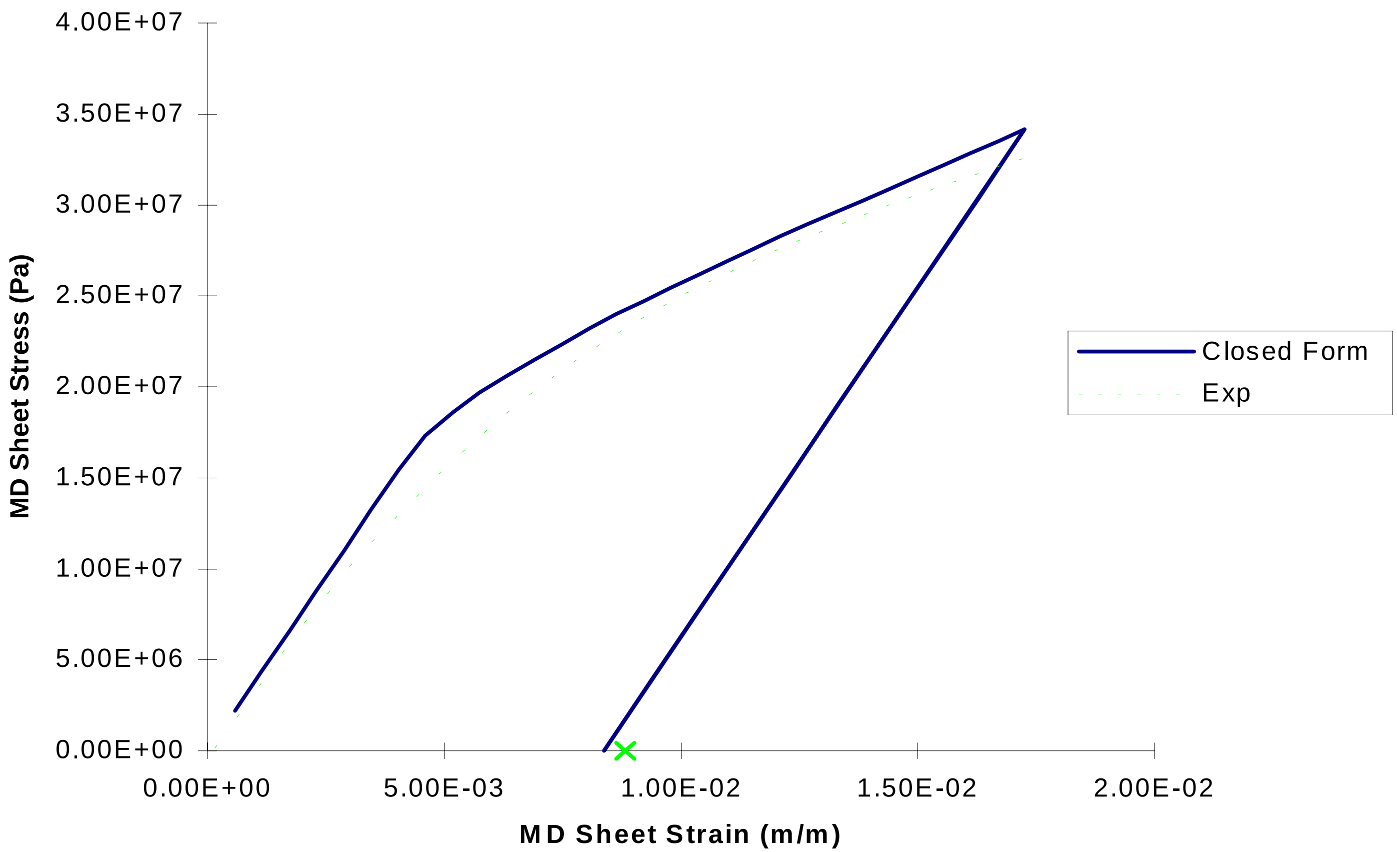

Figure 5.3 MD stress-strain curves from micromechanics model for the 1 inch x 7 inch sample during loading and unloading.

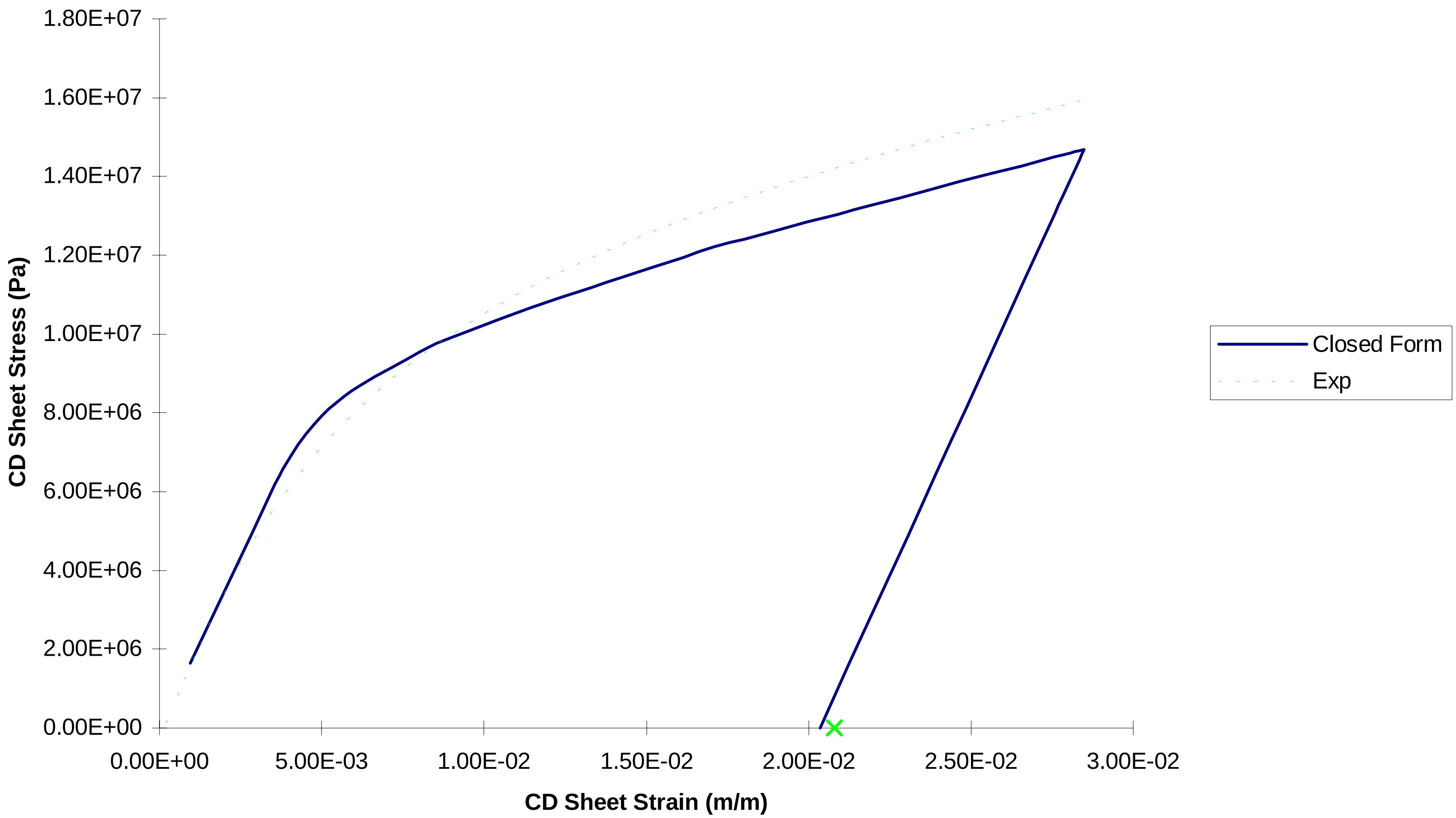

Figure 5.4 CD stress-strain curves from micromechanics model for the 1 inch x 7 inch sample during loading and

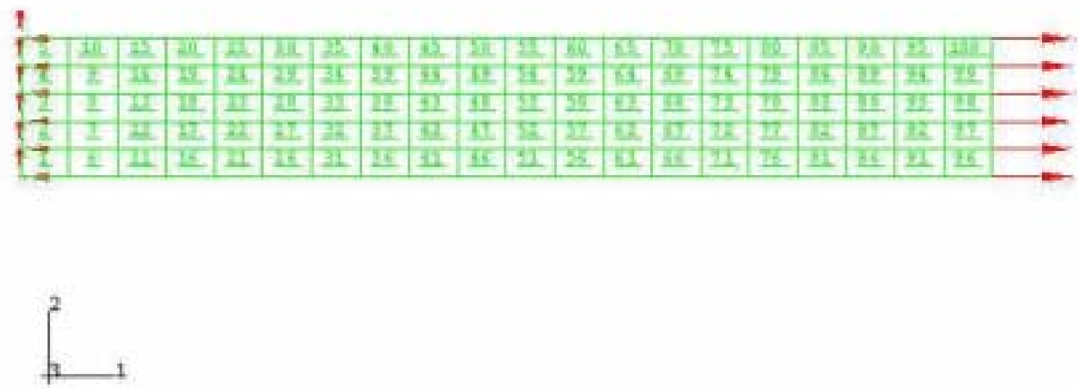

Figure 5.5 The tensile test sample was modeled with 100 4-node bilinear plane stress elements in ABAQUS. The left boundary nodes were constrained in their displacement degrees of freedom, while the right boundary nodes were displaced by the average value obtained experimentally.

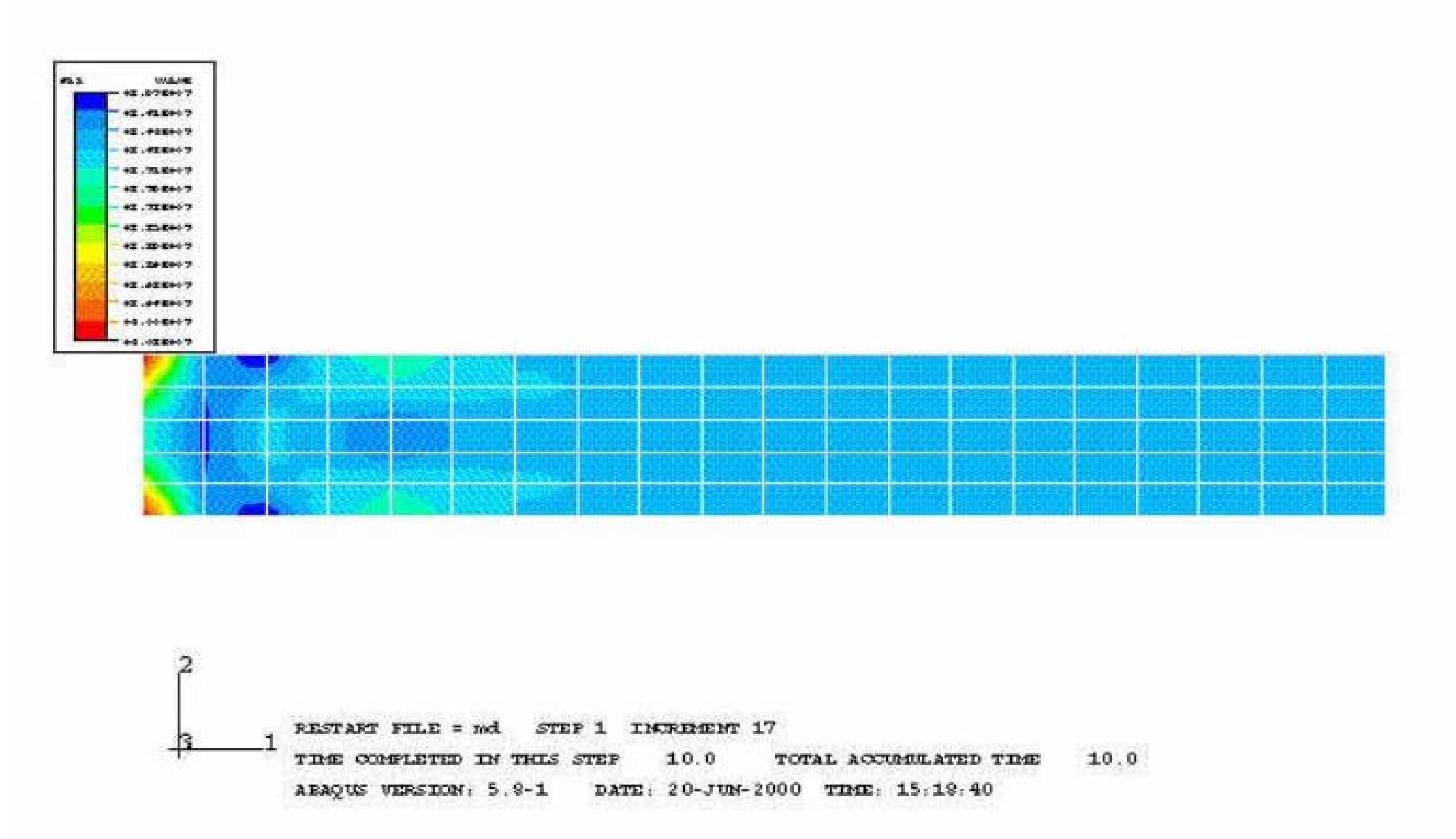

Figure 5.6 σ_{MD} in the 100-element model when loaded. (The right boundary nodes were displaced by 3.120 x 10^{-3} m to the right.)

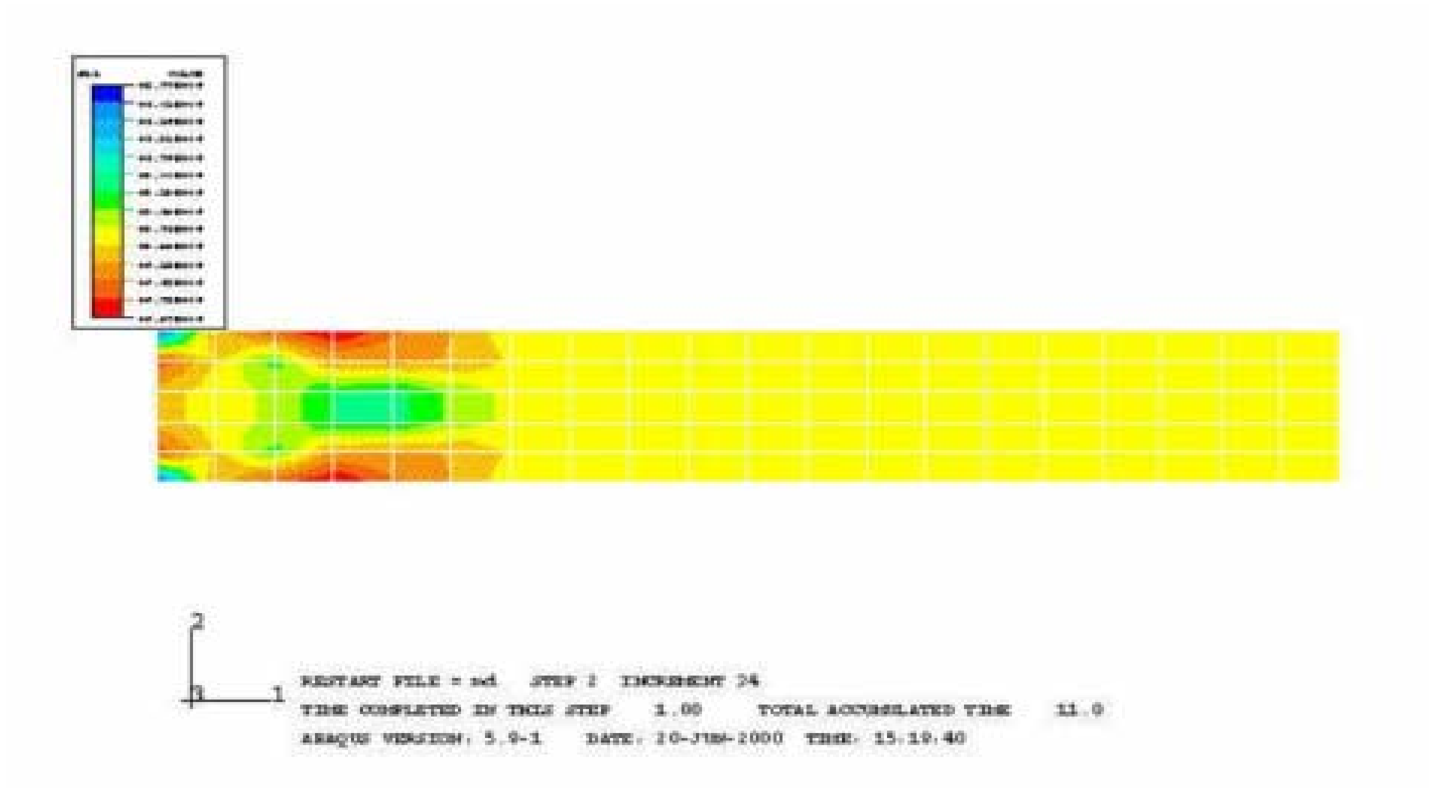

Figure 5.7 σ_{MD} in the 100-element model when unloaded (the right boundary nodes were displaced by 1.692 x 10-3 m to the left).

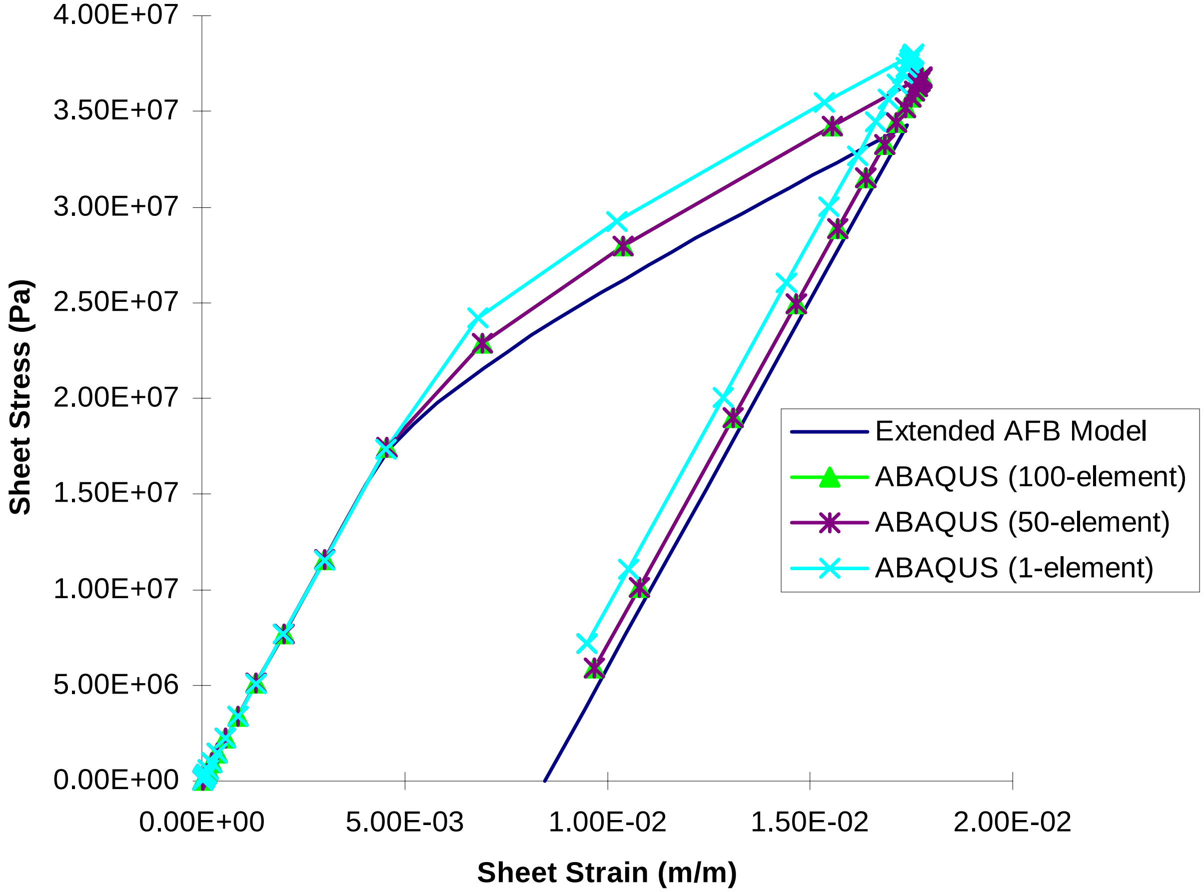

Figure 5.8 MD loading-unloading stress-strain curves for the 1 inch x 7 inch sample. The FEA solution was obtained using the automatic time step increment scheme in ABAQUS.

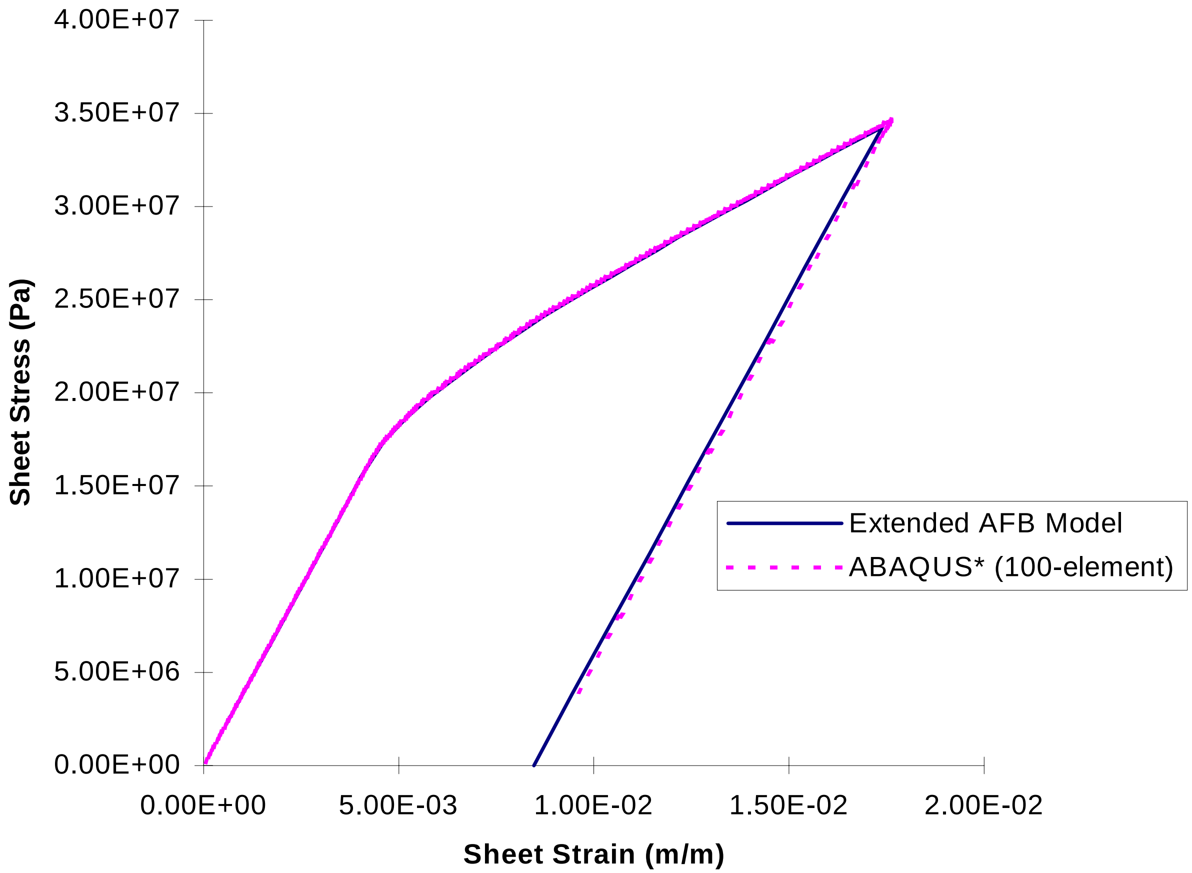

Figure 5.9 The FEA*(100-element model) solution was obtained with a constant step size in ABAQUS.

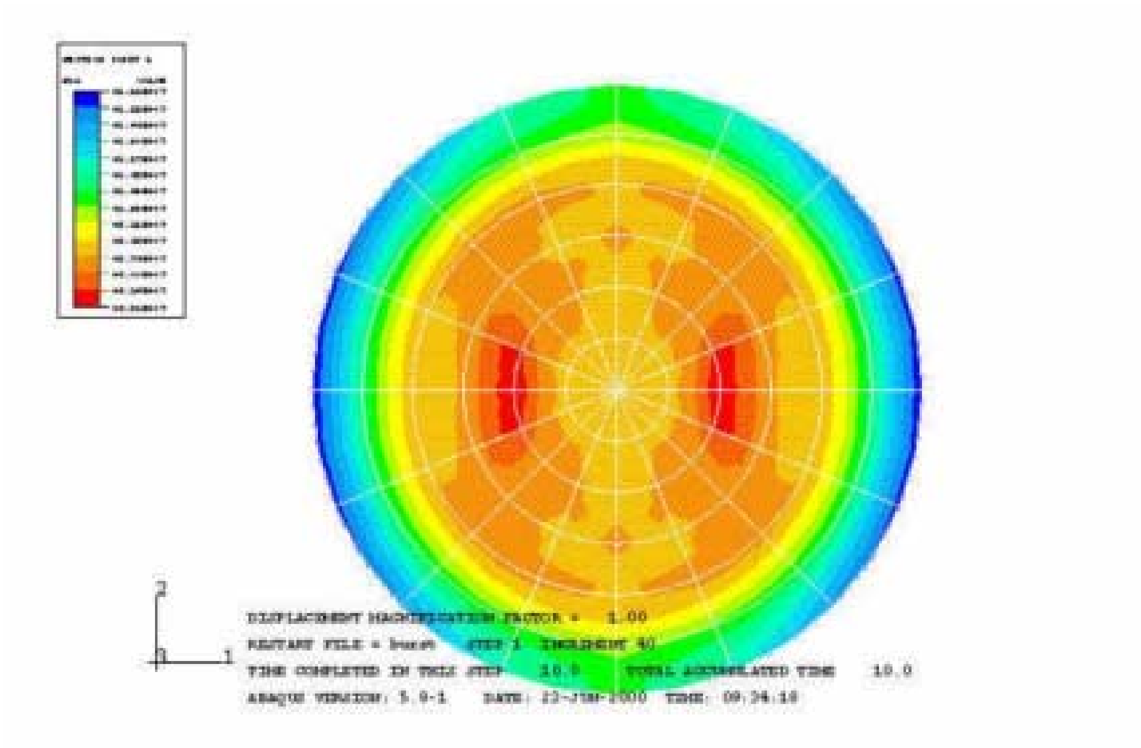

Figure 5.10 σ_{MD} of sample in burst test at P = 0.72MPa. The displacement degrees of freedom were constrained at the boundary.

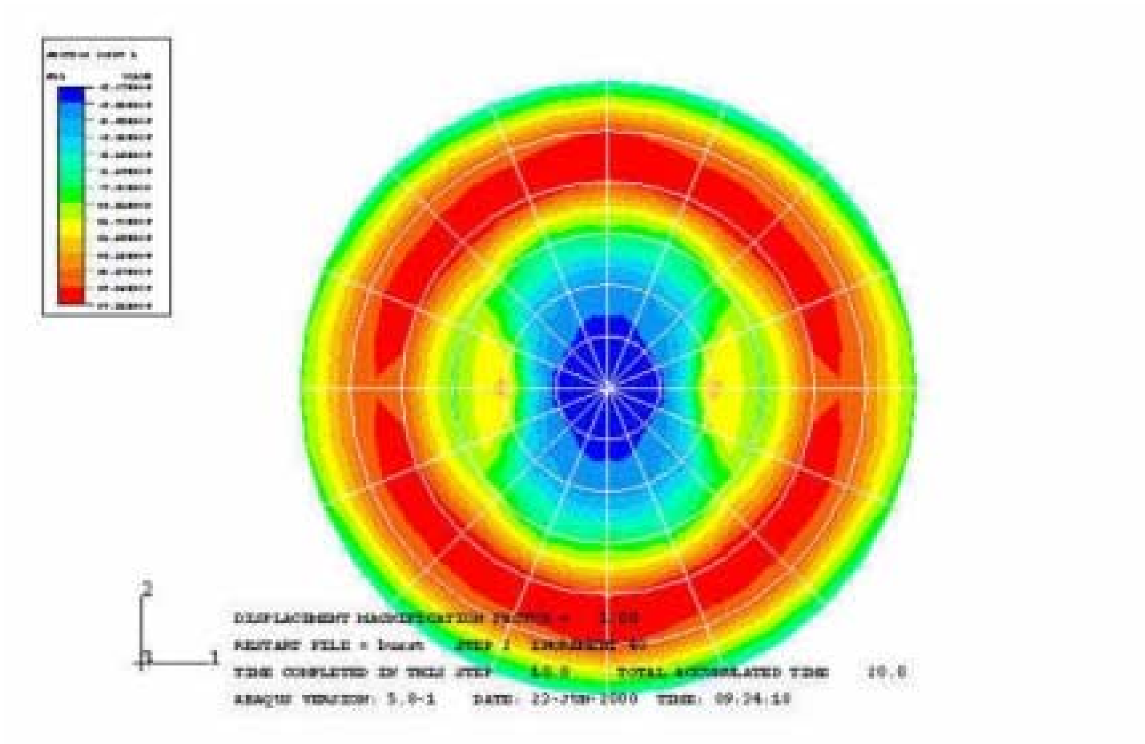

Figure 5.11 σ_{CD} of sample in burst test at P = 0.72MPa. The displacement degrees of freedom were constrained at the boundary.

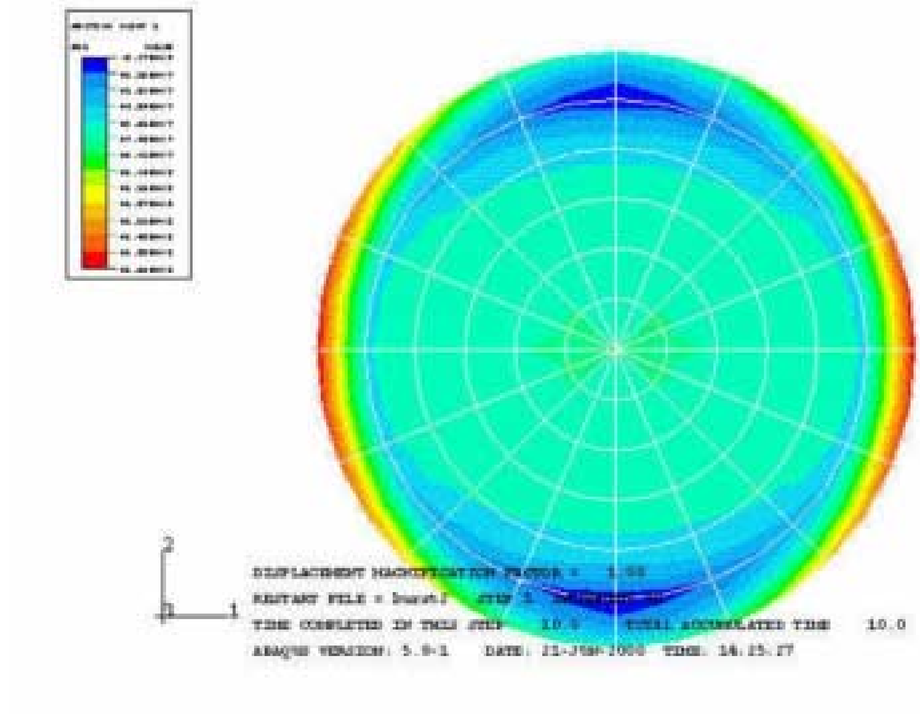

Figure 5.12 σ_{MD} of sample in burst test at P = 0.72MPa. The displacement and rotational degrees of freedom were constrained at the boundary.

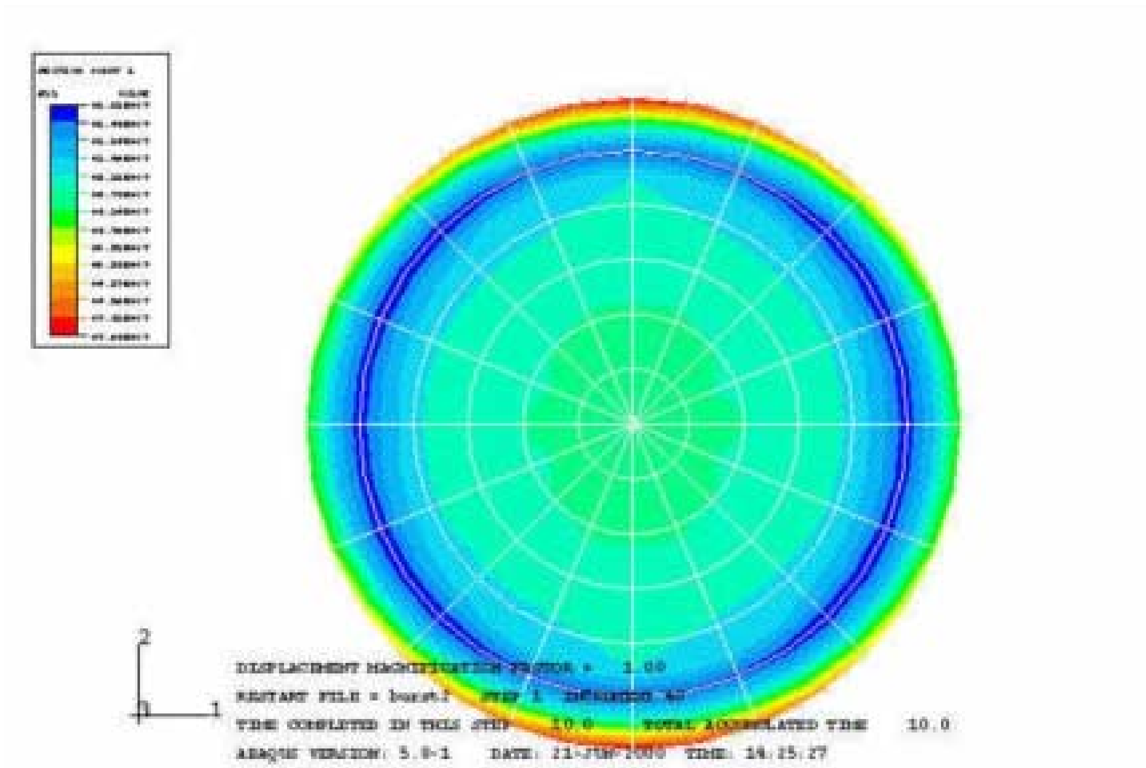

Figure 5.13 σ_{CD} of sample in burst test at P = 0.72MPa. The displacement and rotational degrees of freedom were constrained at the boundary.

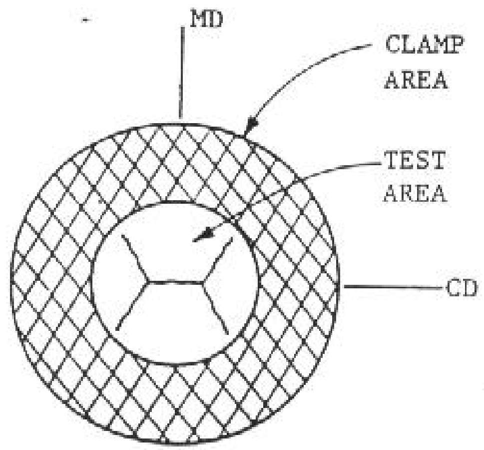

Figure 5.14 In a burst test, the sample generally failed at the center in the shape of the letter H.

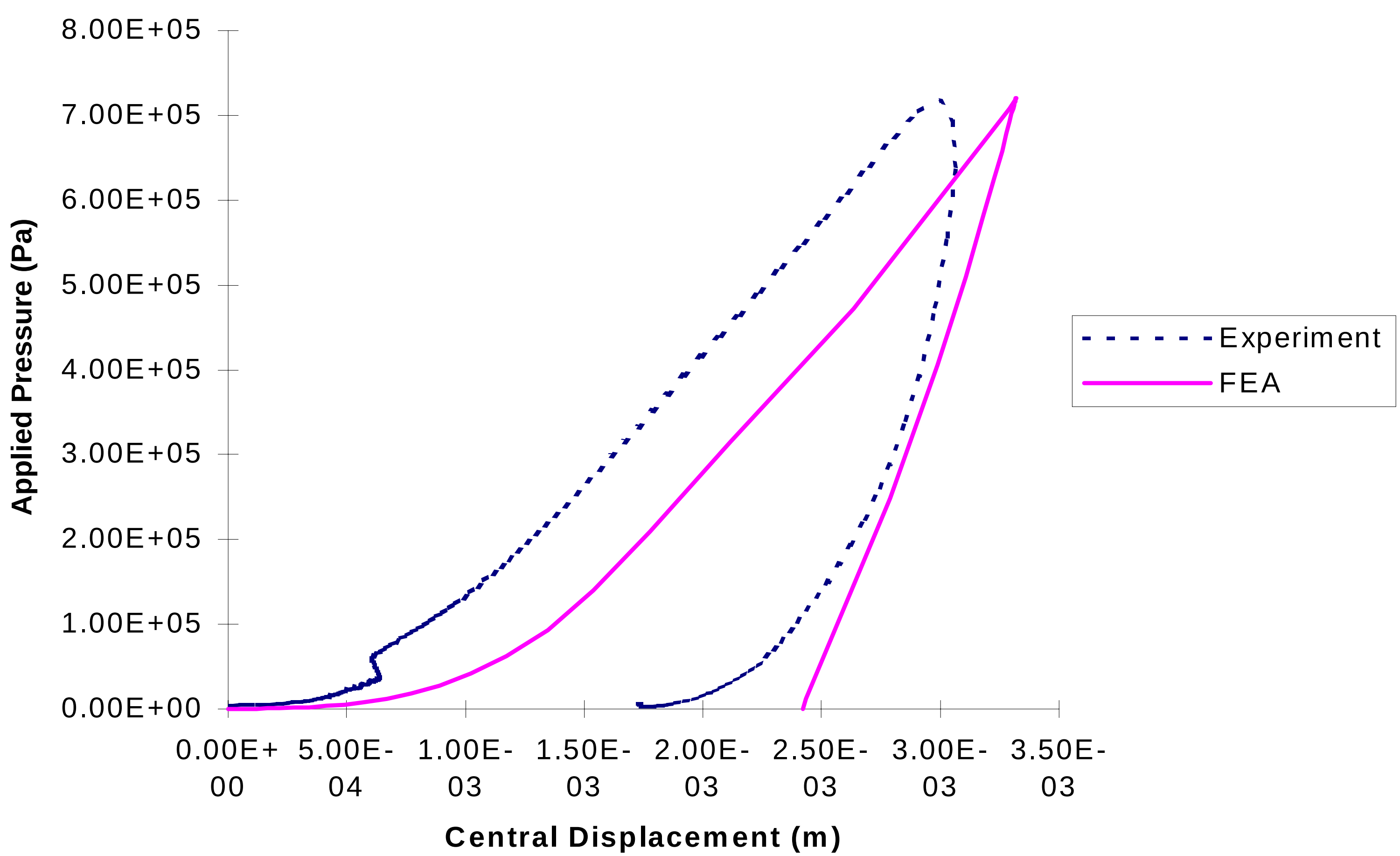

Figure 5.15 Central displacement curve for a sample loaded to 0.72 MPa and unloaded in a Mullen tester.

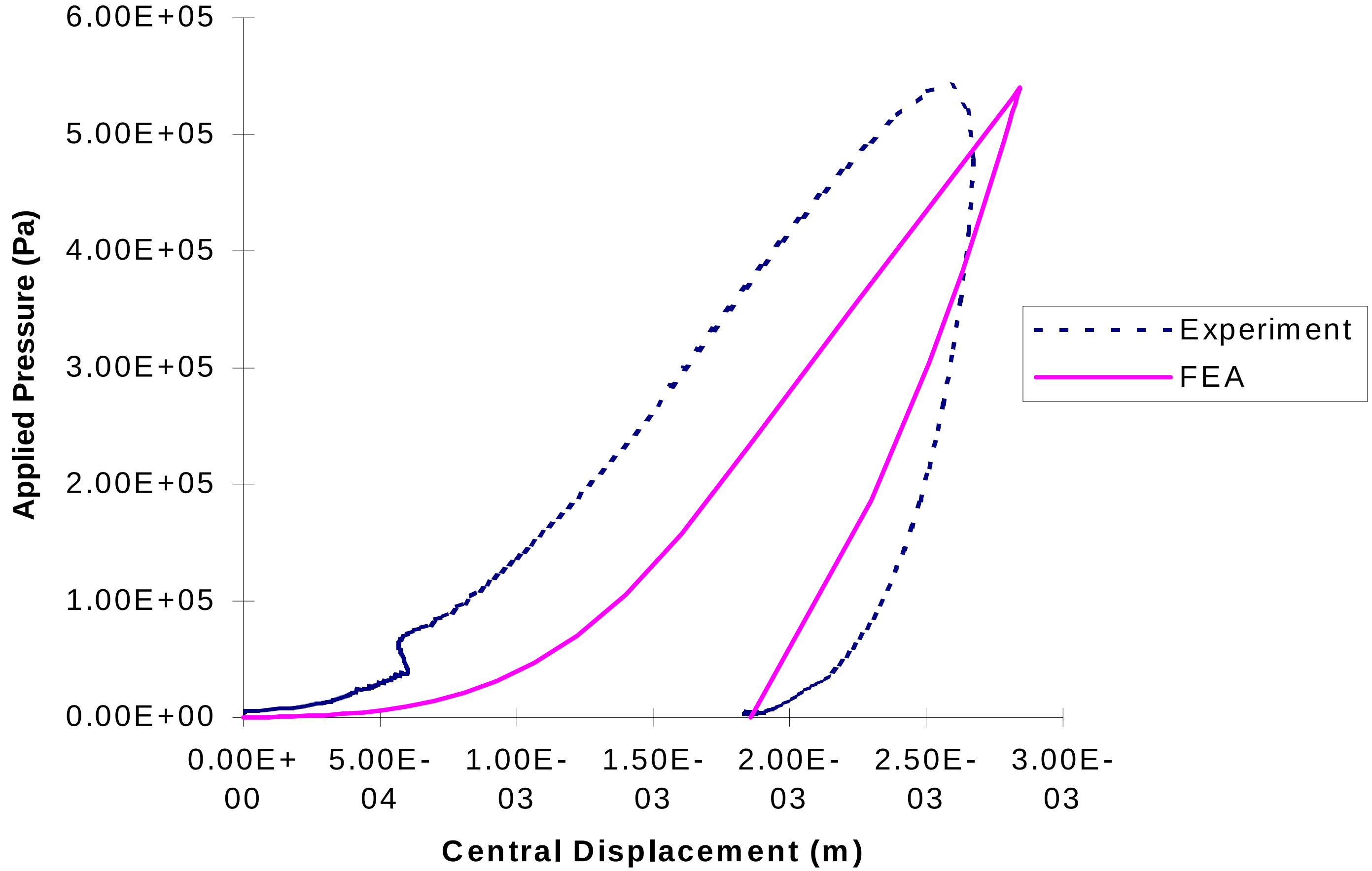

Figure 5.16 Central displacement curve for a sample loaded to 0.54 MPa and unloaded in a Mullen tester.

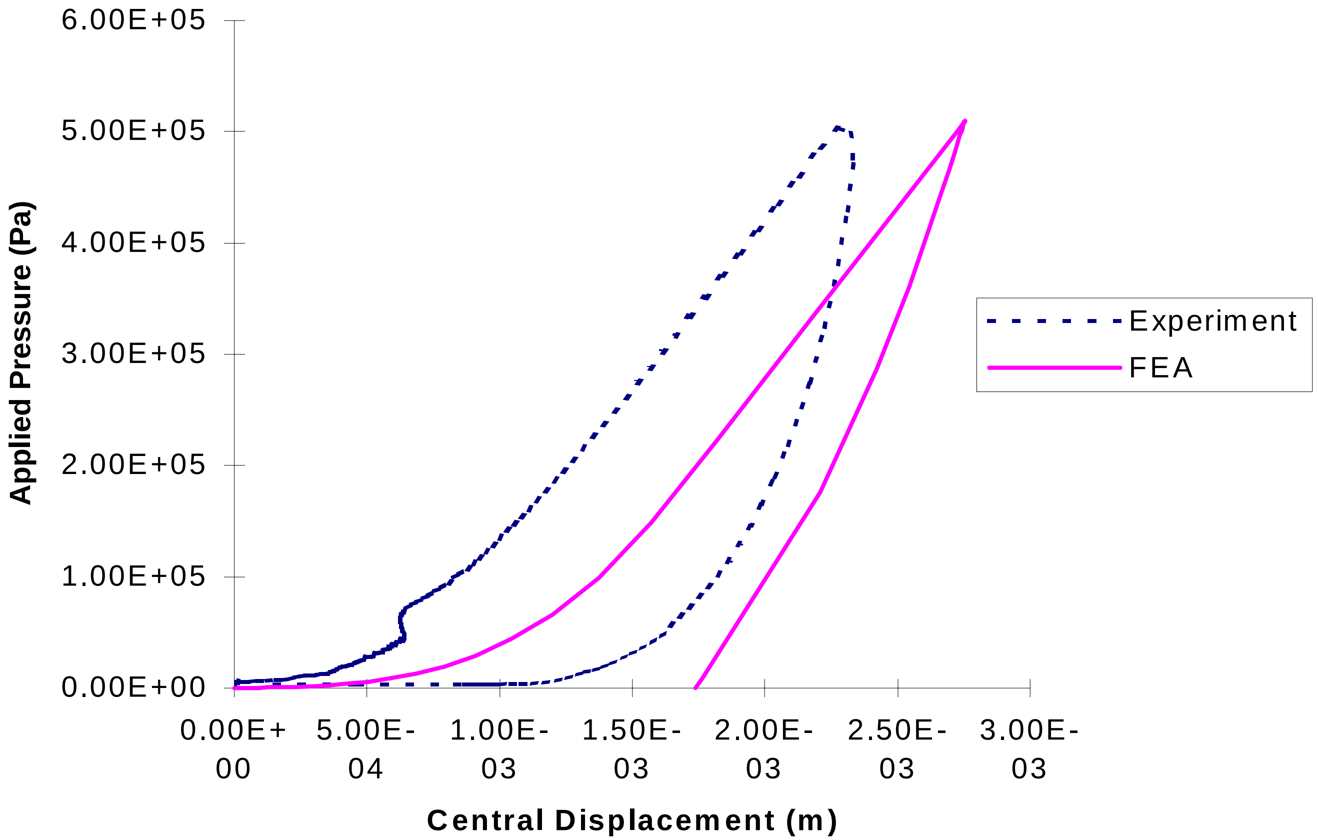

Figure 5.17 Central displacement curve for a sample loaded to 0.51 MPa and unloaded in a Mullen tester.

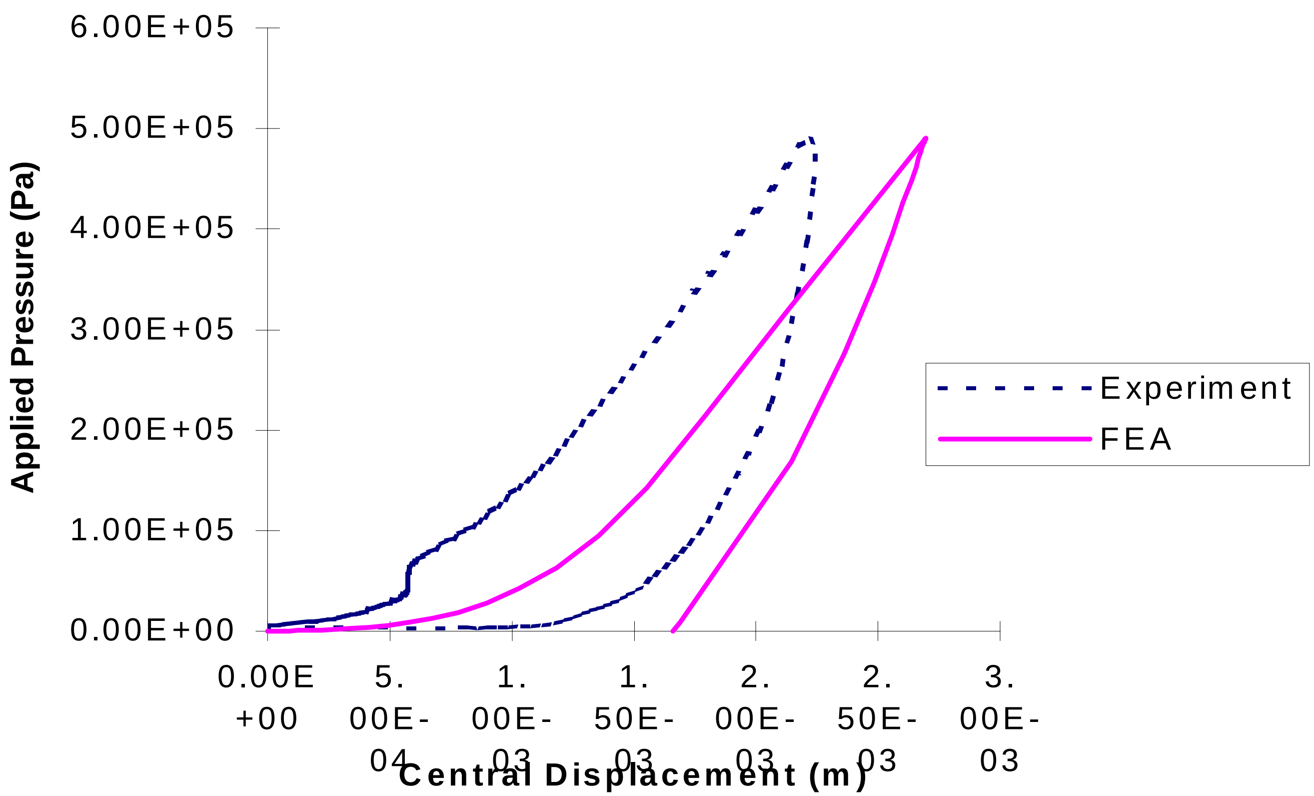

Figure 5.18 Central displacement curve for a sample loaded to 0.49 MPa and unloaded in a Mullen tester.

6. Conclusions and Future Work

A review of the constitutive models for paper material has shown that currently available models focus mainly on the loading process. In practice, some amount of strain is recovered during the unloading process. In this work, the asymptotic fiber and bond model (Sinha, 1994) was extended to include the unloading behavior of paper material subjected to cyclic loading. The asymptotic fiber and bond model, which is a micromechanics model, was chosen in this work due to its ability to address many of the factors that affect the constitutive behavior of paper material. The factors addressed by this model include the material properties of fiber and bond, the effects of drying restraints, fiber orientation, and degree of bonding.

In the asymptotic fiber and bond model, the load-bearing unit consists of a fiber segment that is bonded on one side. A two-slope model describes the fiber and bond constitutive behavior. In this work, as the applied strain increases, the bond eventually yields and this leads to the nonlinearity in the sheet stress-strain behavior. Fiber remains elastic throughout the loading process. When unloading, both fiber and bond behave elastically. From the deformation of the load-bearing unit, the fiber stress is derived. The sheet stress in the loading unloading process is then derived from the integral sum of the appropriate component of the fiber stress for all fiber orientation and concentration.

The model was applied on a paper cup stock of 720 kg/m^3. The model parameters were obtained by curve-fitting the model to experimental data from uniaxial tensile tests of the material in the machine and cross-machine direction. Using the model parameters, the sheet elastic modulus is calculated. The division of the final sheet stress by the sheet elastic modulus provides the amount of elastic strain component, which is recovered upon unloading. This elastic strain component is subtracted from the final sheet strain to obtain the permanent plastic strain, which remains after unloading. The model prediction of the plastic strain showed good agreement with experimental data for the machine and cross-machine direction. Admittedly, in a uniaxial loading problem, the unloading path could be graphically determined, rendering the application of the model unnecessary. However, the success of the model in the uniaxial loading problem showed the feasibility of applying the model in the unloading process, by assuming that fiber and bond behave elastically during unloading. This served as a stepping stone for the model application in a two-dimensional problem, whose unloading process is not as easy to determine such as by graphical means.

The extended model was further tested in a two-dimensional problem, i.e. a burst test. A Mullen tester was used to obtain the experimental data. The pressure transducer attached to the tester provided the pressure data, while a capacitance sensor provided the displacement data at the center of the samples. The samples were not tested to failure. Instead, they were deformed into hemispherical form and then unloaded. The model was used to predict the pressure-displacement curve for the center of the sample during the loading and unloading process.

In order to apply the model in the two-dimensional problem, the finite element approach was used. The 3 inch diameter sample of the burst test was discretized into 96 shear deformable shell elements in ABAQUS, whose elemental stress-strain equation was derived from the asymptotic fiber and bond model and implemented in ABAQUS via its UMAT subroutine. Loading and unloading was applied in incremental steps. At each step, the yield criteria and critical stresses was checked and updated when necessary to correctly model the cyclic loading process. The accuracy of the solution from the finite element model was verified by varying the step size and the number of elements used in setting up the finite element model. In the process, it was observed that over prediction of the yield point and stress-strain curve in the plastic region could result if the step size is not sufficiently small when the applied load is approaching the yield point.

The model prediction of the pressure-central displacement curves was also satisfactory, even though the model over-predicted the central displacement. To a lesser extent, the discrepancy could be attributed to the choice of model parameter values. More importantly, the discrepancy could be due to the effects of the coating of polyethylene on one side of the paper cup stock. Experimental results have shown that the coating affects the pressure at which the sample fails. When the pressure was applied to the coated surface, the samples tend to fail at lower pressure and vice versa.

Therefore, for future work the coating should be included in the finite element model as a thin layer of substance with properties of its own defined. Alternately, the model could be tested on laboratory made samples with no coating. An added advantage to this alternative would be the knowledge of the drying restraints applied during the papermaking process and free shrinkage experienced by the samples for a given moisture content. This eliminates the need for fitting the drying restraint parameters to experimental data to obtain their values.

In addition to the experimental work suggested above, the interlaminar shear between layers of fiber network which form the sheet could also be explored. In this work, the shear elastic modulus of the sheet used in the finite element analysis for the two-dimensional problem was experimentally determined using ultrasonic technique. The composite laminate theory could be used to model a sheet as layers of fiber network, whose constitutive behavior is governed by the asymptotic fiber and bond model. This could extend the micromechanics model to address the constitutive behavior of paper material in the thickness direction.

Reference

1. G. A. Baum, D. C. Brenna, C. C. Habeger, Orthotropic Elastic Constants of Paper, Tappi, August, 1981, Vol. 64, No. 8, pp. 97 –101.
2. Gary A. Baum, Subfracture Mechanical Properties, Product of Papermaking, Transactions of the Tenth Fundamental Research Symposium, Vol.1, pp. 1-126, Oxford, September 1993.
3. Leif Carlsson, Christer Fellers, and Bo Westerlind, Finite Element Analysis of the Creasing and Bending of Paper, Svensk Papperstidning, pp. R121-R126, 1982
4. D. F. Dumbleton, Tappi 55(1):127, 1972.
5. H. Giertz and G. Rodland, Elongation of Segments-bonds in the Secondary regime of the Load-Elongation Curve, Proc. International Paper Physics Conference, Harrison Hot Springs, September, 1979.
6. B. A. Jayne, Mechanical Properties of Wood Fibers, Tappi 42(6):461-467, 1959.
7. C. A. Jentzen, Tappi 47(7):412, 1964
8. M. W. Johnson, Jr., and T. J. Urbanik, A Nonlinear Theory for Elastic Plates with Application to Characterizing Paper Properties, Journal of Applied Mechanics, Vol. 51, March 1984, pp. 146 – 152.
9. T. Komori and K. Makashima, Textile Research J., 47:13, 1977.
10. Wentao Lu, Leif A. Carlsson, and Ylva Andersson, ‘Micro-model of Paper, Part 1: Bounds on Elastic Properties’, Tappi Journal, Vol. 78, No. 12, 1995.
11. Wentao Lu and Leif A. Carlsson, ‘Micro-model of Paper, Part 2: Statistical Analysis of the Paper Structure’, Tappi Journal, Vol. 79, No. 1, 1996.
12. Wentao Lu, Leif A. Carlsson, and Ylva Andersson, ‘Micro-model of Paper, Part 3: Mosaic Model’, Tappi Journal, Vol. 79, No. 2, 1996.
13. R. W. Mann, G. A. Baum, and C. C. Habeger, Determination of All Nine Orthotropic Elastic Constants for Machine-made Paper, Tappi 63 (1980):2, 163.
14. Kasyap Muthuraman, A Computational Mechanics Model for the Brim Forming Process in Paperboard Container Manufacturing, M.S. Thesis, North Carolina State University, 1998.
15. Kaarlo Niskanen, Paper Physics, Fapet Oy 1998.

16. D. H. Page, F. El-Hosseiny, K. Winkler, et al., Tappi 60(4):114, 1977
17. D. H. Page and F. El-Hosseiny, Pulp Pap. Can., 84(9):TR99, 1983
18. D. H. Page and P. A. Tydeman, A New Theory of the Shrinkage, Structure, and Properties of Paper, Formation and Structure of Paper, Transactions of the Fundamental Research Symposium, pp. 397-413, Oxford, September, 1961.
19. D. H. Page and R. S. Seth, The Elastic Modulus of Paper. II. The Importance of Fiber Modulus, Bonding, and Fiber Length, Tappi, 63(6): 113-116, 1980a.
20. D. H. Page and R. S. Seth, The Elastic Modulus of Paper. III. The Effects of Dislocations, Microcompressions, Curl, Crimps, and Kinks, Tappi, 63(10): 99-109, 1980b
21. M. K. Ramasubramanian and R. W. Perkins, Computer Simulation of the Uniaxial Elastic-Plastic Behavior of Paper, Journal of Engineering Materials and Technology, 110: 117-123, April 1988.
22. M. K. Ramasubramanian and Yun Y. Wang, Constitutive Models for Paper and Other Ribbon-like Nonwovens - A Literature Review, AMD-Vol. 231/MD-Vol.85, Mechanics of Cellulosic Materials, ASME 1999.
23. R. W. Perkins and R. E. Mark, Some New Concepts of the Relation between Fiber Orientation, Fiber Geometry, and Mechanical Properties, The Role of Fundamental Research in Paper Making, Trans. Symp. 1981, Mech. Eng. Publ. Lts., London, pp. 479-525, 1983.
24. R. W. Perkins, Micromechanics Models for Predicting the Elastic and Strength Behavior of Paper Materials, Mat. Res. Soc. Symp. Proc., 197:99-118, 1990.
25. Richard W. Perkins, Jr., Richard E. Mark, and Sanjiv Sinha, Micromechanics and Continuum Models for Paper Materials of Medium to High Density, International Paper Physics Conference 1991, Tappi Proceedings, pp. 413–435.
26. Richard W. Perkins and Sanjiv Sinha, A Micromechanics Plasticity Model for the Uniaxial Loading of Paper Materials, AMD-Vol. 135/MD-Vol. 31, Plastic Flow and Creep, 1992a, pp. 117 –135.
27. Richard W. Perkins, Sanjiv K. Sinha, Vera Bares, and Richard E. Mark, A Micromechanics Model for the Uniaxial Constant Strain Rate Loading of Paper

Materials, AMD-Vol. 145/MD-Vol. 36, Mechanics of Cellulosic Materials, ASME 1992b, pp. 49-67.

28. Adel S. Saada, ‘Elasticity: Theory and Applications’, Pergamon Press Inc., 1974, pp.187.
29. Lennart Salmén, Leif Carlsson, Alf de Ruvo, Christer Fellers, and Myat Htun, A Treatise on the Elastic and Hygroexpansional Properties of Paper by a Composite Laminate Approach, Fibre Science and Technology, 20, 1984, pp. 283 –296.
30. Sanjiv K. Sinha and Richard W. Perkins, Jr., A Micromechanics Constitutive Model for Use in Finite Element Analysis, AMD-Vol. 209/MD-Vol.60, Mechanics of Cellulosic Materials, ASME 1995.
31. Sanjiv K. Sinha, Viscoplastic Micromechanics and Continuum Models of Fibrous Cellulosic Materials, Ph.D. Dissertation, Syracuse University, December, 1994.
32. J. C. Suhling, M. W. Johnson, R. E. Rowlands, and D. E. Gunderson, Nonlinear Elastic Constitutive Relations for Cellulosic Materials, Mechanics of Cellulosic and Polymeric Materials, AMD - Vol. 99/MD - Vol. 13, 1989.
33. J. A. Van Den Akker, in The Formation and Structure of Paper (F. Bolam, Ed.), B.P.B.M.A., London, 1962, vol. 1, pp.205-245.
34. L. Wong, M. T. Kortschot, and C. T. J. Dodson, Finite Element Analysis and Experimental Measurement of Strain Fields and Failure in Paper, 1995 International Paper Physics Conference, pp. 131 - 135.

APPENDIX I

```
      SUBROUTINE UMAT(STRESS,STATEV,DDSDDE,SSE,SPD,SCD,
     1  RPL,DDSDDT,DRPLDE,DRPLDT,
     2  STRAN,DSTRAN,TIME,DTIME,TEMP,DTEMP,PREDEF,DPRED,CMNAME,
     3  NDI,NSHR,NTENS,NSTATV,PROPS,NPROPS,COORDS,DROT,PNEWDT,
     4  CELENT,DFGRD0,DFGRD1,NOEL,NPT,LAYER,KSPT,KSTEP,KINC)
C
      INCLUDE 'ABA_PARAM.INC'
C
C*********************************************************************
C  AXIAL, LINEAR WORK-HARDENING FIBER AND BOND PLASTICITY MODEL      *
C  USING ASYMPTOTIC BEHAVIOR(LB=0,LF=L), RESTRAINED DRYING INCLUDED  *
C  MICROMECHANICS PROGRAM FOR CALCULATING STRESSES FOR NEXT INCREMENT*
C  AND JACOBIAN MATRIX FOR BOUNDARY VALUE PROBLEM USING ABAQUS "UMAT"*
C*********************************************************************
        IMPLICIT REAL*8(A-H,O-Z)
        REAL*8 M
        REAL*8 L,KAPPA
C****************************************************************
      PARAMETER(MAXNP1=31,MAXNP2=15,MAXNP3=11)
C****************************************************************
C
      DIMENSION SIGBAR(MAXNP1),EPS(MAXNP1),DEPS(MAXNP1),
     1  T(MAXNP1),F(MAXNP1),FX(MAXNP1),FY(MAXNP1),FXY(MAXNP1),
     2  FXZ(MAXNP1),FYZ(MAXNP1)
C
      DIMENSION GAMMA(MAXNP2)
C*********************************************************************
      CHARACTER*8 CMNAME
      DIMENSION STRESS(NTENS),STATEV(NSTATV),
     1  DDSDDE(NTENS,NTENS),
     2  DDSDDT(NTENS),DRPLDE(NTENS),
```

```
     3  STRAN(NTENS),DSTRAN(NTENS),PREDEF(1),DPRED(1),
     4  PROPS(NPROPS),COORDS(3),DROT(3,3)
C
     DIMENSION DSTRES(6),D(3,3)
C
C*******MODEL INPUTS*********************************************
C*******STRUCTURAL PARAMETERS OF FIBERS
     DATA L,WF,TF,TB/ 1.D-3,4.D-5,4.D-6,4.D-7 /
C*******DENSITY AND ORIENTATION CONCENTRATION PARAMETERS
        DATA RHOS, RHOF, KAPPA / 720., 1500., 0.6 /
C*******ELASTIC CONSTANTS FOR MESOELEMENTS
        DATA EFO,GBO /18.E9,15.E6 /
C*******YIELD STRESSES FOR MESOELEMENTS
        DATA SCRPO, SCRNO, TCRO / 19.E9, 5.E9, 6.5E6 /
C*******PLASTIC SLOPES FOR MESOELEMENTS
        DATA HFPPO, HFPNO, HBPO / 19.E9, 1.E9,.010E6 /
C*******HARDENING PARAMETERS
     DATA FS,BS,FPP,FPN,BP,HFP,HFN,HBP/ 0.0,0.0,0.0,0.0,2.0,
     *  0.0,0.0,70.0 /
C*******DRYING PARAMETERS
     DATA ALPHAXM,EXD,ALPHAYM,EYD/ 0.045,0.0,0.0,0.0 /
C*********************************************************************
c        WRITE (7,5) L, WF, RHOS, KAPPA
5       FORMAT (1X,'L=',F5.4,3X,'WF=',F5.4,3X,'RHOS=',F7.2,3X,
     *  'KAPPA=',F5.2)
c        WRITE (7,6) EFO, GBO
6       FORMAT (1X,'EFO=',E13.2,5X,'GBO=',E13.2)
c        WRITE (7,7) SCRPO, SCRNO, TCRO
7       FORMAT (1X,'SCRPO=',E13.2,5X,'SCRNO=',E13.2,5X,'TCRO=',E13.2)
c        WRITE (7,8) HFPPO, HFPNO, HBPO
8       FORMAT (1X,'HFPPO=',E13.2,5X,'HFPNO=',E13.2,5X,'HBPO=',E13.2)
```

```
C
     M=0.0
C
     ALPHA=0.0
     W1=.98*WF
     AF=WF*TF
     CF=RHOS/RHOF
C
     PI=3.141592654
C
     DT=PI/DFLOAT(MAXNP1-1)
C
C************************************************C
C    Determine value of zeroth order modified   C
C    Bessel Function                           C
C***********************************************C
     IF(KAPPA .EQ. 0.0)THEN
          BF=1.0
     ELSE
C         GAMMA FUNCTION: FACTORIAL
          GAMMA(1)=1.0
          DO I=2,15
               GAMMA(I)=GAMMA(I-1)*(I-1)
          END DO
C         CALCULATION OF IO(KAPPA)
          SUM=0.0
          DO  I=1,15
               SUM=SUM+(((KAPPA/2.0)**(2.0*(I-1)))/(GAMMA(I)**2.0))
          END DO
          BF=SUM
     ENDIF
```

```
c    WRITE (7,90) BF, KAPPA
90      FORMAT (1X,'BF=',F5.3,3X,'KAPPA=',F5.3)
c    WRITE (7,101) GAMMA
101     FORMAT (1X,'GAMMA=',7x,F15.3)
C
C***************************************************C
C    Calculate average fiber stress and            C
C    F functions for the Jacobian Matrix         C
C***************************************************C
     DO I=1,MAXNP1
          T(I)=(-PI/2.0)+((I-1)*DT)
C         Determine macroscopic drying restraint strain measure ...
          EDR=((ALPHAXM+EXD)*(DCOS(T(I))**2))+((ALPHAYM+EYD)
     +                *(SIN(T(I))**2))
C         Address effects of drying restraints ...
          EF=EFO*(1.0+(FS*EDR))
          GB=GBO*(1.0+(BS*EDR))
          SIGCRP=SCRPO*(1.0+(FPP*EDR))
          SIGCRN=SCRNO*(1.0+(FPN*EDR))
          TAUMCR=TCRO*(1.0+(BP*EDR))
          EFPP=HFPPO*(1.0+(HFP*EDR))
          EFPN=HFPNO*(1.0+(HFN*EDR))
          GBP=HBPO*(1.0+(HBP*EDR))
C         Calculate local sheet strain ...
          EX=STRAN(1)
          EY=STRAN(2)
          EXY=STRAN(3)
          EPS(I)=(EX*DCOS(T(I))**2)+(EY*DSIN(T(I))**2)+(EXY*
     +    DSIN(T(I))*DCOS(T(I)))
          EPSI=EPS(I)
C         Calculate local incremental sheet strain ...
```

```
      EX=DSTRAN(1)
      EY=DSTRAN(2)
      EXY=DSTRAN(3)
      DEPS(I)=(EX*DCOS(T(I))**2)+(EY*DSIN(T(I))**2)+(EXY*
     1        DSIN(T(I))*DCOS(T(I)))
      DEPSI=DEPS(I)
C     Calculate the a parameters in the tanh functions ...
      IF(DEPSI .LT. 0.0)THEN
           SIGMCR=-SIGCRN
           EFP=EFPN
           TAUCR=-TAUMCR
      ELSE
           SIGMCR=SIGCRP
           EFP=EFPP
           TAUCR=TAUMCR
      END IF
C
      A=DSQRT((GB*(W1/WF))/(TB*TF*EF))
      AA1=DSQRT((GB*(W1/WF))/(TB*TF*EFP))
      BB1=DSQRT((GBP*(W1/WF))/(TB*TF*EF))
      CC1=DSQRT((GBP*(W1/WF))/(TB*TF*EFP))
C
      AL=A*L
      IF(AL .GE. 70.0)THEN
           AL=70.0
      END IF
C
      AA1L=AA1*L
      IF(AA1L .GE. 70.0)THEN
           AA1L=70.0
      END IF
```

```
C
          BB1L=BB1*L
          IF(BB1L .GE. 70.0)THEN
               BB1L=70.0
          END IF
C
          CC1L=CC1*L
          IF(CC1L .GE. 70.0)THEN
               CC1L=70.0
          END IF
C
C         CRITICAL FIBER AND BOND STRAINS
C         These are the initial critical strains ...
          ECRB=((TAUCR*W1)/(EF*AF))*(1.0/(A*TANH(A*L)))
          ECRF=(SIGMCR/EF)/(1.0-(1.0/COSH(A*L)))
          ECRBF=(SIGMCR/EF)/(1.0-(1.0/COSH(BB1*L)))
          ECRFB=ECRF+(((TAUCR*W1)-(EF*AF*ECRF*A*
     1          TANH(A*L)))/(EF*AF*AA1*TANH(AA1*L)))
C
C*****************C
C    Loading   C
C*****************C
          FIBSTRS=STATEV(I)
          EET=STATEV(MAXNP1+I)
          EEC=STATEV((2*MAXNP1)+I)
          PLASTIC=STATEV((3*MAXNP1)+I)
C
          IF ((FIBSTRS*DEPSI).GE.0) THEN
C         LOADING OR RELOADING IN PROGRESS
               IF (DEPSI.GE.0) THEN
C              TENSILE LOADING/RELOADING
```

```
                    SIGMCR=-SIGCRN
                    EFP=EFPN
                    TAUCR=-TAUMCR
                    CECRB=((TAUCR*W1)/(EF*AF))*(1.0/(A*TANH(A*L)))
                    CECRF=(SIGMCR/EF)/(1.0-(1.0/COSH(A*L)))
                    IF (DABS(CECRF).GT.DABS(CECRB)) THEN
C                   BOND WOULD YIELD FIRST IN COMPRESSION
                         IF (DABS(EEC).LT.DABS(CECRB)) THEN
C                        BOND HAS NOT YIELDED IN COMPRESSION.
                                   CALL BLOADT(ECRF,ECRB,ECRBF,ECRFB,EPSI,DEPSI,
     1                             SIGBAR,I,MAXNP1,EF,EFP,AL,A,L,AA1,BB1,CC1,
     1                             PLASTIC,EET,EEC,STATEV,NSTATV)
                              ELSE
C                        BOND HAS YIELDED IN COMPRESSION
                              IF (ECRF.GT.ECRB) THEN
                              IF (STATEV((9*MAXNP1)+I).LT.ECRB) THEN
C                             BOND HAS NOT YIELDED IN TENSION
                                   CALL LOADT(ECRF,ECRB,ECRBF,ECRFB,EPSI,DEPSI,
     1                                  SIGBAR,I,MAXNP1,EF,EFP,AL,A,L,AA1,BB1,CC1,
     1                                  PLASTIC,EET,EEC,STATEV,NSTATV,SHIFT)
                                   ELSE
C                             BOND HAS YIELDED IN TENSION
                                   CALL LOADT2(ECRF,ECRB,ECRBF,ECRFB,EPSI,DEPSI,
     1                                  SIGBAR,I,MAXNP1,EF,EFP,AL,A,L,AA1,BB1,CC1,
     1                                  PLASTIC,EET,EEC,STATEV,NSTATV,SHIFT)

                                   END IF
                                   END IF
                                   IF (ECRB.GT.ECRF) THEN
                                   IF (STATEV((9*MAXNP1)+I).LT.ECRF) THEN
C                             FIBER HAS NOT YIELDED IN TENSION
```

```
                                        CALL LOADT(ECRF,ECRB,ECRBF,ECRFB,EPSI,DEPSI,
     1                                  SIGBAR,I,MAXNP1,EF,EFP,AL,A,L,AA1,BB1,CC1,
     1                                  PLASTIC,EET,EEC,STATEV,NSTATV,SHIFT)
                                   ELSE
C                             FIBER HAS YIELDED IN TENSION
                                   CALL LOADT2(ECRF,ECRB,ECRBF,ECRFB,EPSI,DEPSI,
     1                                  SIGBAR,I,MAXNP1,EF,EFP,AL,A,L,AA1,BB1,CC1,
     1                                  PLASTIC,EET,EEC,STATEV,NSTATV,SHIFT)
                                   END IF
                                   END IF
                              END IF
                         END IF
                    IF (DABS(CECRB).GT.DABS(CECRF)) THEN
C                   FIBER WOULD YIELD FIRST IN COMPRESSION
                         IF (DABS(EEC).LT.DABS(CECRF)) THEN
C                        FIBER HAS NOT YIELDED IN COMPRESSION
                                   CALL BLOADT(ECRF,ECRB,ECRBF,ECRFB,EPSI,DEPSI,
     1                             SIGBAR,I,MAXNP1,EF,EFP,AL,A,L,AA1,BB1,CC1,
     1                             PLASTIC,EET,EEC,STATEV,NSTATV)
                              ELSE
C                        FIBER HAS YIELDED IN COMPRESSION
                              IF (ECRF.GT.ECRB) THEN
                              IF (STATEV((9*MAXNP1)+I).LT.ECRB) THEN
C                             BOND HAS NOT YIELDED IN TENSION
                                   CALL LOADT(ECRF,ECRB,ECRBF,ECRFB,EPSI,DEPSI,
     1                                  SIGBAR,I,MAXNP1,EF,EFP,AL,A,L,AA1,BB1,CC1,
     1                                  PLASTIC,EET,EEC,STATEV,NSTATV,SHIFT)
                                   ELSE
C                             BOND HAS YIELDED IN TENSION
                                   CALL LOADT2(ECRF,ECRB,ECRBF,ECRFB,EPSI,DEPSI,
     1                                  SIGBAR,I,MAXNP1,EF,EFP,AL,A,L,AA1,BB1,CC1,
```

```
     1                                  PLASTIC,EET,EEC,STATEV,NSTATV,SHIFT)
                                   END IF
                                   END IF
                                   IF (ECRB.GT.ECRF) THEN
                                   IF (STATEV((9*MAXNP1)+I).LT.ECRF) THEN
C                             FIBER HAS NOT YIELDED IN TENSION

                                        CALL LOADT(ECRF,ECRB,ECRBF,ECRFB,EPSI,DEPSI,
     1                                  SIGBAR,I,MAXNP1,EF,EFP,AL,A,L,AA1,BB1,CC1,
     1                                  PLASTIC,EET,EEC,STATEV,NSTATV,SHIFT)
                                   ELSE
C                             FIBER HAS YIELDED IN TENSION
                                   CALL LOADT2(ECRF,ECRB,ECRBF,ECRFB,EPSI,DEPSI,
     1                                  SIGBAR,I,MAXNP1,EF,EFP,AL,A,L,AA1,BB1,CC1,
     1                                  PLASTIC,EET,EEC,STATEV,NSTATV,SHIFT)
                                   END IF
                                   END IF

                              END IF
                         END IF
               END IF
               IF (DEPSI.LT.0) THEN
C              COMPRESSIVE LOADING/RELOADING
                         SIGMCR=SIGCRP
                    EFP=EFPP
                    TAUCR=TAUMCR
                    TECRB=((TAUCR*W1)/(EF*AF))*(1.0/(A*TANH(A*L)))
                    TECRF=(SIGMCR/EF)/(1.0-(1.0/COSH(A*L)))
                    IF (DABS(TECRF).GT.DABS(TECRB)) THEN
C                   BOND WOULD YIELD FIRST IN TENSION
                         IF(DABS(EET).LT.DABS(TECRB)) THEN
```

```
C                        BOND HAS NOT YIELDED IN TENSION
                                   CALL BLOADC(ECRF,ECRB,ECRBF,ECRFB,EPSI,DEPSI,
     1                             SIGBAR,I,MAXNP1,EF,EFP,AL,A,L,AA1,BB1,CC1,
     1                             PLASTIC,EET,EEC,STATEV,NSTATV)
                         ELSE
C                        BOND HAS YIELDED IN TENSION
                              IF (DABS(ECRF).GT.DABS(ECRB)) THEN
                              IF (DABS(STATEV((10*MAXNP1)+I)).LT.DABS(ECRB)) THEN
C                             BOND HAS NOT YIELDED IN COMPRESSION

                                   CALL LOADC(ECRF,ECRB,ECRBF,ECRFB,EPSI,DEPSI,
     1                                  SIGBAR,I,MAXNP1,EF,EFP,AL,A,L,AA1,BB1,CC1,
     1                                  PLASTIC,EET,EEC,STATEV,NSTATV,SHIFT)
                                   ELSE
C                             BOND HAS YIELDED IN COMPRESSION
                                        CALL LOADC2(ECRF,ECRB,ECRBF,ECRFB,EPSI,DEPSI,
     1                                  SIGBAR,I,MAXNP1,EF,EFP,AL,A,L,AA1,BB1,CC1,
     1                                  PLASTIC,EET,EEC,STATEV,NSTATV,SHIFT)
                                   END IF
                                   END IF
                              IF (DABS(ECRB).GT.DABS(ECRF)) THEN
                              IF (DABS(STATEV((10*MAXNP1)+I)).LT.DABS(ECRF)) THEN
C                             FIBER HAS NOT YIELDED IN COMPRESSION
                                   CALL LOADC(ECRF,ECRB,ECRBF,ECRFB,EPSI,DEPSI,
     1                                  SIGBAR,I,MAXNP1,EF,EFP,AL,A,L,AA1,BB1,CC1,
     1                                  PLASTIC,EET,EEC,STATEV,NSTATV,SHIFT)
                                   ELSE
C                             FIBER HAS YIELDED IN COMPRESSION
                                        CALL LOADC2(ECRF,ECRB,ECRBF,ECRFB,EPSI,DEPSI,
     1                                  SIGBAR,I,MAXNP1,EF,EFP,AL,A,L,AA1,BB1,CC1,
     1                                  PLASTIC,EET,EEC,STATEV,NSTATV,SHIFT)
```

```
                                   END IF
                                   END IF
                         END IF
                         END IF
                    IF (DABS(TECRB).GT.DABS(TECRF)) THEN
C                   FIBER WOULD YIELD FIRST IN TENSION
                         IF(DABS(EET).LT.DABS(TECRF)) THEN
C                        FIBER HAS NOT YIELDED IN TENSION
                                   CALL BLOADC(ECRF,ECRB,ECRBF,ECRFB,EPSI,DEPSI,
     1                             SIGBAR,I,MAXNP1,EF,EFP,AL,A,L,AA1,BB1,CC1,
     1                             PLASTIC,EET,EEC,STATEV,NSTATV)
                              ELSE
C                        FIBER HAS YIELDED IN TENSION
                              IF (DABS(ECRF).GT.DABS(ECRB)) THEN
                              IF (DABS(STATEV((10*MAXNP1)+I)).LT.DABS(ECRB)) THEN
                                   CALL LOADC(ECRF,ECRB,ECRBF,ECRFB,EPSI,DEPSI,
     1                                  SIGBAR,I,MAXNP1,EF,EFP,AL,A,L,AA1,BB1,CC1,
     1                                  PLASTIC,EET,EEC,STATEV,NSTATV,SHIFT)
                                   ELSE
                                        CALL LOADC2(ECRF,ECRB,ECRBF,ECRFB,EPSI,DEPSI,
     1                                  SIGBAR,I,MAXNP1,EF,EFP,AL,A,L,AA1,BB1,CC1,
     1                                  PLASTIC,EET,EEC,STATEV,NSTATV,SHIFT)
                                   END IF
                                   END IF
                              IF (DABS(ECRB).GT.DABS(ECRF)) THEN
                              IF (DABS(STATEV((10*MAXNP1)+I)).LT.DABS(ECRF)) THEN
                                   CALL LOADC(ECRF,ECRB,ECRBF,ECRFB,EPSI,DEPSI,
     1                                  SIGBAR,I,MAXNP1,EF,EFP,AL,A,L,AA1,BB1,CC1,
     1                                  PLASTIC,EET,EEC,STATEV,NSTATV,SHIFT)
                                   ELSE
                                        CALL LOADC2(ECRF,ECRB,ECRBF,ECRFB,EPSI,DEPSI,
```

```
     1                                  SIGBAR,I,MAXNP1,EF,EFP,AL,A,L,AA1,BB1,CC1,
     1                                  PLASTIC,EET,EEC,STATEV,NSTATV,SHIFT)
                                   END IF
                                   END IF
                         END IF
                         END IF
               END IF
          ELSE
C         UNLOADING IN PROGRESS
               PREVIOUS=STATEV(I)
               SIGBAR(I)=EF*(1.0-((DTANH(AL))/(A*L)))
               STATEV(I)=STATEV(I)+(SIGBAR(I)*DEPSI)
               IF ((PREVIOUS*STATEV(I)).LT.0) THEN
C              THE PROCESS HAS GONE FROM UNLOADING TO LOADING/RELOADING
                    CALL OFFSET(ECRF,ECRB,DEPSI,I,MAXNP1,
     1                   PLASTIC,EET,EEC,STATEV,NSTATV,SHIFT)
               END IF
          END IF
200       FORMAT (1X,I2,5X,E13.5,5X,E13.5,5X,E13.5,5X,E13.5)
C***********************************************C
C    FIBER ORIENTATION DISTRIBUTION FUNCTION   C
C***********************************************C
          F(I)=DEXP(KAPPA*DCOS(2.0*T(I)))
          FX(I)=(DCOS(T(I))**4)*SIGBAR(I)*F(I)
          FY(I)=(DSIN(T(I))**4)*SIGBAR(I)*F(I)
          FXY(I)=((DSIN(T(I))**2)*(DCOS(T(I))**2))*SIGBAR(I)*F(I)
          FXZ(I)=(DSIN(T(I))*(DCOS(T(I))**3))*SIGBAR(I)*F(I)
          FYZ(I)=((DSIN(T(I))**3)*DCOS(T(I)))*SIGBAR(I)*F(I)
     END DO
c         WRITE (7,105) SIGBAR
105       FORMAT (1X,'SIGBAR=',7x,F20.4)
```

```
C*****************************************************************C
C    SIMPSON'S RULE OF INTEGRATION FOR ORIENTATION DISTRIBUTION  C
C*****************************************************************C
     FY1=0.0
     FY2=0.0
     FX1=0.0
     FX2=0.0
     FXY1=0.0
     FXY2=0.0
     FXZ1=0.0
     FXZ2=0.0
     FYZ1=0.0
     FYZ2=0.0
C
     DO JJ=2,MAXNP1-1,2
          FY1=FY1+FY(JJ)
          FX1=FX1+FX(JJ)
          FXY1=FXY1+FXY(JJ)
          FXZ1=FXZ1+FXZ(JJ)
          FYZ1=FYZ1+FYZ(JJ)
     ENDDO
C
     DO JJ=3,MAXNP1-2,2
          FY2=FY2+FY(JJ)
          FX2=FX2+FX(JJ)
          FXY2=FXY2+FXY(JJ)
          FXZ2=FXZ2+FXZ(JJ)
          FYZ2=FYZ2+FYZ(JJ)
     ENDDO
C
      EXPRS1=(1.0/(PI*BF))*(RHOS/RHOF)
```

```
c    WRITE (7,110) EXPRS1
110       FORMAT (1X,'EXPRS1=',F20.3)
C
C***************************C
C    THE JACOBIAN MATRIX   C
C***************************C
     DDSDDE(2,2)=EXPRS1*(DT/3.0)*(FY(1)+FY(MAXNP1)+(4.0*FY1)
     +  +(2.0*FY2))
C
     DDSDDE(1,1)=EXPRS1*(DT/3.0)*(FX(1)+FX(MAXNP1)+(4.0*FX1)
     +  +(2.0*FX2))
C
     DDSDDE(1,2)=EXPRS1*(DT/3.0)*(FXY(1)+FXY(MAXNP1)+(4.0*FXY1)
     +  +(2.0*FXY2))
C
     DDSDDE(1,3)=EXPRS1*(DT/3.0)*(FXZ(1)+FXZ(MAXNP1)+(4.0*FXZ1)
     +  +(2.0*FXZ2))
C
     DDSDDE(2,3)=EXPRS1*(DT/3.0)*(FYZ(1)+FYZ(MAXNP1)+(4.0*FYZ1)
     +  +(2.0*FYZ2))
C
     DDSDDE(3,3)=DDSDDE(1,2)
     DDSDDE(2,1)=DDSDDE(1,2)
     DDSDDE(3,1)=DDSDDE(1,3)
     DDSDDE(3,2)=DDSDDE(2,3)
C
C********************************C
C    THE INCREMENTAL STRESSES   C
C********************************C
     DSTRES(1)=DDSDDE(1,1)*DSTRAN(1)+DDSDDE(1,2)*DSTRAN(2)
     +  +DDSDDE(1,3)*DSTRAN(3)
```

```
C
     DSTRES(2)=DDSDDE(2,1)*DSTRAN(1)+DDSDDE(2,2)*DSTRAN(2)
     +  +DDSDDE(2,3)*DSTRAN(3)
C
     DSTRES(3)=DDSDDE(3,1)*DSTRAN(1)+DDSDDE(3,2)*DSTRAN(2)
     +  +DDSDDE(3,3)*DSTRAN(3)
C
C************************C
C    THE TOTAL STRESSES C
C************************C
     STRESS(1)=STRESS(1)+DSTRES(1)
     STRESS(2)=STRESS(2)+DSTRES(2)
     STRESS(3)=STRESS(3)+DSTRES(3)
C
     RETURN
     END
C
C
C
     SUBROUTINE BLOADT(ECRF,ECRB,ECRBF,ECRFB,EPSI,DEPSI,
     1    SIGBAR,I,MAXNP1,EF,EFP,AL,A,L,AA1,BB1,CC1,
     1  PLASTIC,EET,EEC,STATEV,NSTATV)
C****************************************************************C
C    THIS IS THE INITIAL LOADING SUBROUTINE WHERE THE PLASTIC  C
C    STRAIN IN TENSION AND COMPRESSION ARE BOTH ZERO           C
C***************************************************************C
        IMPLICIT REAL*8(A-H,O-Z)
        REAL*8 L
     DIMENSION SIGBAR(MAXNP1),STATEV(NSTATV)
C
     IF ((EPSI+DEPSI).GE.(PLASTIC+EET)) THEN
```

```
C    LOADING PROCESS
C*************************************************C
C    Case 1: Bond yield first, i.e. ECRF > ECRB   C
C*************************************************C
          IF(DABS(ECRF) .GT. DABS(ECRB))THEN
               IF(DABS(EPSI).LE.DABS(ECRB)) THEN
                    SIGBAR(I)=EF*(1.0-((DTANH(A*L))/(A*L)))
               END IF
               IF ((DABS(EPSI).GT.DABS(ECRB)).AND.(DABS(EPSI).LE.DABS(ECRBF))) THEN
                    SIGBAR(I)=(EF*(1.0-((DTANH(BB1*L))/
     1                   (BB1*L))))
               END IF
               IF(DABS(EPSI).GT.DABS(ECRBF)) THEN
                    SIGBAR(I)=(EFP*(1.0-((DTANH(CC1*L))/
     1                   (CC1*L))))
               END IF
          END IF
C**************************************************C
C    Case 2: Fiber yield first, i.e. ECRF < ECRB   C
C**************************************************C
          IF(DABS(ECRF).LT.DABS(ECRB))THEN
               IF(DABS(EPSI).LE.DABS(ECRF)) THEN
                    SIGBAR(I)=EF*(1.0-((DTANH(A*L))/(A*L)))
               END IF
               IF((DABS(EPSI).GT.DABS(ECRF)).AND.(DABS(EPSI).LE.DABS(ECRFB))) THEN
                    SIGBAR(I)=(EFP*(1.0-((DTANH(AA1*L))/
     1                   (AA1*L))))
               END IF
               IF(DABS(EPSI).GT.DABS(ECRFB)) THEN
                    SIGBAR(I)=(EFP*(1.0-((DTANH(CC1*L))/
     1                   (CC1*L))))
```

```
               END IF
          END IF
          STATEV(I)=STATEV(I)+(SIGBAR(I)*DEPSI)
          CALL CRITICAL(ECRF,ECRB,ECRBF,ECRFB,EPSI,DEPSI,
     1         SIGBAR,I,MAXNP1,A,L,EF,STATEV,NSTATV)
     END IF
     IF ((EPSI+DEPSI).LT.(PLASTIC+EET))THEN
C         RELOADING
          SIGBAR(I)=EF*(1.0-((DTANH(A*L))/(A*L)))
          STATEV(I)=STATEV(I)+(SIGBAR(I)*DEPSI)
     END IF
200  FORMAT (1X,I2,5X,E13.5,5X,E13.5,5X,E13.5,5X,E13.5)
     RETURN
     END
C
C
C
     SUBROUTINE BLOADC(ECRF,ECRB,ECRBF,ECRFB,EPSI,DEPSI,
     1    SIGBAR,I,MAXNP1,EF,EFP,AL,A,L,AA1,BB1,CC1,
     1  PLASTIC,EET,EEC,STATEV,NSTATV)
C****************************************************************C
C    THIS IS THE INITIAL LOADING SUBROUTINE WHERE THE PLASTIC   C
C    STRAIN IN TENSION AND COMPRESSION ARE BOTH ZERO            C
C****************************************************************C
        IMPLICIT REAL*8(A-H,O-Z)
        REAL*8 L
     DIMENSION SIGBAR(MAXNP1),STATEV(NSTATV)
C
     IF((EPSI+DEPSI).LE.(PLASTIC+EEC)) THEN
C    INITIAL LOADING PROCESS IS COMPRESSIVE
**************************************************C
```

```
C    Case 1: Bond yield first, i.e. ECRF > ECRB  C
C************************************************C
          IF(DABS(ECRF) .GT. DABS(ECRB))THEN
               IF(EPSI.GE.ECRB) THEN
                    SIGBAR(I)=EF*(1.0-((DTANH(A*L))/(A*L)))
               END IF
               IF((EPSI.LT.ECRB).AND.(EPSI.GE.ECRBF)) THEN
                    SIGBAR(I)=(EF*(1.0-((DTANH(BB1*L))/
     1                   (BB1*L))))
               END IF
               IF(EPSI.LT.ECRBF) THEN
                    SIGBAR(I)=(EFP*(1.0-((DTANH(CC1*L))/
     1                   (CC1*L))))
               END IF
          END IF
C**************************************************C
C    Case 2: Fiber yield first, i.e. ECRF < ECRB   C
C**************************************************C
          IF(DABS(ECRF) .LT. DABS(ECRB))THEN
               IF(EPSI.GE.ECRF) THEN
                    SIGBAR(I)=EF*(1.0-((DTANH(A*L))/(A*L)))
               END IF
               IF((EPSI.LT.ECRF).AND.(EPSI.GE.ECRFB)) THEN
                    SIGBAR(I)=(EFP*(1.0-((DTANH(AA1*L))/
     1                   (AA1*L))))
               END IF
               IF(EPSI.LT.ECRFB) THEN
                    SIGBAR(I)=(EFP*(1.0-((DTANH(CC1*L))/
     1                   (CC1*L))))
               END IF
          END IF
```

```
          STATEV(I)=STATEV(I)+(SIGBAR(I)*DEPSI)
          CALL CRITICAL(ECRF,ECRB,ECRBF,ECRFB,EPSI,DEPSI,
     1         SIGBAR,I,MAXNP1,A,L,EF,STATEV,NSTATV)
     END IF
     IF ((EPSI+DEPSI).GT.(PLASTIC+EEC))THEN
C    RELOADING WITH NO SHIFT TO ECRB, ECRF,ECRBF,AND ECRFB
          SIGBAR(I)=EF*(1.0-((DTANH(A*L))/(A*L)))
          STATEV(I)=STATEV(I)+(SIGBAR(I)*DEPSI)
     END IF
     RETURN
     END
C
C
C
     SUBROUTINE LOADT(ECRF,ECRB,ECRBF,ECRFB,EPSI,DEPSI,
     1    SIGBAR,I,MAXNP1,EF,EFP,AL,A,L,AA1,BB1,CC1,
     1  PLASTIC,EET,EEC,STATEV,NSTATV,SHIFT)
C****************************************************************C
C    THIS IS THE INITIAL LOADING SUBROUTINE WHERE THE PLASTIC   C
C    STRAIN IN TENSION AND COMPRESSION ARE BOTH ZERO            C
C****************************************************************C
        IMPLICIT REAL*8(A-H,O-Z)
        REAL*8 L
     DIMENSION SIGBAR(MAXNP1),STATEV(NSTATV)
C
C    STATEV((5*MAXNP1)+I) STORES THE PLASTIC STRAIN AT THE POINT
C    WHEN UNLOADING IN COMPRESSION STATE CROSS INTO LOADING IN TENSION.
     SHIFT=STATEV((5*MAXNP1)+I)
     IF ((EPSI+DEPSI).GE.(SHIFT+EET)) THEN
C    LOADING PROCESS
C**************************************************C
```

```
C    Case 1: Bond yield first, i.e. ECRF > ECRB   C
C**************************************************C
          IF(DABS(ECRF) .GT. DABS(ECRB))THEN
               IF(EPSI.LE.(ECRB+SHIFT)) THEN
                    SIGBAR(I)=EF*(1.0-((DTANH(AL))/(A*L)))
               END IF
               IF ((EPSI.GT.(ECRB+SHIFT)).AND.
     1              (EPSI.LE.(ECRBF+OFFSET))) THEN
                    SIGBAR(I)=(EF*(1.0-((DTANH(BB1*L))/
     1                   (BB1*L))))
               END IF
               IF(EPSI.GT.(ECRBF+SHIFT)) THEN
                    SIGBAR(I)=(EFP*(1.0-((DTANH(CC1*L))/
     1                   (CC1*L))))
               END IF
          END IF
C***************************************************C
C    Case 2: Fiber yield first, i.e. ECRF < ECRB   C
C***************************************************C
          IF(DABS(ECRF).LT.DABS(ECRB))THEN
               IF(EPSI.LE.(ECRF+SHIFT)) THEN
                    SIGBAR(I)=EF*(1.0-((DTANH(A*L))/(A*L)))
               END IF
               IF((EPSI.GT.(ECRF+SHIFT)).AND.
     1              (EPSI.LE.(ECRFB+SHIFT))) THEN
                    SIGBAR(I)=(EFP*(1.0-((DTANH(AA1*L))/
     1                   (AA1*L))))
               END IF
               IF(EPSI.GT.(ECRFB+SHIFT)) THEN
                    SIGBAR(I)=(EFP*(1.0-((DTANH(CC1*L))/
     1                   (CC1*L))))
```

```
               END IF
          END IF
          STATEV(I)=STATEV(I)+(SIGBAR(I)*DEPSI)
          CALL CRITICAL(ECRF,ECRB,ECRBF,ECRFB,EPSI,DEPSI,
     1         SIGBAR,I,MAXNP1,A,L,EF,STATEV,NSTATV)
     END IF
     IF ((EPSI+DEPSI).LT.(SHIFT+EET))THEN
C    RELOADING
          SIGBAR(I)=EF*(1.0-((DTANH(A*L))/(A*L)))
          STATEV(I)=STATEV(I)+(SIGBAR(I)*DEPSI)
     END IF
200  FORMAT (1X,I2,5X,E13.5,5X,E13.5,5X,E13.5,5X,E13.5)
     RETURN
     END
C
C
C
     SUBROUTINE LOADC(ECRF,ECRB,ECRBF,ECRFB,EPSI,DEPSI,
     1    SIGBAR,I,MAXNP1,EF,EFP,AL,A,L,AA1,BB1,CC1,
     1  PLASTIC,EET,EEC,STATEV,NSTATV,SHIFT)
C****************************************************************C
C    THIS IS THE INITIAL LOADING SUBROUTINE WHERE THE PLASTIC   C
C    STRAIN IN TENSION AND COMPRESSION ARE BOTH ZERO            C
C****************************************************************C
        IMPLICIT REAL*8(A-H,O-Z)
        REAL*8 L
     DIMENSION SIGBAR(MAXNP1),STATEV(NSTATV)
C
C    STATEV((4*MAXNP1)+I) STORES THE PLASTIC STRAIN AT THE POINT
C    WHEN UNLOADING IN TENSION CROSS INTO LOADING IN COMPRESSION.
     SHIFT=STATEV((4*MAXNP1)+I)
```

```
     IF((EPSI+DEPSI).LE.(SHIFT+EEC)) THEN
C    LOADING PROCESS
***************************************************C
C    Case 1: Bond yield first, i.e. ECRF > ECRB   C
C**************************************************C
          IF(DABS(ECRF) .GT. DABS(ECRB))THEN
               IF(EPSI.GE.(ECRB+SHIFT)) THEN
                    SIGBAR(I)=EF*(1.0-((DTANH(AL))/(A*L)))
               END IF
               IF(EPSI.LT.(ECRB+SHIFT) .AND.
     1         EPSI.GE.(ECRBF+SHIFT)) THEN
                    SIGBAR(I)=(EF*(1.0-((DTANH(BB1*L))/
     1                   (BB1*L))))
               END IF
               IF(EPSI.LT.(ECRBF+SHIFT)) THEN
                    SIGBAR(I)=(EFP*(1.0-((DTANH(CC1*L))/
     1                   (CC1*L))))
               END IF
          END IF
C***************************************************C
C    Case 2: Fiber yield first, i.e. ECRF < ECRB   C
C***************************************************C
          IF(DABS(ECRF) .LT. DABS(ECRB))THEN
               IF(EPSI.GE.(ECRF+SHIFT)) THEN
                    SIGBAR(I)=EF*(1.0-((DTANH(A*L))/(A*L)))
               END IF
               IF((EPSI).LT.(ECRF+SHIFT) .AND.
     1              (EPSI).GE.(ECRFB+SHIFT)) THEN
                    SIGBAR(I)=(EFP*(1.0-((DTANH(AA1*L))/
     1                   (AA1*L))))
               END IF
```

```
               IF((EPSI).LT.(ECRFB+SHIFT)) THEN
                    SIGBAR(I)=(EFP*(1.0-((DTANH(CC1*L))/
     1                   (CC1*L))))
               END IF
          END IF
          STATEV(I)=STATEV(I)+(SIGBAR(I)*DEPSI)
          CALL CRITICAL(ECRF,ECRB,ECRBF,ECRFB,EPSI,DEPSI,
     1         SIGBAR,I,MAXNP1,A,L,EF,STATEV,NSTATV)
     END IF
     IF ((EPSI+DEPSI).GT.(SHIFT+EEC))THEN
C    RELOADING
          SIGBAR(I)=EF*(1.0-((DTANH(A*L))/(A*L)))
          STATEV(I)=STATEV(I)+(SIGBAR(I)*DEPSI)
     END IF
     RETURN
     END
C
C
C
     SUBROUTINE LOADT2(ECRF,ECRB,ECRBF,ECRFB,EPSI,DEPSI,
     1    SIGBAR,I,MAXNP1,EF,EFP,AL,A,L,AA1,BB1,CC1,
     1  PLASTIC,EET,EEC,STATEV,NSTATV,SHIFT)
C*****************************************************************C
C    THIS IS THE INITIAL LOADING SUBROUTINE WHERE THE PLASTIC   C
C    STRAIN IN TENSION AND COMPRESSION ARE BOTH ZERO            C
C*****************************************************************C
        IMPLICIT REAL*8(A-H,O-Z)
        REAL*8 L
     DIMENSION SIGBAR(MAXNP1),STATEV(NSTATV)
C
     YIELD=STATEV((6*MAXNP1)+I)
```

```
      SHIFT=STATEV((7*MAXNP1)+I)
      IF ((EPSI+DEPSI).GE.YIELD) THEN
C     LOADING PROCESS
C**************************************************C
C     Case 1: Bond yield first, i.e. ECRF > ECRB   C
C**************************************************C
           IF(DABS(ECRF) .GT. DABS(ECRB))THEN
                IF(EPSI.LE.YIELD) THEN
                     SIGBAR(I)=EF*(1.0-((DTANH(AL))/(A*L)))
                END IF
                IF ((EPSI.GT.YIELD).AND.
     1               (EPSI.LE.(ECRBF-SHIFT))) THEN
                     SIGBAR(I)=(EF*(1.0-((DTANH(BB1*L))/
     1                    (BB1*L))))
                END IF
                IF(EPSI.GT.(ECRBF-SHIFT)) THEN
                     SIGBAR(I)=(EFP*(1.0-((DTANH(CC1*L))/
     1                    (CC1*L))))
                END IF
           END IF
C***************************************************C
C     Case 2: Fiber yield first, i.e. ECRF < ECRB   C
C***************************************************C
           IF(DABS(ECRF).LT.DABS(ECRB))THEN
                IF(EPSI.LE.YIELD) THEN
                     SIGBAR(I)=EF*(1.0-((DTANH(A*L))/(A*L)))
                END IF
                IF((EPSI.GT.YIELD).AND.
     1               (EPSI.LE.(ECRFB-SHIFT))) THEN
                     SIGBAR(I)=(EFP*(1.0-((DTANH(AA1*L))/
     1                    (AA1*L))))
```

```
               END IF
               IF(EPSI.GT.(ECRFB-SHIFT)) THEN
                    SIGBAR(I)=(EFP*(1.0-((DTANH(CC1*L))/
     1                   (CC1*L))))
               END IF
          END IF
          STATEV(I)=STATEV(I)+(SIGBAR(I)*DEPSI)
          CALL CRITICAL(ECRF,ECRB,ECRBF,ECRFB,EPSI,DEPSI,
     1         SIGBAR,I,MAXNP1,A,L,EF,STATEV,NSTATV)
     END IF
     IF ((EPSI+DEPSI).LT.YIELD)THEN
C    RELOADING
          SIGBAR(I)=EF*(1.0-((DTANH(A*L))/(A*L)))
          STATEV(I)=STATEV(I)+(SIGBAR(I)*DEPSI)
     END IF
200  FORMAT (1X,I2,5X,E13.5,5X,E13.5,5X,E13.5,5X,E13.5)
     RETURN
     END
C
C
C
     SUBROUTINE LOADC2(ECRF,ECRB,ECRBF,ECRFB,EPSI,DEPSI,
     1    SIGBAR,I,MAXNP1,EF,EFP,AL,A,L,AA1,BB1,CC1,
     1  PLASTIC,EET,EEC,STATEV,NSTATV,SHIFT)
C****************************************************************C
C    THIS IS THE INITIAL LOADING SUBROUTINE WHERE THE PLASTIC   C
C    STRAIN IN TENSION AND COMPRESSION ARE BOTH ZERO            C
C****************************************************************C
        IMPLICIT REAL*8(A-H,O-Z)
        REAL*8 L
     DIMENSION SIGBAR(MAXNP1),STATEV(NSTATV)
```

```
C
     YIELD=STATEV((6*MAXNP1)+I)
     SHIFT=STATEV((8*MAXNP1)+I)
     IF((EPSI+DEPSI).LE.YIELD) THEN
C    LOADING PROCESS
     write(7,*)'CALLING LOADC2'
*************************************************C
C    Case 1: Bond yield first, i.e. ECRF > ECRB  C
C************************************************C
          IF(DABS(ECRF) .GT. DABS(ECRB))THEN
               IF(EPSI.GE.YIELD) THEN
                    SIGBAR(I)=EF*(1.0-((DTANH(AL))/(A*L)))
               END IF
               IF((EPSI.LT.YIELD) .AND.
     1         EPSI.GE.(ECRBF+SHIFT)) THEN
                    SIGBAR(I)=(EF*(1.0-((DTANH(BB1*L))/
     1                   (BB1*L))))
               END IF
               IF(EPSI.LT.(ECRBF+SHIFT)) THEN
                    SIGBAR(I)=(EFP*(1.0-((DTANH(CC1*L))/
     1                   (CC1*L))))
               END IF
          END IF
C**************************************************C
C    Case 2: Fiber yield first, i.e. ECRF < ECRB   C
C**************************************************C
          IF(DABS(ECRF) .LT. DABS(ECRB))THEN
               IF(EPSI.GE.YIELD) THEN
                    SIGBAR(I)=EF*(1.0-((DTANH(A*L))/(A*L)))
               END IF
               IF((EPSI.LT.YIELD) .AND.
```

```
     1              (EPSI).GE.(ECRFB-SHIFT)) THEN
                    SIGBAR(I)=(EFP*(1.0-((DTANH(AA1*L))/
     1                   (AA1*L))))
               END IF
               IF((EPSI).LT.(ECRFB-SHIFT)) THEN
                    SIGBAR(I)=(EFP*(1.0-((DTANH(CC1*L))/
     1                   (CC1*L))))
               END IF
          END IF
          STATEV(I)=STATEV(I)+(SIGBAR(I)*DEPSI)
          CALL CRITICAL(ECRF,ECRB,ECRBF,ECRFB,EPSI,DEPSI,
     1         SIGBAR,I,MAXNP1,A,L,EF,STATEV,NSTATV)
     END IF
     IF ((EPSI+DEPSI).GT.PLASTIC)THEN
C    RELOADING
          SIGBAR(I)=EF*(1.0-((DTANH(A*L))/(A*L)))
          STATEV(I)=STATEV(I)+(SIGBAR(I)*DEPSI)
     END IF
     RETURN
     END
C
C
C
     SUBROUTINE CRITICAL(ECRF,ECRB,ECRBF,ECRFB,EPSI,DEPSI,SIGBAR,I,
     1  MAXNP1,A,L,EF,STATEV,NSTATV)
C***********************************************************************C
C    THE CRITICAL SUBROUTINE UPDATES THE ELASTIC COMPONENT OF THE     C
C    TOTAL STRAIN. IT IS CALLED ONLY DURING TENSILE LOADING PROCESS.  C
C***********************************************************************C
     IMPLICIT REAL*8(A-H,O-Z)
     REAL*8 L
```

```
      DIMENSION SIGBAR(MAXNP1),STATEV(NSTATV)
C     STATEV(I) STORES THE CURRENT FIBER STRESS FOR ORIENTATION I
C     STATEV(MAXNP1+I) STORES THE CURRENT ELASTIC COMPONENT OF THE TOTAL STRAIN IN TENSION
C     STATEV((2*MAXNP1)+I) STORES THE CURRENT ELASTIC COMPONENT OF THE TOTAL STRAIN IN
COMPRESSION
C     STATEV((3*MAXNP1)+I) STORES THE CURRENT PLASTIC STRAIN
C
      IF (STATEV(I).GT.0) THEN
           STATEV(MAXNP1+I)=STATEV(I)/(EF*(1.0-((DTANH(A*L))/(A*L))))
           STATEV((3*MAXNP1)+I)=EPSI+DEPSI-STATEV(MAXNP1+I)
         ELSE IF (STATEV(I).LT.0) THEN
           STATEV((2*MAXNP1)+I)=STATEV(I)/(EF*(1.0-((DTANH(A*L))/(A*L))))
           STATEV((3*MAXNP1)+I)=EPSI+DEPSI-STATEV((2*MAXNP1)+I)
      ELSE
      END IF
      RETURN
      END
C
C
C
      SUBROUTINE OFFSET(ECRF,ECRB,DEPSI,I,MAXNP1,
      1    PLASTIC,EET,EEC,STATEV,NSTATV,SHIFT)
C******************************************************************************C
C     THE OFFSET SUBROUTINE DETERMINES THE SHIFT OF THE CRITICAL STRAINS      C
C******************************************************************************C
      IMPLICIT REAL*8(A-H,O-Z)
      DIMENSION STATEV(NSTATV)
C
      EET=STATEV(MAXNP1+I)
      EEC=STATEV((2*MAXNP1)+I)
      PLASTIC=STATEV((3*MAXNP1)+I)
```

```
     STATEV((9*MAXNP1)+I)=EET
     STATEV((10*MAXNP1)+I)=EEC
C****************************************************************************************
**C
C    WHEN THE PROCESS HAS CROSSED FROM UNLOADING IN COMPRESSION INTO LOADING IN TENSION
C
C****************************************************************************************
**C
C    STATEV((5*MAXNP1)+I) STORES THE PLASTIC STRAIN AT WHICH THIS DEPARTURE FROM
COMPRESSION INTO
C    TENSION TAKES PLACE.
C    STATEV((6*MAXNP1)+I) STORES THE MOST CURRENT YIELD STRAIN IN TENSION.
C    STATEV((8*MAXNP1)+I) STORES THE TOTAL AMOUNT OF PLASTIC STRAIN ACCUMULATED IN
COMPRESSION SO FAR.
          IF (DEPSI.GE.0) THEN
               IF (DABS(ECRF).GT.DABS(ECRB)) THEN
                    IF (DABS(EET).LT.DABS(ECRB)) THEN
C                   ALL CRITICAL STRAINS MOVE BY AN AMOUNT OF CURRENT PLASTIC STRAIN
                         STATEV((5*MAXNP1)+I)=PLASTIC
                         STATEV((8*MAXNP1)+I)=PLASTIC
                    ELSE
                         STATEV((5*MAXNP1)+I)=PLASTIC
                         STATEV((6*MAXNP1)+I)=PLASTIC+EET
                    STATEV((8*MAXNP1)+I)=STATEV((8*MAXNP1)+I)+
     1                   DABS(STATEV((4*MAXNP1)+I)-STATEV((5*MAXNP1)+I))
                    END IF
               ELSE
               IF (DABS(EET).LT.DABS(ECRF)) THEN
C                   ALL CRITICAL STRAINS MOVE BY AN AMOUNT OF CURRENT PLASTIC STRAIN
                    STATEV((5*MAXNP1)+I)=PLASTIC
                    STATEV((8*MAXNP1)+I)=PLASTIC
```

```
                    ELSE
                         STATEV((5*MAXNP1)+I)=PLASTIC
                         STATEV((6*MAXNP1)+I)=PLASTIC+EET
                    STATEV((8*MAXNP1)+I)=STATEV((8*MAXNP1)+I)+
     1                   DABS(STATEV((4*MAXNP1)+I)-STATEV((5*MAXNP1)+I))
                    END IF
               END IF
          END IF
C****************************************************************************************
**C
C    WHEN THE PROCESS HAS CROSSED FROM UNLOADING IN TENSION INTO LOADING IN COMPRESSION
C
C****************************************************************************************
**C
C    STATEV((4*MAXNP1)+I) STORES THE PLASTIC STRAIN AT WHICH THIS DEPARTURE FROM TENSION
INTO
C    COMPRESSION TAKES PLACE.
C    STATEV((6*MAXNP1)+I) STORES THE MOST CURRENT YIELD STRAIN IN COMPRESSION
C    STATEV((7*MAXNP1)+I) STORES THE TOTAL AMOUNT OF PLASTIC STRAIN ACCUMULATED IN
TENSION SO FAR.
          IF (DEPSI.LT.0) THEN
               IF (DABS(ECRF).GT.DABS(ECRB)) THEN
                    IF (DABS(EEC).LT.DABS(ECRB)) THEN
C                   ALL CRITICAL STRAINS MOVE BY AN AMOUNT OF CURRENT PLASTIC STRAIN
                         STATEV((4*MAXNP1)+I)=PLASTIC
                         STATEV((7*MAXNP1)+I)=PLASTIC
                    ELSE
                         STATEV((4*MAXNP1)+I)=PLASTIC
                         STATEV((6*MAXNP1)+I)=PLASTIC+EEC
                    STATEV((7*MAXNP1)+I)=STATEV((7*MAXNP1)+I)+
     1                   DABS(STATEV((4*MAXNP1)+I)-STATEV((5*MAXNP1)+I))
```

```
                  END IF
            ELSE
               IF (DABS(EET).LT.DABS(ECRF)) THEN
C                 ALL CRITICAL STRAINS MOVE BY AN AMOUNT OF CURRENT PLASTIC STRAIN
                  STATEV((4*MAXNP1)+I)=PLASTIC
                  STATEV((7*MAXNP1)+I)=PLASTIC
                  ELSE
                     STATEV((4*MAXNP1)+I)=PLASTIC
                     STATEV((6*MAXNP1)+I)=PLASTIC+EEC
                  STATEV((7*MAXNP1)+I)=STATEV((7*MAXNP1)+I)+
     1               DABS(STATEV((4*MAXNP1)+I)-STATEV((5*MAXNP1)+I))
               END IF
               END IF
            END IF
         RETURN
         END
```